NANOPARTICLE-STABILIZED CO_2-FOAM AS A HYDRAULIC FRACTURING FLUID-AN EXPERIMENTAL STUDY

A Dissertation

by

AREZOO SADAT EMRANI

Submitted to the Office of Graduate and Professional Studies of
Texas A&M University
in partial fulfillment of the requirements for the degree of

DOCTOR OF PHILOSOPHY

Chair of Committee,	Hisham A. Nasr-El-Din
Committee Members,	Stephen A. Holditch
	Maria A. Barrufet
	Mahmoud El-Halwagi
Head of Department,	A. Daniel Hill

May 2017

Major Subject: Petroleum Engineering

ABSTRACT

Foamed fluids have been used for decades to diminish formation damage in nearly all kinds of reservoirs over a wide range of pressures and temperatures. Although water-based fluids are widely used in the oil industry as one of the most economic hydraulic fracturing methods, foam is another viable alternative to fracture water-sensitive reservoirs where damage to pore throats is caused by swelling clays or fines migration. CO_2-foam not only reduces formation damage by minimizing the quantity of aqueous fluid that enters the formation but also significantly improves sweep efficiency. Even though surfactant is widely used to generate stable foam in high-temperature and high-salinity environments such foam can degrade in these harsh conditions.

Oil production using enhanced oil recovery techniques and especially through performing hydraulic fracturing has been increased in recent years. This in turn significantly escalates the demand for high performance fracturing fluids which cause low formation damage in porous medium. Traditional fracturing fluids use water viscosifying agents such as guar gum and its derivatives to support and carry the proppant. However, guar gum forms an insoluble residue in the formation, and these insoluble materials plug pore throats, causing formation damage that could be fatal to the reservoirs.

The purpose of this dissertation is to develop nanoparticle-stabilized CO_2 foam by adding nanoparticles such as SiO_2 and Fe_2O_3 in combination with guar-gum polymer, and viscoelastic surfactant (VES) to surfactant solutions stabilize CO_2-foam to enhance its stability. Additional objectives include measuring contact angle and surface tension of nanoparticle solutions, and measuring the zeta potential of nanoparticle solutions to better understand the parameters that affect CO_2-foam stability. Moreover, in this work, mobility reduction factor (MRF) of CO_2-foam was investigated for foam generated with polymer-

based solution, e.g., guar gum, in the presence and absence of nanoparticles to assess the apparent fluid viscosity at high temperature and high salinity. To achieve this objective, coreflood tests were conducted on different Buff Berea sandstone cores at both 77 and 250°F. CO_2 gas was injected with the different solutions simultaneously to generate foam with 80% quality. The pressure drop across the core was then measured to estimate the MRF.

Experimental results of this work indicated that the critical micelle concentration (CMC) value increases as temperature increases. The CMC value also decreased while salt concentration increased. Furthermore, for a given temperature and salinity, the results did not exhibit changes in the CMC value when the pressure increased. Temperature and pressure had a negative effect on the foam stability when surfactant was used. However, adding nanoparticles and/or polymers could overcome this drawback and improve the foam stability. Polymer-surfactant-based solutions such as guar-gum/AOS generate foams with significantly shorter half-life time than that of the surfactant-nanoparticle dispersion like AOS-SiO_2. That is, under same conditions, polymer-surfactant based foams are less stable compared to surfactant-nanoparticle based foams. Coreflood results also show that AOS improves MRF by 300% compared to that of brine solution. Adding SiO_2 nanoparticles and guar-gum to the AOS solution improves foam stability and MRF simultaneously.

Choice of surfactant concentration is a critical parameter in generating stable foams. However, the economical use of surfactants is limited by various factors such as surface adsorption, process cost, surfactant loss, and surfactant degradation at high-temperature reservoirs. Nanoparticle solutions can be employed to improve CO_2 foam stability as well as MRF factor. Adding nanoparticles is highly recommended for hydraulic fracturing applications, particularly in fracturing stimulation at high-temperatures.

To Sardar

ACKNOWLEDGMENTS

I would like to express my deepest gratitude and appreciation to my advisor, Dr. H. A. Nasr-El-Din, for his guidance, support, and for patient motivation.

I would also like to acknowledge my committee members: Dr. Stephen A. Holditch, Dr. Maria A. Barrufet, and Dr. Mahmoud El-Halwagi, who graciously agreed to serve on my committee. Thank you and the best of luck in your future endeavors.

My warmest thanks to my parents and my brother for allowing me to realize my own potential. All the support they have provided me over the years was the greatest gift anyone has ever given me. Also, I need to thank Sardar, my lovely husband, for his continued and unfailing love, support and for believing in me, and for sharing my wish to reach the goal of completing this task, but caring enough to love me even if I never achieved it.

Thanks also go to my friends and colleagues and the department faculty and staff for making my time at Texas A&M University a great experience. Finally, I would like to acknowledge financial support from the Crisman Institute at Texas A&M University.

CONTRIBUTORS AND FUNDING SOURCES

Contributors

This work was supported by a dissertation committee consisting of Professor Hisham A. Nasr-El-Din and Professors Stephen A. Holditch and Maria A. Barrufet of the Department of Petroleum Engineering and Professor Mahmoud El-Halwagi of the Department of Chemical Engineering. All other work conducted for the dissertation was completed by the student independently.

Funding Sources

Graduate study was supported by a grant from the Crisman institute for petroleum research at Texas A&M University.

ABBREVIATIONS

AOS	Alpha olefin sulfonate
CMC	Critical micelle concentration (wt%)
DI	Deionized water
DLVO	Derjaguin-landau-verwey-overbeek
DSA	Drop shape analysis
EOR	Enhanced oil recovery
HP/HT	High pressure and high temperature
HPVC	High pressure view chamber
HPAM	Poly-Acrylamide polymer
IFT	Interfacial tension
MRF	Mobility reduction factor
PVAm	Polyvinylamine
PALS	Phase-analysis light-scattering
PPT	Pound per gallon
RT	Room temperature
SDS	Sodium dodecyl sulphate
SDBS	Sodium dodecylbenzene sulfonate
TEM	Transmission electron micro
VES	Viscoelastic surfactant

NOMENCLATURE

A	Cross-section area for the core, cm^2
E	Detachment energy, KT
H_{gas}	Height of the dense CO_2 layer at the time, cm
H_{foam}	Initial height of the foam layer, cm
k	Absolute core permeability, md
L	Core length, in.
Δp	Pressure drop, psi
Q	Total flow rate, cm^3/min
q_{liquid}	Liquid flow rate, cm^3/min
q_{gas}	Gas flow rate, cm^3/min
r	Particle radius, in.
μ	Fluid viscosity subscripts, cp
f	Experiment with foam
g	Experiment without foam
θ	Contact angle
γ	Surface tension, Nm^2/m
V_p	Pore volume, cm^3
ρ	Brine density, g/cm^3

TABLE OF CONTENTS

Page

1. INTRODUCTION AND LITERATURE REVIEW 1

1.1 Foam Characteristics 3
1.2 Foam Quality 4
1.3 Foaming Agent 6
1.4 Viscoelastic Surfactants 11
1.5 Polymers 11
1.6 Nanoparticles 13
1.7 Brine 15

2. EXPERIMENTAL STUDY 16

2.1 Material 16
2.1.1 Surfactant 16
2.1.2 Brine 17
2.1.3 Gas 17
2.1.4 Nanoparticles 17
2.1.5 VES 17
2.1.6 Polymer 18
2.1.7 Cores 18
2.2 Method and Equipment 18
2.2.1 Surface Tension 18
2.2.2 Contact Angle 22
2.2.3 Rock Samples to Determine Contact Angle 23
2.2.4 Foam Stability 23
2.2.5 Foam Texture 26
2.2.6 Zeta Potential 27
2.2.7 Coreflood 28

3. EXPERIMENTAL RESULTS 34

3.1 Surface Tension Measurement 34
3.1.1 Effect of Surfactant Concentration, Temperature and Pressure on Surface Tension and the CMC of AOS 35
3.1.2 Effect of Salt Concentration on Surface Tension and the CMC of AOS 38

3.1.3 Effect of Nanoparticles on Surface Tension and the CMC of AOS 40
3.2 Foam Texture 42
3.3 Foam Stability 43
3.3.1 Foam Stability in Absence of Nanoparticles 43
3.3.2 Foam Stability in Presence of Nanoparticles 46
3.3.3 Foam Stability in Presence of Polymer 59
3.4 Contact Angle 69
3.5 Zeta Potential 74
3.6 Coreflood 76
3.6.1 Foamability 77
3.6.2 Foam Stability 79
3.6.3 Nanoparticles Effect 83
3.6.4 Temperature Effects 86
3.6.5 Polymer Effect 88

4. CONCLUSIONS AND RECOMMENDATIONS 93

4.1 Surface Tension Measurement to Find the CMC Value 93
4.2 Foam Stability 94
4.3 Core Flood 95
4.4 Recommendation 96

REFERENCES 97

APPENDIX A. 108

LIST OF FIGURES

FIGURE		Page
1.1	Illustration of foam structure.	3
1.2	Generalized 2D slice of a bulk foam system.	4
1.3	Pendant drop geometry [15]	6
1.4	Schematic diagram of surface-active molecule [16]	7
1.5	Schematic illustration of the reversible monomer-micelle thermodynamic equilibrium [16].	9
1.6	The mechanism of surface tension based on surfactant concentration [25].	9
1.7	Molecular structure of partially hydrolyzed polyacrylamide [38].	12
2.1	Molecular structure of AOS.	16
2.2	Molecular structure of VES [60].	18
2.3	A schematic of DSA equipment and setup used in the current experiments. The left panel is the setup for HPHT experiments to measure contact angle and surface tension. The right panel is the focused image of the output of the system.	20
2.4	A photo of density meter used to study liquid density.	21
2.5	Density of CO_2 gas as a function of temperature and pressures.	21
2.6	A schematic diagram illustrating the work flow process and equipment to measure foam stability. A and B are ball valves, and C, D, and E are needle valves.	25
2.7	Determination of foam stability at HP/HT. Hgas is the height of the dense CO_2 layer at the time, cm, Hliquid is the height of the liquid at the time, and Hfoam is the initial height of the foam layer, cm.	26
2.8	A photo of microscope used to study foam texture.	27

2.9 A photo of the ZetaPals setup used to measure the zeta potential. 28

2.10 Schematic for coreflood setup, where 1 = CO_2 accumulator, 2 = brine and solution accumulators, 3 = Core Holder, 4 = Pressure Transducer, 5 = PC Recorder, 6 = hand pump for overburden pressure, 7 = syringe pump, 8 = CO_2 cylinder, 9 = N_2 cylinder, 10 = Back pressure regulator, 11 = Oven. . 30

3.1 The surface tension of CO_2/AOS solution as a function of (a) time and (b) bubble surface area (0.1 wt% of AOS at 176°F and 73 psi). 35

3.2 Surface tension as a function of surfactant concentration at 1 wt% salinity at various pressures and temperatures. 37

3.3 A comparison of the CMC value as a function of temperature for 1, 3 and 5 wt% of NaCl. 38

3.4 AOS is not soluble at high NaCl concentrations (8 wt% of NaCl). 39

3.5 Surface tension as a function of surfactant concentration for 1, 3, and 5 wt% of NaCl (77°F and 435 psi). 40

3.6 A comparison of the equilibrium time on the solution containing both surfactants and nanoparticles (435 psi and 302°F). 41

3.7 A comparison of the CMC value as a function of temperature on the solution containing both surfactants and nanoparticles. 41

3.8 Threshold image, of selected section at initial time (0.1 wt% of nanoparticles and 0.5 wt% of AOS). 42

3.9 Foam height as a function of surfactant concentration at 75°F and 300 psi. 44

3.10 Effect of surfactant concentrations on foam texture for 0.05, 0.8, and 1 wt% of AOS solution. 45

3.11 Foam shake test for all solutions examined in this study. Concentrations of chemical are 0.5 wt% of AOS, 0.1 wt% of nanoparticles, SiO_2 and Fe_2O_3, 20 ppt guar gum, and 2 vol% of VES. 47

3.12 A comparison of the foam height in the absence and presence of nanoparticles at 75°F and 300 psi (0.1 wt% of nanoparticles and 0.5 wt% of AOS). 48

3.13 Log (half-life time) as a function of nanoparticle concentrations at 75°F and 290 psi. 50

3.14 The optimal surfactant and nanoparticle concentrations (SiO_2 with 100 nm) for line-bar at 75°F, and dashed-line at 140°F. 51

3.15 Contact angle between solution/sandstone/CO_2 for 0.5 wt% of AOS at 75°F. 52

3.16 The bubble size for 0.5 wt% of AOS at 75°F and initial time. 53

3.17 A comparison of the foam made by 0.5 wt% of AOS and two different nanoparticle sizes at 75°F. 54

3.18 Contact angle between solution/sandstone/CO_2 for 0.5 wt% of AOS and SiO_2 with 100 nm (left) and 140 nm (right) at 75°F. 54

3.19 Log (half-life) as a function of pressure at 75°F in the presence of 0.1 wt% of SiO_2 with 100 nm for 0.1 and 0.5 wt% of AOS. 55

3.20 The bubble size increases as temperature increases. 56

3.21 Log (half-life time) as a function of temperature at 300 psi and 0.5 wt% of AOS. 56

3.22 Log (half-life time) as a function of a nanoparticle concentration for 75°F and 140°F at 300 psi for 0.5 wt% of AOS. 57

3.23 A comparison of the log (half-life) of CO_2 foam at 75°F temperature and 300 psi for 0.5 wt% of AOS in the presence of SiO_2 with 100 nm for different salt concentrations. 59

3.24 A comparison of the foamability at ambient conditions for: (a) 20 ppt guar + 0.1 wt% SiO_2, (b) 0.5 wt% AOS + 20 ppt guar + 0.1 wt% SiO_2, (c) 0.5 wt% AOS + 20 ppt guar + 0.1 wt% Fe_2O_3, and (d) 0.5 wt% AOS + 0.1 wt% SiO_2. Experiments showed that all dispe dispersions ((b), (c), and (d)) could generate foam except for the dispersion (a) which contains no surfactant. 60

3.25 Effect of pressure on log (half-life) for the AOS-guar and AOS solutions in the presence of nanoparticles at 77°F. 61

3.26 Compression of the thickness for (a) 0.5 wt% AOS + 20 ppt guar, and (b) 0.5 wt% AOS + 20 ppt guar + 0.1 wt% SiO_2. Nanoparticles create lamella layer two times thicker than that of the solution without nanoparticles. . . 62

3.27 Optical micrographs of foams stabilized by 0.5 wt% AOS solutions with 20 ppt guar gum in the presence of 0.1 wt% nanoparticles at initial time (a, b, and c) and after two days (d, e, and f). (a, b, and c) show that the nanoparticles attach to the lamella between bubbles that help to stabilize foam. (d) and (e) show that the bubble size and shape changes with time. (f) shows clearly that there is agglomeration for Fe_2O_3 into the AOS + guar-gum solutions. 63

3.28 Agglomeration of nanoparticles for the AOS-guar solution in the presence of Fe_2O_3 at ambient conditions. (a) foam at ambient conditions, (b)-(d) magnified images of the squared areas in (a)-(c) using electron microscope to show Fe_2O_3 agglomeration. 64

3.29 TEM image of Fe_2O_3 nanoparticle agglomeration in the AOS-guar solution. 65

3.30 Log (Half-life) for the AOS-guar and AOS solutions in the presence of nanoparticles at various temperatures and 300 psi. 66

3.31 The behavior of the foam over time for AOS solution: (a) and (c) in the presence of SiO_2, and (b) and (d) in the absence of SiO_2. Small bubbles merge to form and expand larger bubbles as time passes (c) and (d). . . . 67

3.32 Optical micrographs showing a 3D network structure in the lamella layer for: (a) 0.5 wt% AOS and (b) 0.5 wt% AOS + 0.1 wt% SiO_2. 68

3.33 Contact angle for 0.5 wt% of AOS and (a) 0.1 wt% of SiO_2 (b) 20 ppt guar + 0.1 wt% of SiO_2, (c) 20 ppt guar + 0.2 wt% SiO_2, and (d) 20 ppt guar + 0.1 wt% Fe_2O_3 at 77°F. 70

3.34 Comparison of the detachment energy for different dispersions at 77°F. KT represents an energy unit which is called Boltzmann constant (KT = 4.11 $\times 10^{-21}$ Joule). 72

3.35 Contact angle for 0.5 wt% AOS + 0.1 wt% SiO_2 at (a) 77°F, (b) 100°F, (c) 140°F, and (d) 180°F. 73

3.36 Detachment energy for the AOS solutions in the presence of 0.1 wt% of SiO_2 nanoparticles as a function of temperature. 74

3.37 Zeta potential of nanoparticles for the AOS solution and the AOS-guar solution in the presence of nanoparticles at 77°F. 75

3.38 Foam shake test for 0.5 wt% of AOS in the absence (a), presence of 0.1 wt% of SiO_2 (b), and presence of 4 ppt guar-gum and SiO_2 (c) at ambient conditions for 5 wt% of NaCl. 79

3.39 Log (half-life) for room temperature (77°F) and 140°F at 300 psi for 0.5 wt% of AOS. 81

3.40 Threshold image, of selected section at initial time (polymer-based). The bubble size increases as temperature increases. 81

3.41 A comparison of the drop pressure across the core between CO_2-Foam injection and brine-CO_2 Coinjection at 77°F. 82

3.42 A comparison of the pressure drop between AOS solution in the absence and presence of nanoparticles and 77°F. 83

3.43 A comparison of the foam height for AOS solution in the (a) presence and (b) absence of SiO_2 nanoparticles at 77°F. 84

3.44 A comparison of the outlet production (a) before breakthrough and (b) after breakthrough for AOS + SiO_2 solution. 85

3.45 A comparison of the MRF between AOS solution in the absence and presence of nanoparticles and 77°F. 86

3.46 A comparison of the pressure drop between CO_2-Foam (AOS and AOS + Guar) and CO_2 Gas at 250°F. 87

3.47 A comparison of the MRF between AOS in the presence and absence of SiO_2 at 250°F 88

3.48 A comparison of the drop pressure between CO_2-Foam injection (AOS + Guar) and brine-CO_2 Coinjection at 77°F. 89

3.49 A comparison of the MRF between guar solution, CO_2-Foam (AOS+ guar) in the presence, and absence of SiO_2 at 77°F. 90

3.50 A comparison of the MRF between CO_2-Foam and CO_2-Foam + guar in the presence and absence of SiO_2 at 140°F. 91

3.51 A comparison of the MRF between CO_2-Foam + guar in the presence and absence of SiO_2 at 250°F. 91

LIST OF TABLES

TABLE Page

1.1 Common surfactants to form foam. 10

2.1 Physical properties of sandstone core and detailed information of the chemical used. 32

3.1 The surface tension between CO_2 and different aqueous dispersions at 300 psi. 71

1. INTRODUCTION AND LITERATURE REVIEW

Today, many unconventional resources are widely developed so as to enhance the amount of hydrocarbon production to meet increasing worldwide energy demands. Reservoirs with low permeability cannot produce at economic flow rates. Thus, developing these resources requires a different approach from conventional gas reservoirs. New technologies such as horizontal drilling, hydraulic fracturing and de-watering have been introduced in the oil and gas industry to develop these resources on a commercial scale.

Employing carbon dioxide and surfactant as an effective hydraulic fracturing fluid has been recently addressed in enhanced oil recovery (EOR). Due to a variety of CO_2 advantages compared to other solvents, it has been used in the oil industry for the past 30 years. CO_2 is inexpensive, relatively nontoxic, nonflammable, and a nonpolar solvent that is abundant and has a mild critical point value [1, 2].

Most hydraulic fracturing fluids are water-based; however, they should be used with extreme care in water-sensitive formations. Employing water as a hydraulic fracturing fluid may accordingly results in clay swelling or fines migration in the formation while replacing foam can eliminate such drawbacks and minimize water consumption [3].

Generally, CO_2-foams are generated and stabilized by surfactants. However, surfactants tend to degrade at high temperatures and high salinity environments. Moreover, surfactant dissipation in reservoirs due to adsorption in porous media results in an increasing chemical consumption volume in CO_2-foam flooding.

A solution to this problem is discussed in [4]. They reported that using nanoparticles not only solve aforementioned issue, but also may increase foam stability more than surfactants. Also, they showed that the successful application of nanoparticles and nonionic surfactants in foam remain stable at 95°C and 0.05wt% for a month. Nanoparticles are of

high interest in the oil industry because of its size, high absorption, and heat conductivity. It should be mentioned that in many of the previous research studies only the application of nanoparticles in CO_2-foam was investigated [5, 6, 7, 4].

To prepare nanoparticle-dispersion, nanoparticles (silica powder in the range of 100-150 nm with concentration between 4000-6000 ppm) are added to DI water and Brine according to [5, 6]. Shape and size of nanoparticle as well as contact angle, concentration, and particle-particle interactions at the gas/liquid interface can affect particle stabilization. It would take into account that other types of nanoparticles also may be utilized in industry. For instance, [8] used three types of nanoparticles (MgO, Al_2O_3 and SiO_2) to reduce fines migration into the fluid [8].

Physical properties of CO_2 can significantly vary with changes in environmental circumstances such as temperature and pressure changes which might affect CO_2-foam performance. [9] showed that weaker CO_2-foams were generated at supercritical conditions, but [10] had studied supercritical CO_2-foam in Berea sandstone at pressures from 90 to 280 bar and temperatures of $50 - 90$°C. They mentioned that strong CO_2-foam could be generated even at supercritical conditions.

Foams have two phases; gas and liquid (Figure 1.1). The gas phase might be either N_2 or CO_2 and the liquid phase may contain some alternatives such as water, linear gel, cross linker gel or a viscoelastic surfactant. It must be taken into account that CO_2 has a higher solubility than N_2 and consequently could outperform N_2 in most cases. Each system has its advantages and its physical limitations. Moreover, most foam requires either a foaming agent or a cross linker to maintain the foam structure and prevent phase separation.

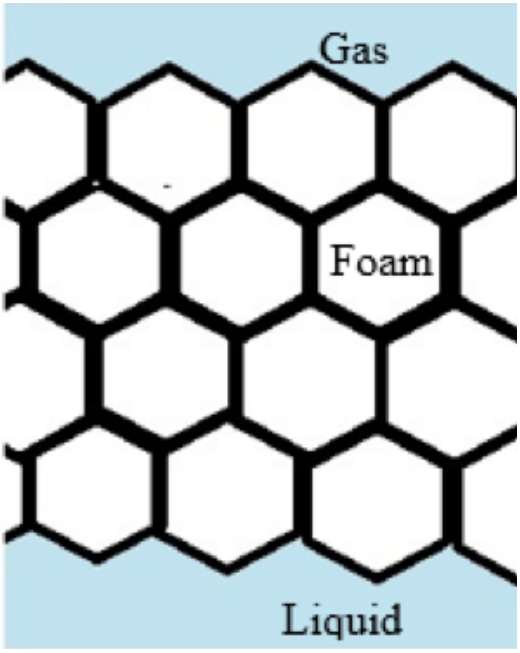

Figure 1.1: Illustration of foam structure.

1.1 Foam Characteristics

Injecting gas bubbles into a liquid can generate a foaming structure with a rate at which the injected liquid trapped between bubbles cannot drain away. A self-explanatory scheme is depicted in (Figure 1.2). describing the most important terminology of a foam system. Lamella defines as a thin liquid film that separates the gas phases from each other. As is shown in the schematic foaming structure bellow, the foam bubbles tend to form a connected network with an angle of 120 at junction points called the Plateau border [11]. It has been reported in literature that lamellae drive mobility reduction owing to the dominant interactions between pore walls and lamellae that govern foam flow behavior. There are two distinct types of foam with respect to the geometry and shape of bubbles referred to as wet-foam and dry-foam. Compact structures of accumulated spherical shape foam bubbles detached by rather thick layers of liquid generate a wet-foam structure while

dry-foam is known as a connected network of polyhedral foam bubbles with thin and solid film separators [12].

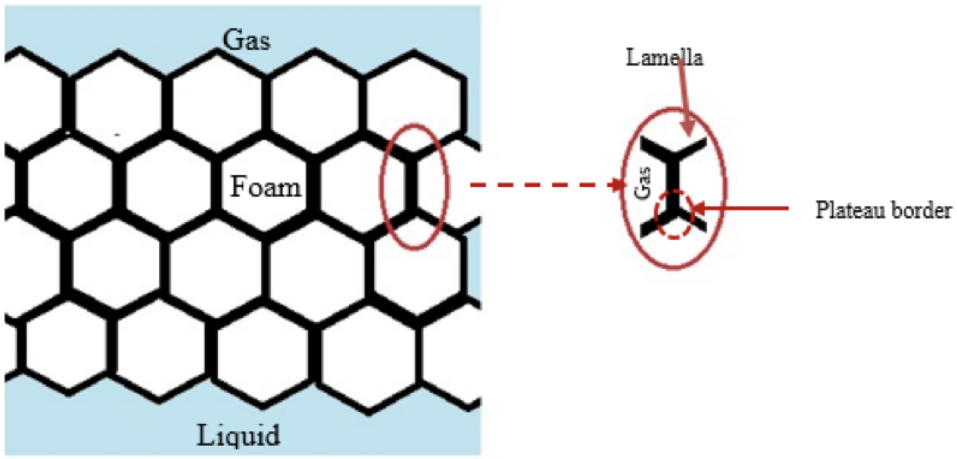

Figure 1.2: Generalized 2D slice of a bulk foam system.

1.2 Foam Quality

One of the most important factors affecting foam behavior is the foam quality [13]. Foam quality is the ratio of gas volume (or gas flow rate) to total liquid and gas volume (or total flow foam rate) shown in Eq.1.1:

$$f_g = \frac{q_{gas}}{q_{liquid} + q_{gas}} \tag{1.1}$$

where; f_g is the foam quality, q_{gas} is the gas flow rate and $q_{liquid}$is the liquid flow rate [14].

The size of foam bubbles significantly affects foam quality and foam stability. The larger the foam bubbles become, the less stable the foam will be which technically translate to lower quality foam [12].

The objective of this work is to investigate the effects of reservoir temperature, pressure, surfactant type, and salt concentrations on the CMC value of the AOS solution with and without nanoparticle in solution. The pendant drop method was employed to measure the surface tension between gas and solution. The pendant drop method is utilized to measure gas/liquid interfacial tension (IFT) at high-pressure and high-temperature conditions. Pendant drop method uses the balance between buoyancy and gravitational forces to measure IFT. A liquid drop is generated at the bottom of a gas immersed capillary tube or column which the liquid drop shape is governed by how the gravitational and buoyancy forces are balanced.

Young-Laplace equation explains the difference in pressure of the inside and outside of a curved liquid interface (Laplace pressure) using the principal radii of curvature r_i (Eq.1.2):

$$\Delta P = \gamma\left(\frac{1}{r_1} + \frac{1}{r_2}\right) \tag{1.2}$$

Wherein the principal radii of curvature for different planes shown in pendant drop schematic in (Figure 1.3).are denoted by. Further, pressure difference between the inside and outside of the drop and the interfacial tension are denoted with respectively.

For the best effectiveness, surfactants must be used at concentrations above the CMC value.

The aim of second part is to study foam stability in the absence and presence of nanoparticles, polymers, and VES at reservoir conditions and a wide range of parameters including surfactant, salt, and nanoparticle concentrations. Contact angle was measured to obtain an optimal concentration of nanoparticles. This work also highlights the effects of nanoparticle based foams on the foam stability and provides a comprehensive comparison between the nanoparticle foams and the polymer-based foam in terms of their effects on

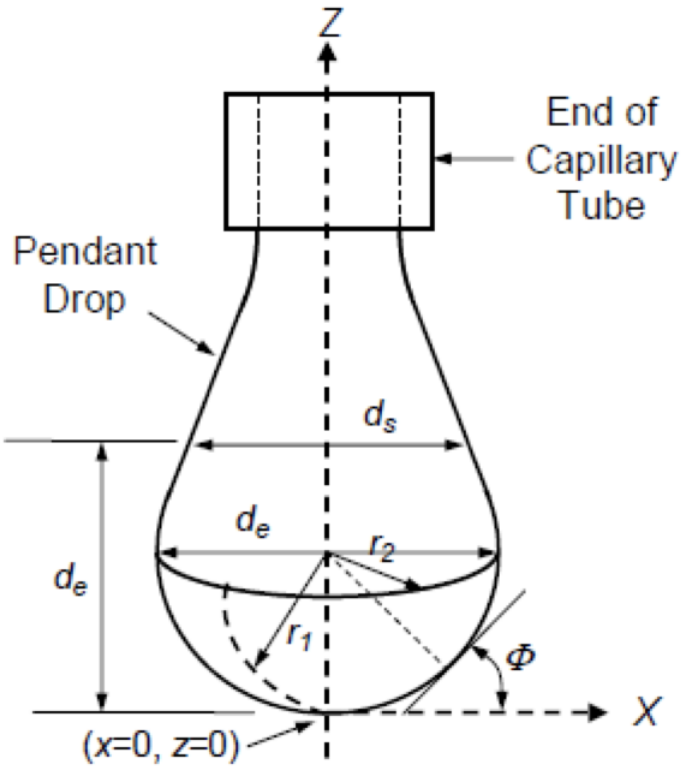

Figure 1.3: Pendant drop geometry [15]

the foam stability at reservoir conditions. The temperature ranged from 75 to 302°F, while the pressure increased from atmospheric up to 800 psi.

Zeta potential is another factor that can affect stability of colloidal dispersion. A high absolute zeta potential values show high stability for nanoparticle suspensions. The lower the values are, the less the repulsion force is comparing to the attraction force, which causes particles start to aggregate.

1.3 Foaming Agent

A foaming agent plays a critical role in forming foam. For instance, surfactant could be a foaming agent in this purpose. Surfactants are a polar compound, consisting of an amphiphilic molecule, with a hydrophobic part and a hydrophilic part (Figure 1.4).

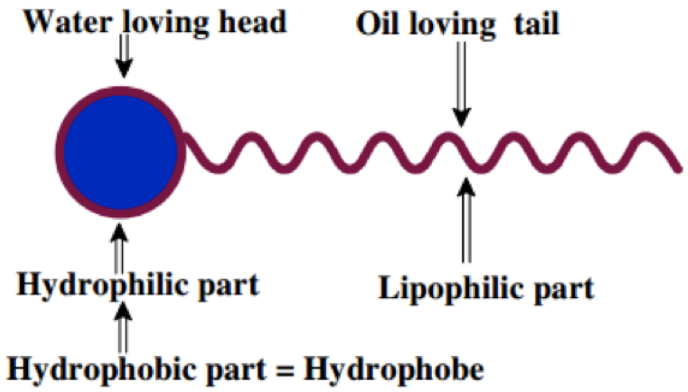

Figure 1.4: Schematic diagram of surface-active molecule [16]

Foaming agent is classified according to the nature of the molecular polar part. Depending upon the nature of molecular polar (or hydrophilic part), the surfactants are categorized as follows: (1) Anionic; (2) Cationic; (3) Amphoteric or Zwitterion; and (4) Nonionic [17]. The first category is distinguished by anionic groups such as phosphates, carboxylates, sulfonates, and sulphates attached to their head. The second class of surfactants is determined with cationic groups like pyridinium and quaternary ammonium salts into their structures. Amphoteric category owns cationic and anionic groups including betaine, sultaine and amino acid together. The last class of surfactants like glucoside and ethoxylated alcohol/glycols contains no function group in their structure.

Surfactants not only increase liquid viscosity but also can reduce the surface tension of a liquid, and the IFT between liquid/gas which helps to significantly increase oil recovery [18]. The difference in pressure through the boundary of two immiscible fluids or between the wetting and non-wetting phases is described as capillary pressure (Eq.1.3). Brine is usually the wetting phase and thus oil is the non-wetting phase in a brine and oil systems [19].

$$p_c = \frac{2\gamma \cos\theta}{r} \tag{1.3}$$

where; p_c is capillary pressure, γ is the IFT between the two fluids; θ is the contact angle and r is the effective radius of the interface.

A surfactant like zwitterionic surfactant is used as the cleanest version of a foamed system which means it contains no formation damage solids [20, 21].

The selection of foaming agents depends on the type of gas that generates foam. Anionic and nonionic surfactants with a relatively high number of hydrophilic ethylene oxide groups are used to generate CO_2-foam. Most previous studies have used a nonionic surfactant as a foaming agent to generate CO_2-foam. The cloud point is very important for this surfactant.[22] mentioned that these surfactants should be employed at temperatures below their cloud point. A common surfactant used in several research studies [23, 24] is ChaserTM CD1045 (CD). A combination of different types of surfactants exhibit better foaming properties than those of individual components. However, these surfactants tend to have a poor performance in high salinity reservoir conditions.

Unlike the normal behavior of surfactant dilute concentration as an electrolyte in aqueous solution, at higher concentrations surfactant express a significantly dissimilar behavior. Formation of organized molecules aggregates, also known as micelles, justify such a strange behavior of surfactant (Figure 1.5).

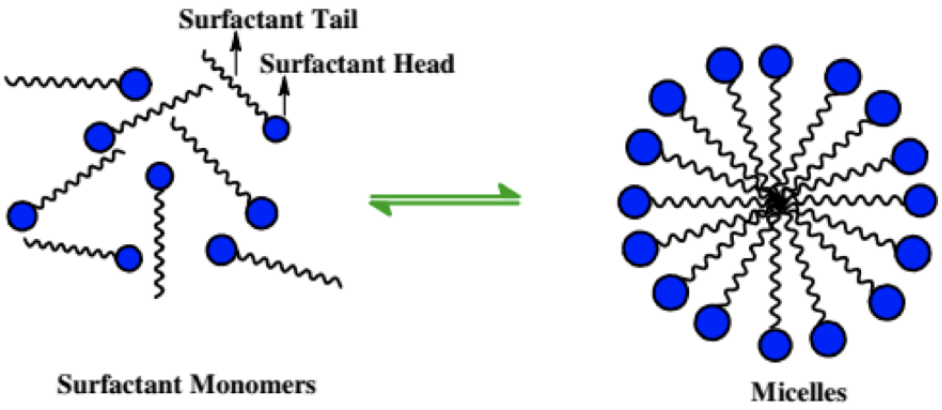

Figure 1.5: Schematic illustration of the reversible monomer-micelle thermodynamic equilibrium [16].

The concentration at which micelle formation becomes significant is called the critical micelle concentration (CMC) (Figure 1.6). A lower CMC value is produced by increasing the molecular mass of the lipophilic part of the molecule, lowering the temperature (commonly), and adding electrolyte (commonly).

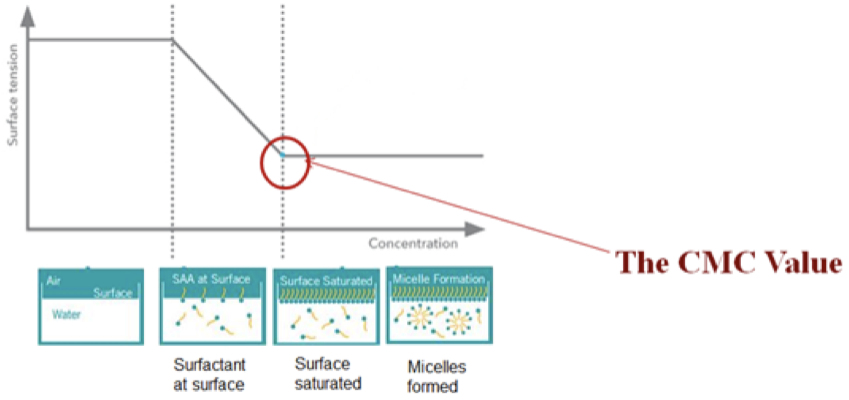

Figure 1.6: The mechanism of surface tension based on surfactant concentration [25].

[7] and [26] reported that above the CMC value, surfactant can transport nanoparticles. In practice, to attain full nanoparticle displacement at the interface and thus preventing nanoparticle emulsions, surfactant concentration is kept above the CMC value.

Commercial surfactants have been utilized in research studies for CO_2-foam generation. In addition to CD, various types of water soluble anionic olefins sulfonates (AOS) have been used as an excellent foam agent for the generation of different foams in the EOR process. Other examples of surfactant which were used in lab or pilot scale are summarized in Table 1.1 (adapted from references).

Foam Agent	Chemical Description	Surfactant Type
Chaser GR-1080	40% active aqueous solution of alpha olefin sulphonates of proprietary	-
PEN-5	Octyl ethoxylated alchohol	Nonionic
Bio-Terge As-40	C_{14-16} sodium olefin sulfonate	Anionic
AOS	C_{14-16} alpha olefin sulfonate	Anionic
Triton x -100	Octylphenol	Nonionic
Dow XSS-84321.05	Mixture of C10 diphenyletherdisulfonate and C_{14-16} AOS	Anionic
Tertigol TMN 6 (10% water)	Dodecyl Tergitol	Nonionic
Surfonic, OP-100	Octylphenol	Nonionic
Surfonic, N-Series	Nonylphenol	Nonionic
Surfonic, TDA-Series	Tridecyl alcohol ethoxylatetes with multiple methyl	Nonionic
Surfonic, L12-8	The 8 mol ethoxylates of linear, primary C10-12 alcohol	Nonionic
Empilan KR-8	Ethoxylate of an Îś-methyl C_{9-11} alchohol	Nonionic
Surfonic, DDP-100, 120	Dodecylphenol	Nonionic
XOF-315, 318	Di (branched nonyl) phenol ethoxylate	Nonionic
XOF-700	Di (branched nonyl) phenol ethoxylate	Nonionic
TSP (XOF-501)	Tristyrylphenol ethoxylates	Nonionic
Lutensol OP-10	Octylphenol	Nonionic
Lutensol XP-70, 80	Alkyl polyethylene glycol ethers based on C_10âĂŞGuerbet alcohol and ethylene oxide	Nonionic
Lutensol TO-8, 10	Iso C_13 oxoalcohol ethoxylates and 8 or 10 EO groups	Nonionic
Lutensol AO-8,11	Alcohol ethoxylate	Nonionic
Enordet X-2001	Alcohol ethoxyglycerylsulfonate	Nonionic
FC-4434	Mixture of AOS and polymeric fluorocarbon esther	Nonionic
Fluorad FC-751	Fluoro alkylsulfobetaine	Nonionic
Rhodapex CD-128	Ammonium alky ether sulfate	Nonionic
SDS	Sodium dodecyl sulfate	Anionic
CTAB	Cetyl trimethylammonium bromide	Cationic
Enordet IOS	Sodium (C_{15-18}) internal olefin sulfonate	Anionic
NG-VES	Composed of a zwitterionic surfactant	Zwitterionic
Alipal CD-128	Sulfate-ester-type (ammonium sulfate ester)	Anionic
Witcolate 259,1276	Alcohol ether sulfate	Anionic

Table 1.1: Common surfactants to form foam.

AOS surfactants are selected as foam stabilizer in this study because they have a lower

adsorption values due to repulsion forces between negative charges of sandstone. AOS surfactants offer remarkable characteristics such as foamability, excellent detergency, and high compatibility with hard water and particularly in contact with CO_2 in a partially oil-saturated porous medium. Owing to such properties, AOS surfactants become the agent of choice in many CO_2-foam applications [27, 28, 29]. AOS has been used in several successful field applications as well [9, 28].

1.4 Viscoelastic Surfactants

Before the wide application of VES as viscosifier, polymers were the only choice of the oil and gas industry. The first ever application of VES to increase fluid viscosity was introduced in 1986 [30]. Other than a simple viscosifier, the primary characteristic of the surfactant was retained as the VES also functionalized to create foams. VES have been employed in both N_2 and CO_2-foams as well as polymers to stabilize foam. The VES foams minimize the interfacial tension and the amount of water used in the system, which make them a choice of interest for ultra-tight gas reservoirs and coalbed methane wells that contain water. Furthermore, no polymer residue damage will be initiated due to the ability of the VES foams to control leak off into the cleats. However, viscosity loss control over time using breakers results in damage to packs [31]. Moreover, gas mobility decreases dramatically due to migration of surfactant systems to the matrix at the fracture face. This requires using extra chemicals in order to improve water mobility and gas permeability to avoid liquid trapping at the fracture faces [21].

1.5 Polymers

Foam used during petroleum recovery operations requires stabilizers to migrate quickly to the gas/liquid interface to form a boundary around the bubbles that make up the foam. One major concern when using foams for EOR purposes is foam stability over time. To address this concern and to improve foam stability, various types of stabilizers such as poly-

mers are added to the solutions [32, 33, 34]. Enormous union of replicates of monomers constructs large molecules of polymers. Polymer foams tends to be unstable due to low adsorption rate of large polymer molecule to the bubble surface [35]. Adding water soluble polymers to the foaming solution enhances the viscosity of the solution which also supplies mobility control of chemical flood. Extensive studies have been conducted on the applications of the polymer-surfactant solutions to control the stability of the colloidal systems along with the rheological properties of the solutions in EOR projects [36, 37].

Partially hydrolyzed polyacrylamide polymer (HPAM) is widely used to stabilize foams in EOR practices (Figure 1.7). Reacting polyacrylamide with a base transforms amide groups ($CONH_2$) to carboxyl groups (COO-), which results in a decline in adsorption and produces HPAM. The conversion of amide groups to carboxyl groups leads to interactions between negative carboxyl groups and the polymer chains of HPAM which can highly influences the rheological properties of the polymer solution with respect to salinity of the brine.

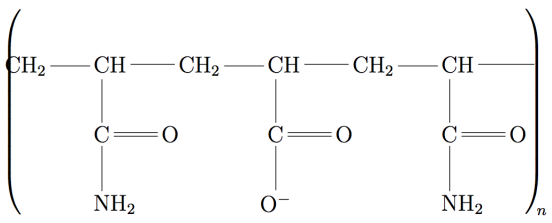

Figure 1.7: Molecular structure of partially hydrolyzed polyacrylamide [38].

[39] showed that using HPAM and AOS could reduce gas mobility and improve the stability of foam. [40] studied a micro model of polymer-enhanced foam flow into porous media. They used AOS foaming agent with polyacrylamides. Their results indicated that capillary pressure and coalescence do not govern polymer-enhanced foam flow in porous

media as they do for conventional foams. [41] also used HPAM polymer and two different surfactants to measure foam mobility for sandstone reservoirs. Solutions of HPAM and AOS can reduce gas mobility and improve the foam stability. Previous research has shown that charges of polymer and surfactant play a key role in stabilizing foam [41, 42, 39, 43]. Previous results also proposed that a mixture of anionic surfactant (sodium dodecyl sulfate (SDS)) and a cationic polymer (polyvinylamine (PVAm)) improves foam stability, but not foamability [44]. Researchers have reported a drop in foamability in these formulations, compared to the surfactant solutions alone [35, 45].

1.6 Nanoparticles

Temperature and salinity cause polymer to lose most of its viscosity-enhancing function. Hence, employing polymer at high temperature and salinity can be another main concern [46]. Once polymer is used in the aqueous phase, the formation might be damaged, because polymer concentration can reach 10 to 15 times the initial polymer concentration. Although, using a breaker is a common way to address this issue, a large portion of the polymer will still be retained in the formation, which can exacerbate formation damage [47].

Nanoparticles can be combined with polymers to improve foam stability with less formation damage in numerous applications such as CO_2 sequestration and EOR [4, 5]. Recent studies have shown that even a small number of nanoparticles can increase foam stability in foams with polymer or surfactant [48]. Silica nanoparticles (SiO_2) and a surfactant can produce stable foam together at a specific surfactant concentration [49]. Foam stabilized by SiO_2 and sodium dodecylbenzenesulfonate (SDBS) or nanoparticles and SDS have been investigated as potential fracturing fluids [50, 51]. Several experiments have been done using cationic and nonionic surfactants with nanoparticles at ambient temperature to assess the performance and the effects of the nanoparticles on the foamability and

foam stability [52, 53]. At proper surfactant concentration and contact angles, nanoparticles are adsorbed onto the gas-liquid interface, and, thus, foam stability can be improved. The surfactant-based solutions' behavior differs completely from that of solutions containing nanoparticles because surfactants actively adsorb and leave the interface, which causes foam bubbles to decay [49, 54].

Recent developments in nanotechnology grant better established techniques to generate and stabilize the CO_2-foam for months or even years. In fact, nanoparticles could increase the foam stability more than surfactants and polymers [5, 4]. The reason is that nanoparticles are not modified based on polymer chain or surfactant chemical structure to deliver stability [7]. It has been indicated that a mixture of silica nanoparticle and surfactant under desirable conditions can generate more stable foams [49]. The irreversible nanoparticle adsorption onto the interface between gas and liquid phases leads to a higher stability. Surfactants can dynamically adsorb to and desorb from two-phase interfaces [13]. Unlike surfactant molecules, the nanoparticles adsorption at gas/liquid interface is usually irreversible. Nanoparticles can also minimize contact area between the two phases. Therefore, they can form a strict barrier that prevents droplet coalescence. Consequently, the involved adsorption energy to move nanoparticles to the bubble interfaces is noticeably large due to the created strict barrier to coalescence. As a matter of fact, the stronger the particle detachment energy is, the more force is necessary to interrupt layers between particles and to make coalescence occur [55].

Contact angle of particles at the interface can explain the interaction between bubbles and particles through the hydrophobicity and hydrophilicity of the particles. One may note that high concentrations of nanoparticles do not always guarantee the formation of stable foam. Ultimately, the deciding factor is the detachment energy, not the nanoparticle concentration. One of the most significant parameters known to have a strong effect on the detachment energy is contact angle [56, 7, 57]. However, minimal work has been

performed to measure contact angle and evaluate its relation to the detachment energy of nanoparticles in EOR literature. In the present work, contact angle measurements are utilized to determine the optimum nanoparticle concentration.

Yu and Espinoza demonstrated in their works [5, 4] that the supercritical CO_2-foams are stabilized with nanoparticle concentrations as low as 0.05 wt%, and foam stabilized at high salinity using high particle concentrations. CO_2-in-water foams were shown to be effectively produced and stay stable using stabilizers such as fumed silica in a column packed with 180 mum glass beads [7]. They showed that foams made by nanoparticles are stable over a long period of time compared to foams stabilized by surfactant molecules.

[5] also showed that surfactants can improve CO_2-foam generation in the presence of nanoparticles. [57] have conducted several experiments using cationic and nonionic surfactants with nanoparticles at ambient temperature. [53] and [52] also studied the mixture of silica nanoparticles and cationic surfactant, hexadecyltrimethylammonium bromide (CTAB), to form foam. They hypothesized that the particle surface changed from hydrophilic to hydrophobic by cationic surfactant CTAB adsorption and would be more hydrophobic with a CTAB concentration increase [53, 52]. [58] investigated two important parameters, the foam stability and the foam durability, for CO_2-foam and AOS solution in the absence and presence of nanoparticles at constant pressure and ambient temperature. All previous work observed that the choice of surfactant and nanoparticle concentrations plays a critical role for having more stable foam.

1.7 Brine

The selection of brine depends on the type of surfactant. Most previous works used NaCl for AOS surfactants to generate foam [59, 10, 29]. Also, NaCl and deionized water (DI) water are selected to make brine because their resulted foam, generated by AOS, is more stable compared to other brine such as KI brine.

2. EXPERIMENTAL STUDY

The objective of the experimental work is to verify the design methodology explained in the previous chapter. This will be done by experimentally identifying the optimum surfactant and nanoparticle concentrations for different temperature, pressure and salt concentrations.

2.1 Material

2.1.1 Surfactant

Anionic alpha-olefin sulfonate (AOS) surfactant is used to prepare the solution for the experiments. The general structure of olefin surfactants is R-$SO_3^-Na^+$ [28], where (R) represents the hydrophobic group (Figure 2.1). In this study, the number of carbon atoms in the surfactant structure is 14-16 with a molecular weight of 315 g/mole, which as supplied by a local chemical company as a solution containing 40 wt% active aqueous solutions.

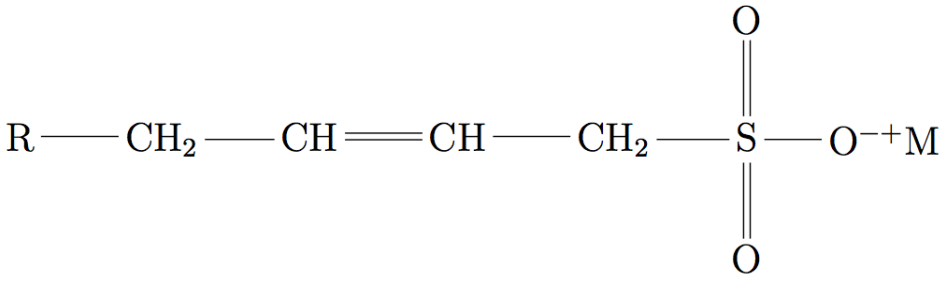

Figure 2.1: Molecular structure of AOS.

2.1.2 Brine

The surfactant solutions were prepared using brine containing 1 to 10 wt% NaCl in de-ionized water at a surfactant concentration in the range of 0.005 to 1 wt%.

2.1.3 Gas

CO_2 gas with a purity of 99.99 mol% was used to pressurize the system and form a droplet to measure the surface tension between gas and AOS solutions.

2.1.4 Nanoparticles

Silica nanoparticles (SiO_2) of sizes 100 and 140 nm were supplied by a chemical company. Iron oxide (Fe_2O_3) of less than 50 nm was obtained from Sigma-Aldrich Company. To prepare the solution in the presence of nanoparticles, the desired AOS concentration was added to the brine. Then, silica nanoparticles at three concentrations (0.1, 0.2, and 0.3 wt%) were added to the AOS solution. This solution and nanoparticles were then stirred moderately with a magnetic stirrer for 2 hours. These solutions were used to examine the effect of nanoparticle concentration on stability of foam.

2.1.5 VES

Another set of experiments were done to compare of the foam stability in the presence of nanoparticles versus those prepared using viscoelastic surfactant (VES) as shown VES molecular structure in figure2.2. In the present work, 2 vol% VES was utilized to stabilize foam.

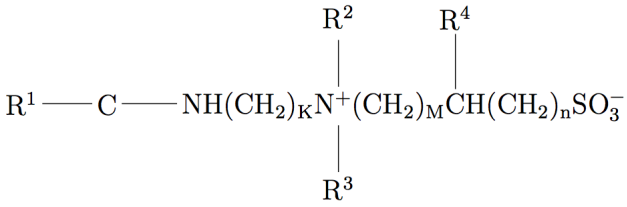

Figure 2.2: Molecular structure of VES [60].

2.1.6 Polymer

The structure of guar resembles that of cellulose, which makes sense as it is derived from plant sources. Guar has historically had uses in the food, textile, drag reduction, and paper industries, and was introduced into the oil industry during the 1960s as a potent viscosifier [61]. In the present work, Guar-gum, 20 ppt (pound per thousand gallon) was used to stabilize foam.

2.1.7 Cores

The cores used were Bandera and Grey Berea sandstone. All cores had a diameter of 1.5 in.in. Berea sandstone cores were used with permeability ranging from 120 to 170 md, and porosity 20%.

2.2 Method and Equipment

2.2.1 Surface Tension

The compositional equilibrium status is a measure of the static surface tension between two immiscible fluids. Although, compositional equilibrium is a common measure of surface tension, many interactions that take place in interface of two immiscible fluids like foaming, injecting surfactant and high-speed wetting cannot reach to the equilibrium and hence exploring dynamic behavior of the system and measuring dynamic surface tension

become of special importance. The surface tension between two immiscible fluid phases is measured by a wide variety of techniques. In this work, drop shape analysis system (DSA) was used to calculate surface tensions between CO_2 gas and different solutions.

(Figure 2.3) shows a schematic diagram illustrating the work flow process and, the equipment for measuring the CO_2/AOS solution surface tension. In these experiments the temperature ranged from ambient conditions to 302°F while the pressure increased from atmospheric up to 435 psi. AOS solutions are prepared using different brine concentrations ranging from 1 to 10 wt% of NaCl and different surfactant concentrations from 0 to 1 wt%.

The system consisted of a stainless steel cylindrical HP/HT cell with two transparent windows, a sample holder inside the chamber to hold the sandstone sample horizontally. A digital image of the drop was obtained via an image data acquisition system. The HP/HT cell was connected to a gas source, a solution accumulator. This piece was connected to a piston high-pressure displacement pump. This pump enabled solution injection to enter into the capillary tube (outside diameter 1/16") that was connected at the top of the cell. To start the experiment for measuring surface tension, the chamber was filled with a mixture of surfactant and brine. The AOS solution was brought to the desired temperature and pressure using a digital temperature controller and CO_2 gas, respectively. At this point, the CO_2 valve at the bottom of the DSA setup was opened. The opened valve allowed CO_2 to flow into the solution inside the chamber through a stainless-steel capillary needle (outside diameter 1/16"). Then, a digital image of the drop was obtained by an image data acquisition system. The accurate interfacial profile of the pendent drop could be achieved by utilizing digital image processing techniques. The pendent drop method is a common technique to determine liquid-liquid or gas-liquid surface tensions from the drop shape that is generated inside a chamber [62, 63]. Finally, the DSA analysis software solves the Laplace equation for capillarity to find the best fit of the numerical interfacial profile to the physical drop.

Interfacial tension versus surfactant concentrations will be plotted. The point that the curve reaches its minimum and starts to be constant is called the CMC.

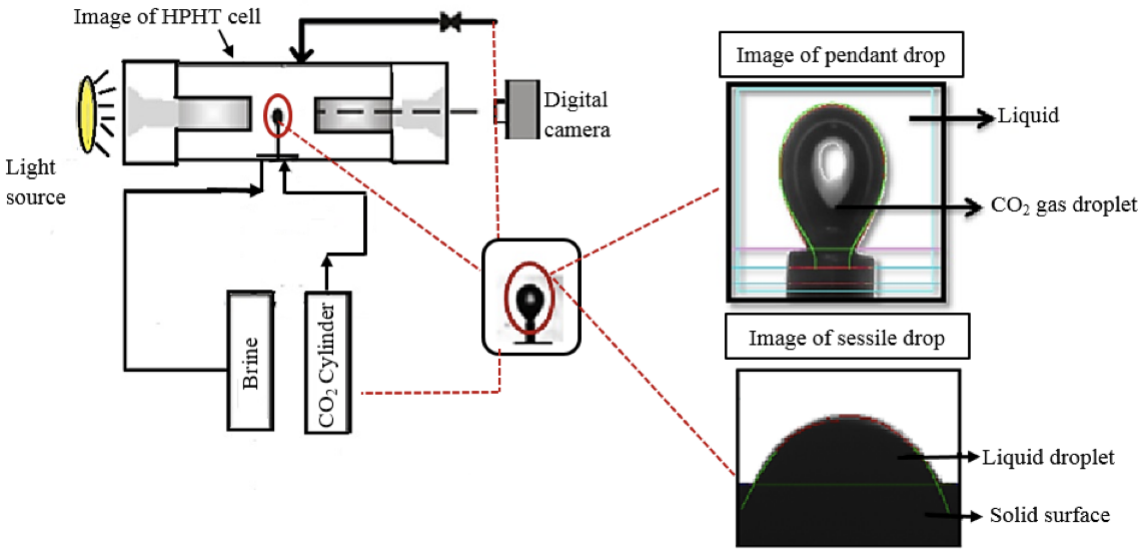

Figure 2.3: A schematic of DSA equipment and setup used in the current experiments. The left panel is the setup for HPHT experiments to measure contact angle and surface tension. The right panel is the focused image of the output of the system.

Determining surface tension requires obtaining liquid and gas densities. The density of the surfactant solution was measured at atmospheric pressure and various temperatures by a Paar model DMA4100 density meter (Figure 2.4).

Figure 2.4: A photo of density meter used to study liquid density.

Similarly, CO_2 density as a function of temperature at various pressures is shown in (Figure 2.5) [64, 65].

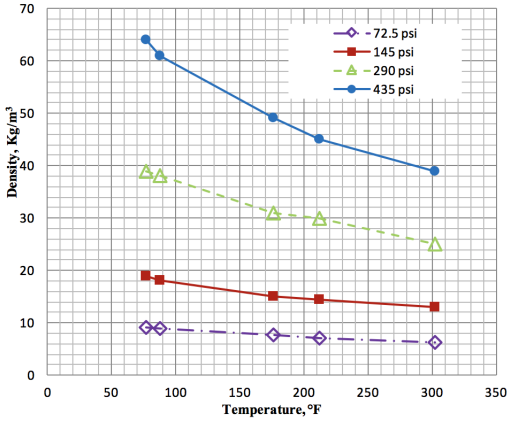

Figure 2.5: Density of CO_2 gas as a function of temperature and pressures.

2.2.2 Contact Angle

The way in which the nanoparticles interact with the bubbles can be predicted by the hydrophobicity and hydrophilicity of the particles, which is described by the contact angle between the particles and the interface. High concentrations of nanoparticles do not always guarantee the formation of a stable foam. Ultimately, the deciding factor is the detachment energy, not the nanoparticle concentration. One of the key parameters to impact the detachment energy is the contact angle [56, 7, 57, 66]. However, minimal work has been performed in order to measure contact angle and evaluate its relationship to the detachment energy of nanoparticles in the EOR literature. In the present work, contact angle measurements were used to determine the optimum nanoparticle concentration.

The energy required to move a particle from the interface to the bulk solution (E) is related to the contact angle (θ) through the aqueous phase, the surface tension (γ), and the particle radius (r) (Eq. 2.1) [55, 4].

$$E = \pi r^2 \gamma_{CO_2-Solution}(1 \pm \cos\theta) \tag{2.1}$$

The sign of the cos (θ) in (Eq. 2.1) becomes negative if the particle is hydrophilic ($\theta <$ 90°), and positive if the particle is hydrophobic ($\theta >$ 90°). Thus, (E) is the energy used to remove the particle from the liquid phase for $\theta <$ 90° or from the CO_2 phase for $\theta >$ 90°. Therefore, the contact angle has a strong effect on the detachment energy. For contact angles between 0 and 30° or between 150 to 180°, the detachment energy is small enough that particles cannot stabilize the foam anymore [55, 67].

The Sessile drop method is a common technique to determine contact angle utilized in the current work to conduct the required analyses. To measure contact angle, the DSA setup was used.

Figure 2.3 also shows a schematic diagram illustrating the equipment and work flow

process employed to measure the CO_2/AOS solution contact angle. Wettability of a solid by a liquid is measured by the concept of contact angle. The contact angle method is used to study the hydrophobicity of the solutions in the presence of nanoparticles. In the present experiments, due to the presence of anionic surfactant, sandstone is utilized as the solid surface base. As discussed previously, to calculate the CMC value, the DSA setup was used. The procedure for measuring the contact angle is similar to that of surface tension. The only difference between the two procedures is that in the process of contact angle measurement, the Berea sandstone sample, i.e., the solid phase, has to be inserted in the chamber using the sample holder. In these experiments, the nanoparticle concentrations ranged from 0.1 to 0.3 wt%. Contact angle of at least 3 drops was determined for each solution.

2.2.3 Rock Samples to Determine Contact Angle

For rock samples, the same procedure with [68] was used. Samples were cut to dimensions of 0.62 in. $\times$ 0.72 in. $\times$ 0.25 in. Then, samples were polished using sand paper (600-mesh and then 300-mesh) to minimize the contact angle hysteresis causes by surface roughness. All samples were loaded into an empty glass flask to apply vacuum for at least 2 hours. At this point, in order to remove the contaminants and surface charges induced by polishing, samples were kept in the formation brine (174 kppm) under vacuum for at least 4 hours. Afterwards, the samples were left in the brine for at least 24 hours. They were then placed in the crude oil and centrifuged at 3000 rpm for 30 minutes to displace the water droplets on the rock surface to keep only the irreducible water.

2.2.4 Foam Stability

In the present work, a high pressure visual cell (HPVC) system is designed to study foam stability and foam texture under the HP/HT conditions. (Figure 2.6) shows a schematic diagram of the CO_2 foam generation apparatus. A piston accumulator is provided for use

of CO_2 as a gas phase. Moreover, a capillary is installed for generating bubbles. Two tongue shaped borosilicate windows that are allocated opposite to each other allowed visualization of main part of the internal volume. The main cell setup consistes of a stainless steel high-pressure part equipped with those two tongue shaped windows for filling with a liquid or a liquid mixture. A stainless-steel capillary needle (outside diameter 1/16") is placed at the bottom of the cell, which is connected to a compressed CO_2 cylinder. The system is pressurized using a CO_2 gas accumulator that has two connections with a compressed CO_2 cylinder and HPVC. The top of the cell is connected to a backpressure regulator which allowed excess gas to flow out after each experiment. Moreover, the cell is heated using a thermocouple. At the end of the experiment, the outlet valve of the observation tube is opened to release CO_2 gas, and the solution was removed. The cell and tube are cleaned with distilled water before the next experiment.

To start the test, the cell was filled with the solution. The AOS solutions were prepared using different brine concentrations ranging from 1 to 10 wt% NaCl and different surfactant concentrations above the CMC value. Then, the system was brought to the desired pressure and temperature using CO_2 gas and a thermocouple. In these experiments, the temperature ranged from 75 to 212°F while the pressure was increased from atmospheric up to 800 psi. At that point, the CO_2 valve at the bottom of cell was opened and allows CO_2 to flow into the solution. Due to the density difference between dense CO_2 gas and the solution, CO_2 bubbles form and move to the top of the cell. In order to study the foam decay, the height of the foam column had to be measured continuously. The foam column formed between the liquid phase at the bottom and the gas phase at the top of the cell. This height had been measured at different times to evaluate the foam stability, as calculated via (Eq. 2.2). The time, when the foam height reduces to half of its initial height, is called the half-life of foam. The stability test was then continued to until the foam completely decayed [69].

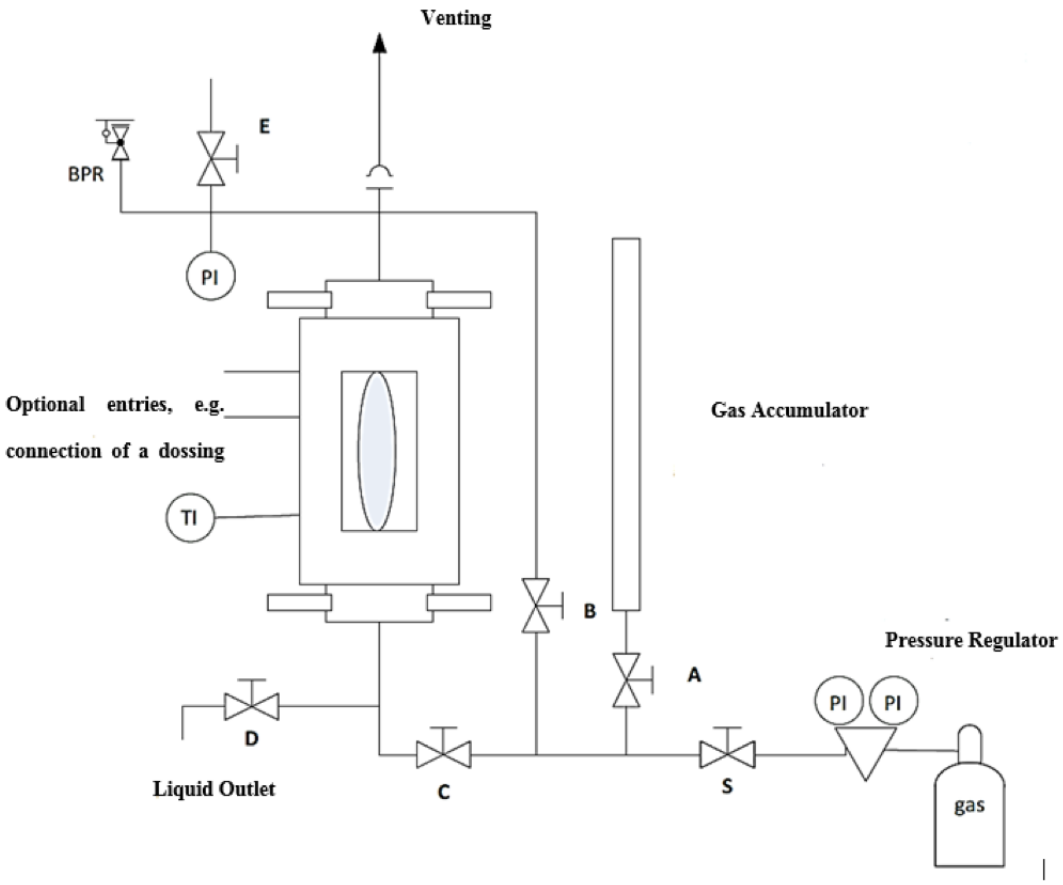

Figure 2.6: A schematic diagram illustrating the work flow process and equipment to measure foam stability. A and B are ball valves, and C, D, and E are needle valves.

$$CO_2 foam stability = 100 - \frac{H_{gas(t)}}{H_{gas(t=0)} + H_{foam(t)}} \times 100 \tag{2.2}$$

where (t) is time, (H_{gas}) is the height in centimeters of the dense CO_2 layer at time, and (H_{foam}) is the initial height of the foam layer, in centimeters (Figure 2.7).

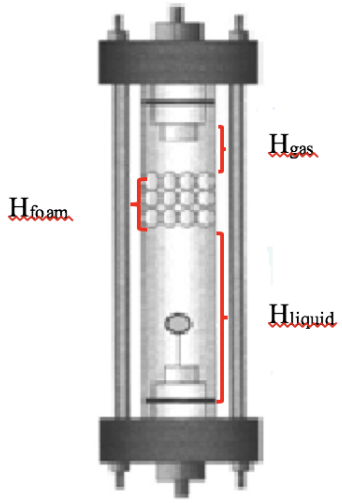

Figure 2.7: Determination of foam stability at HP/HT. Hgas is the height of the dense CO_2 layer at the time, cm, Hliquid is the height of the liquid at the time, and Hfoam is the initial height of the foam layer, cm.

2.2.5 Foam Texture

To study foam texture, which defines the bubble size distribution, and provide better understanding of the relation between foam stability and foam texture, an electron microscope was employed (Figure 2.8). Small spherical bubbles (16-40 μm) indicate a fine foam structure, whereas large and polyhedral bubbles (40-100 μm) characterize coarse foams [70].

Figure 2.8: A photo of microscope used to study foam texture.

2.2.6 Zeta Potential

Zeta potential is another factor can affect stability of colloidal dispersion. A phase-analysis light-scattering (PALS) technique is employed to conduct zeta potential for nanoparticle/solutions interface (Figure 2.9). Zeta potential measurement provides significantly improved results comparing to a traditional electrophoretic light scattering method. Technically speaking, the zeta potential instrument measures electrophoretic mobility in a charged colloidal suspension system and consists of palladium coated electrodes and He-Ne laser which functions as the light source with an overall accuracy of $\pm$ 2% [68].

High repulsion force remarkably enhances foam stability in the system. In fact, the higher the absolute value of zeta potential is, the lower the attraction force will be that leads to a higher repulsion force. Conversely, low zeta potential value of a suspension indicates

that the attraction force is greater than repulsion force and thus particle aggregation can occur.

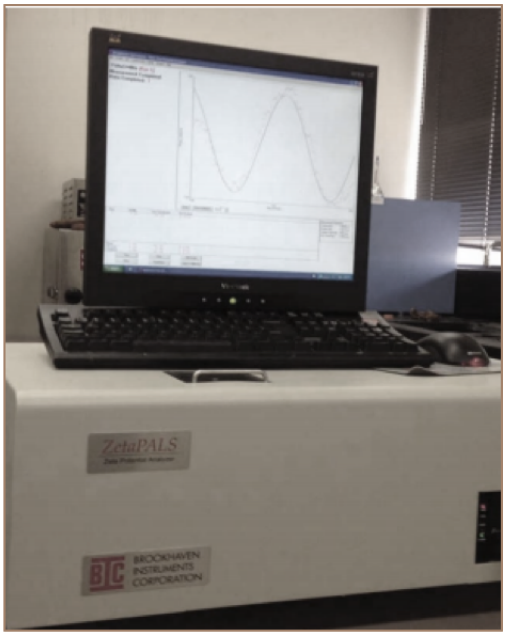

Figure 2.9: A photo of the ZetaPals setup used to measure the zeta potential.

2.2.7 Coreflood

The capacity to reduce the gas/liquid mobility during the injection of foam into a porous media is known as foam blocking ability and hence the larger the blocking ability is, the more stable the foam would be. Mobility reduction factor (MRF) is used as an index to indicate foam blocking ability and stability in the present work. Therefore, performing coreflood experiments in order to obtain mobility reduction factor is of special importance in this dissertation.

(Figure 2.10) shows a schematic diagram of the coreflood setup used. Two stainless-steel piston accumulators with a capacity of two liters each were used to store the synthetic

brine, and the solutions (2). A one-liter accumulator was used to store the CO_2 (1), and was attached to a CO_2 cylinder (8). A syringe pump (7) was used to displace the solutions from the piston accumulators. Valves (v1, v3) was installed at the accumulators outlet to control the fluids alternating during the injection. To monitor the pressure at the core inlet, a pressure gauge was installed at the coreholder inlet (G1). A hassler type core holder (3) was used to hold the core during the coreflood test. The coreholder was installed in an oven (11) that can be used to increase the system temperature. A backpressure regulator (10) was installed at the core outlet to maintain the outlet pressure. It was adjusted by a nitrogen cylinder (9). A hand pump (6) was used to apply overburden pressure around the core. A pressure transducer (4) was used to measure the pressure drop across the core and send the measurement to a data acquisition system (5) to a computer that records the data through LabVIEW software.

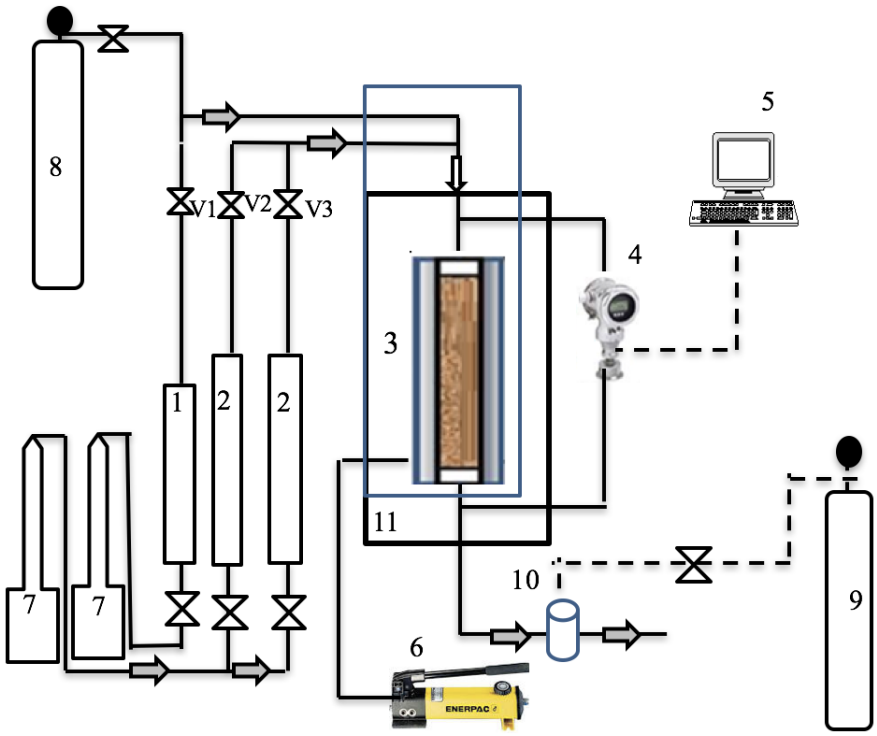

Figure 2.10: Schematic for coreflood setup, where 1 = CO_2 accumulator, 2 = brine and solution accumulators, 3 = Core Holder, 4 = Pressure Transducer, 5 = PC Recorder, 6 = hand pump for overburden pressure, 7 = syringe pump, 8 = CO_2 cylinder, 9 = N_2 cylinder, 10 = Back pressure regulator, 11 = Oven.

Eleven cylindrical Buff Berea sandstone cores were drilled with dimensions of 6 in. $\times$ 1.5 in. The cores were dried in an oven for four hours at 150°F, and then the dry core weight was measured. The cores were saturated under vacuum for four hours with 5 wt% NaCl brine, and then the weight of the saturated cores was measured. The pore volume was calculated from the brine density and weight difference in both the dry and saturated cases. The cores were scanned with a CT-scanner in both dried and saturated cases. Then,

the cores were kept in the brine until it was time to run the experiment.

Each core was placed inside the coreholder; the back pressure was set at 700 psi, and the overburden pressure was set 300 psi above the injection pressure. 5 wt% NaCl brine was injected at 2 cm^3/min. The pressure drop across the core was monitored, and the stabilization pressure was used to calculate the permeability, using Darcy equation for linear and laminar flow. A baseline pressure drop value was measured by CO_2 coinjection with the brine with the same ratios for the foam solutions (quality = 80%). Next the baseline pressure drop was monitored for 6-10 pore volumes (PV), which is represented by Δp_g in (Eq. 2.3).

The injection of CO_2 and the NaCl brine was switched to solution injection. The solution was injected for two pore volumes to satisfy the adsorption requirements for the rock. Finally, the solution and CO_2 were coinjected into the core and the pressure drop across the core was monitored for 6-10 pore volumes, which is represented by in following equation (Eq. 2.3).

$$\begin{aligned} MRF &= \frac{\mu_f}{\mu_g} \\ &= \frac{\left[\frac{kA\Delta P}{qL}\right]_f}{\left[\frac{kA\Delta P}{qL}\right]_g} \\ &= \frac{\Delta P_f}{\Delta P_g} \end{aligned} \tag{2.3}$$

where; Q is the flow rate, k is the absolute core permeability, A is the cross-section area for the core, L is the core length, μ is the viscosity, and is the pressure drop across the core, and the subscripts "f" and "g" represent the experiment with and without foam, respectively.

The ratio of the total mobility of CO_2/brine to the foam mobility defines the MRF which escalates with foam life. High mobility reduction factor describes a more stable foam with stronger resistance to flow. Therefore, mobility is considered the key characteristic in flow behavior and displacement efficiency of foam during the coreflooding process. Using CO_2-foam for mobility control was first proposed by Bond and Holbrook in 1958 [71]. It has been proven that the addition of surfactants aid in the generation of foam wherever the CO_2 flows, especially if they are partially CO_2 soluble. The apparent foam viscosity can be calculated by comparing the pressure drop across the core during foam injection to the pressure drop measured at gas only [71].

Table 2.1 shows the experimental design and physical properties of the cores to investigate the effect of nanoparticles and polymer on the foam stability and on the MRF. Initially and final permeability was measured for each of the core sample before and after foam injection.

Case	Length, in.	Diameter, in.	Permeability, md	PV, in^3	solution	Temperature, °F
1	6	1.5	164	2.12	AOS	77
2	6	1.5	156	2.12	AOS + SiO_2	77
3	6	1.5	160	2.03	AOS + guar-gum	77
4	6	1.5	100	2.12	guar-gum	77
5	6	1.5	160	2.03	AOS + guar-gum + SiO_2	77
6	6	1.5	110	2.03	AOS	140
7	6	1.5	110	2.03	AOS + SiO_2	140
8	6	1.5	113	2.03	AOS + guar-gum	140
9	6	1.5	120	2.03	AOS	250
10	6	1.5	145	2.03	AOS + SiO_2	250
11	6	1.5	160	2.03	AOS + guar-gum	250
12	6	1.5	170	2.03	AOS + guar-gum + SiO_2	250

Table 2.1: Physical properties of sandstone core and detailed information of the chemical used.

Cores were dried in the oven at 250°F for 12 hours and the dry weight of the cores was measured. Then cores were saturated with 5 wt% NaCl under vaccum. The weight of the

saturated core was obtained after the measurement of the initial permeability to ensure that the core is completely saturated. The difference between the dry weight and the weight of the saturated cores was used to calculate the porosity of the cores (Eq. 2.4).

$$V_p = \frac{W_{wet} - W_{dry}}{\rho} \tag{2.4}$$

where; is pore volume (cm^3), and is brine density (g/cm^3). Initial and final permeability measurements were performed seperately from the foam injection. Permeability was measured at room temperature by injecting a 5 wt% NaCl. Darcy's equation for laminar flow was used for the permeability calculation by (Eq. 2.5).

$$k = 122.8\frac{ql\mu}{\Delta P d^2} \tag{2.5}$$

where; k is permeability (md), L is core length (in.), d is the core diameter (in.), q is flow rate (cm^3/min), Îij is dynamic viscosity (cp), and is the pressure drop across the core (psi).

3. EXPERIMENTAL RESULTS[1]

3.1 Surface Tension Measurement

Since, it was found that the surface tension decreased with time, the measurements were carried out until equilibrium was established. Due to mass transfer between CO_2 and AOS solutions at the interface, the drop started to shrink in size. Consequently, the drop size was getting smaller and smaller until both phases were saturated and achieve a stable thermodynamic equilibrium which resulted in a constant drop in volume without any shrinkage. Thus, to generate a stable thermodynamic equilibrium, more CO_2 should be injected into the chamber. The process of injecting CO_2 to reach a constant drop volume of CO_2 in the AOS solution usually took around 2 hours, depending on various factors such as temperature, pressure, salt, and surfactant concentrations. (Figure 3.1) shows the surface tension against time and the bubble volume for the very end of each experiment after the solution was saturated by CO_2.

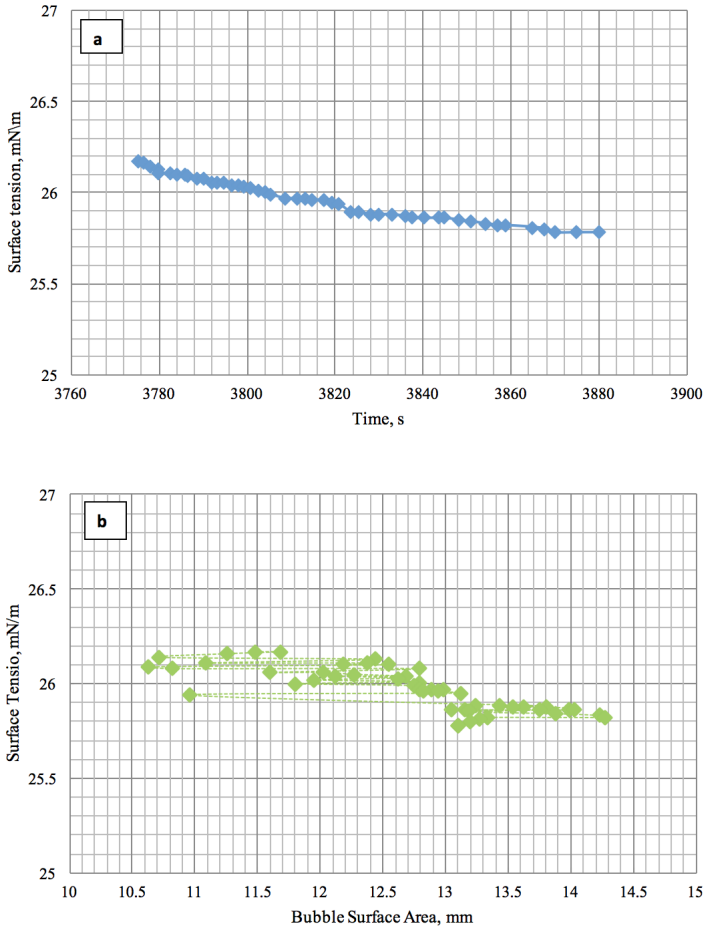

Figure 3.1: The surface tension of CO_2/AOS solution as a function of (a) time and (b) bubble surface area (0.1 wt% of AOS at 176°F and 73 psi).

3.1.1 Effect of Surfactant Concentration, Temperature and Pressure on Surface Tension and the CMC of AOS

AOS surfactant with various concentrations was mixed with NaCl in concentrations of 1 to 10 wt%. As a rule, surfactants normally decrease the surface tension between CO_2/solution. Figure 3.2 presents the results of measuring surface tension between surfactant and CO_2 gas as a function of surfactant concentration for various pressures and

temperatures. As can be seen in Figure 3.2, the surface tension decreased with surfactant concentration and then it became constant. Technically, after this point, the surface tension no longer decreases as surfactant concentration increases. This concentration, at which the interfacial properties between surfactant and CO_2 show no significant changes, is referred to as the CMC value. For instance, the CMC value of an AOS solution is determined to be 0.025 wt% at ambient temperature and 1 wt% of NaCl.

The dependence of surface tension on temperature is more complex than that on either pressure or salinity. Surface tension decreases with temperature at first, and then it increases with temperature. Temperature affects the solubility and interaction energies of hydrophobes and head groups in aqueous solutions. As one can see from the results, temperature as a factor has more effect on surface tension at high surfactant concentrations. The surface tension had a decreasing trend for temperatures below 212°F and had an increasing trend as temperature increased beyond 212°F. As a matter of fact, since molecular adsorption onto the solution can be promoted at temperatures below 212°F, surface tension decreases as temperature increases up to 212°F. For temperatures, greater than 212°F, the surface tension trend is increased. This might be because of the solution phase. The, CO_2 solubility in the solution decreases with increasing temperature which results in an increasing behavior in the surface tension trend when temperature increased above 212°F.

Figure 3.3 shows the CMC value trend of the AOS solution as an ionic surfactant. High temperature not only decreases hydration of the hydrophilic group, which favors micellization, but also disrupts the structured water surrounding the hydrophobic group that disfavors micellization. These two opposing facts can determine whether the CMC value increases or decreases over a particular temperature range. From Figure 3.3, the minimum in the CMC value curve as a function of temperature appears to be around ambient temperature (77°F) for the CO_2/AOS solution.

To investigate the effect of pressure on surface tension and the CMC value, different

pressures were used to measure surface tension. Figure 3.2 also shows the effect of pressure on the CMC value. During the experiment, no effect of pressure for the CMC value was found, however, the surface tension of the CO_2/AOS solution decreases as pressure increases (Figure 3.2). This is because the CO_2 solubility in solution increases as pressure increases.

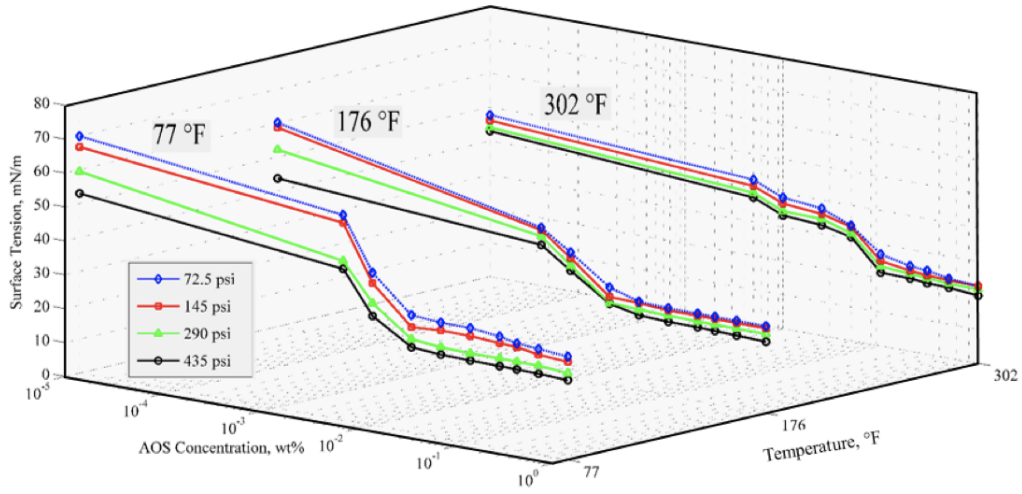

Figure 3.2: Surface tension as a function of surfactant concentration at 1 wt% salinity at various pressures and temperatures.

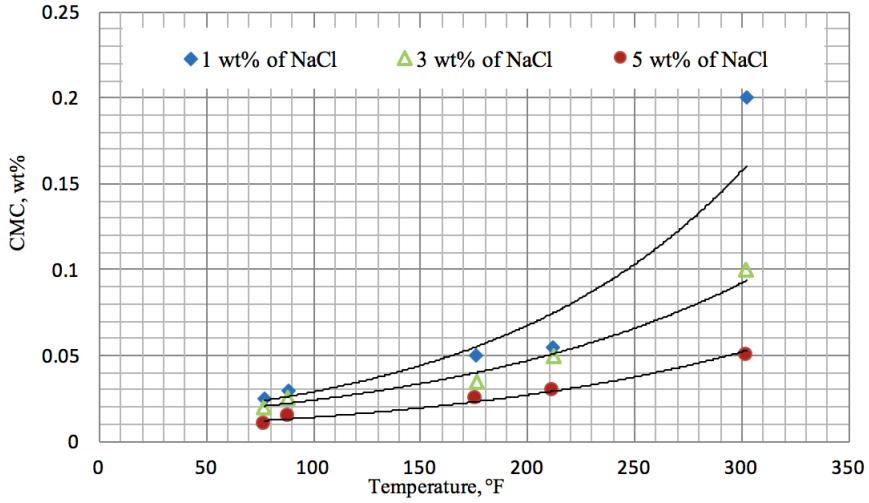

Figure 3.3: A comparison of the CMC value as a function of temperature for 1, 3 and 5 wt% of NaCl.

3.1.2 Effect of Salt Concentration on Surface Tension and the CMC of AOS

Since pressure does not affect the CMC value, the effect of brine salinity on the CO_2/AOS solution surface tension has been studied at 435 psi for different concentrations of NaCl solutions. AOS surfactants become less soluble in brines with more than 5 wt% of NaCl. Therefore, the CMC value of the AOS surfactant could not be determined in these experiments (Figure 3.4).

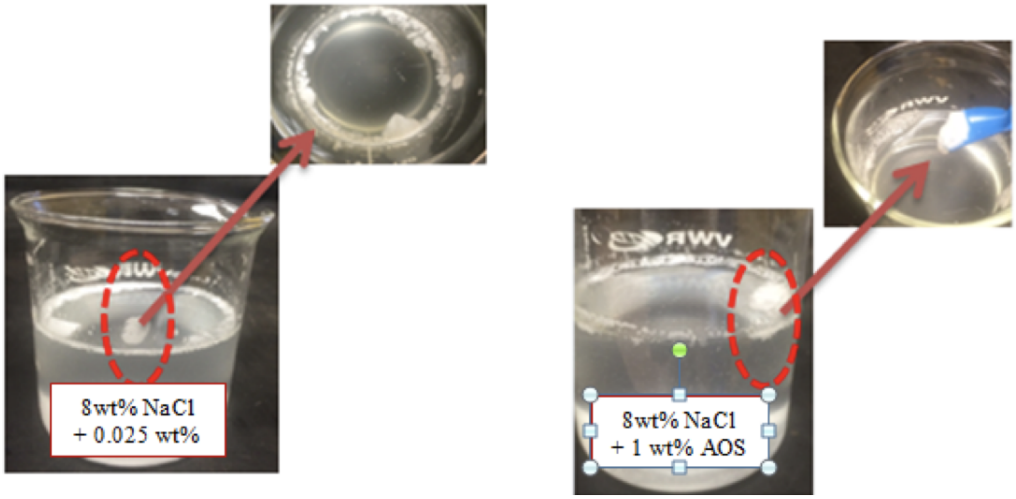

Figure 3.4: AOS is not soluble at high NaCl concentrations (8 wt% of NaCl).

The effect of surfactant concentrations on surface tension measurements at ambient temperature and 435 psi for 1 to 5 wt% of NaCl concentrations is displayed in Figure 3.5. In fact, Figure 3.5 shows the measured surface tension values that are plotted against different AOS concentrations. The additional electrolytes not only can decrease surface tension, but also can decline the CMC value at the same temperature (Figure 3.3). This is because, ionic repulsions between the head-groups and the double-layer thickness decrease as salt concentration increases. In other words, salts have been shown to repress the dissociation of the surfactant and cause a reduction in the desorption rate.

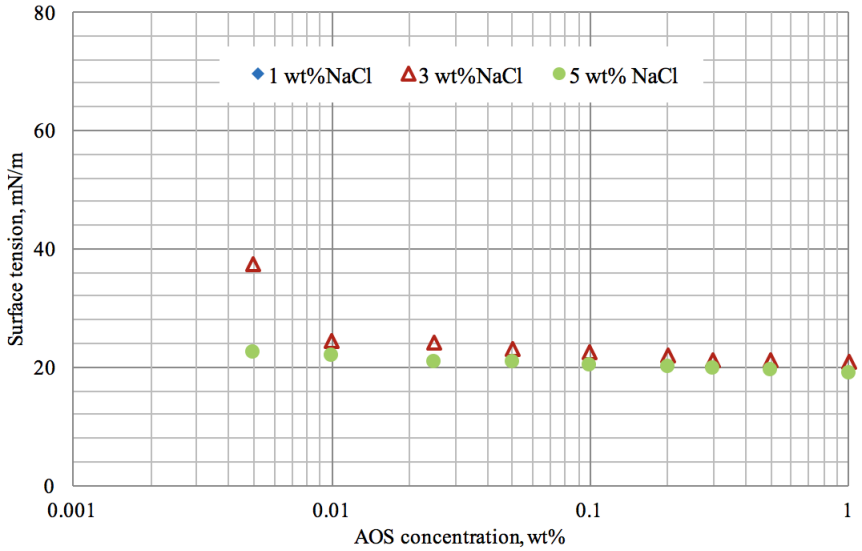

Figure 3.5: Surface tension as a function of surfactant concentration for 1, 3, and 5 wt% of NaCl (77°F and 435 psi).

3.1.3 Effect of Nanoparticles on Surface Tension and the CMC of AOS

Adding nanoparticles to solution brings some benefits. Nanoparticles can help to stabilize the system faster (Figure 3.6). Furthermore, in the presence of nanoparticles, the CMC value was smaller than that of a solution without nanoparticles at constant temperature, pressure and salt concentration (Figure 3.7). Consequently, CO_2 foam can be stabilized at lower surfactant concentrations.

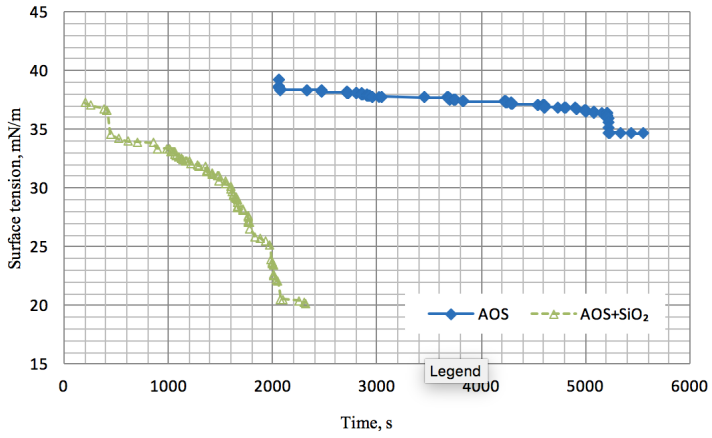

Figure 3.6: A comparison of the equilibrium time on the solution containing both surfactants and nanoparticles (435 psi and 302°F).

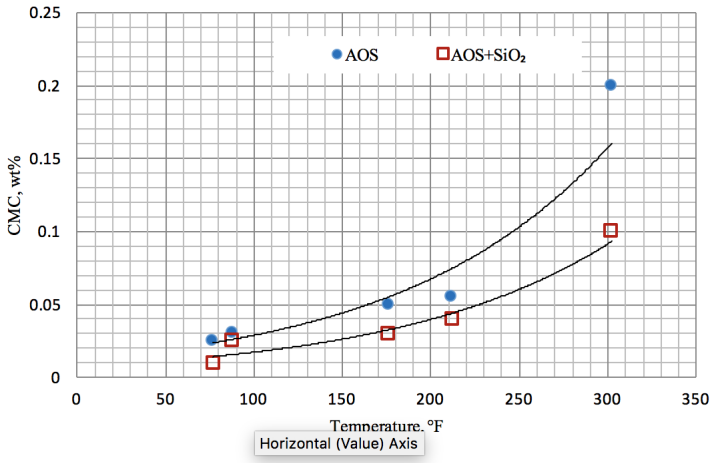

Figure 3.7: A comparison of the CMC value as a function of temperature on the solution containing both surfactants and nanoparticles.

3.2 Foam Texture

The foam bubble size and texture are determined utilizing an image processing software known as 'ImageJ' [72]. Figure 3.8 shows that bubbles are circular in shape, and almost there is no interaction between bubbles at initial time. However, the bubbles, as time passes by, will break down to form polyhedral foams. There are two reasons for foam breaking phenomenon: 1) small bubbles merge to form and expand larger bubbles, 2) bubble walls are thinned. The smaller bubble size is the higher pressure inside the bubble would be. Once bubbles with different sizes interact, the higher pressure within the smaller one disperses to the liquid phase between the bubbles walls. This continues until the bubbles coalesced and formed a larger bubble [73]. Moreover, the observation is that using iron oxide as a stabilizer can generate foam with small bubble size. Smaller bubbles show stronger foam, which is the result of retarded coalescence of bubbles due to adsorption of nanoparticles on the gas-solution interface.

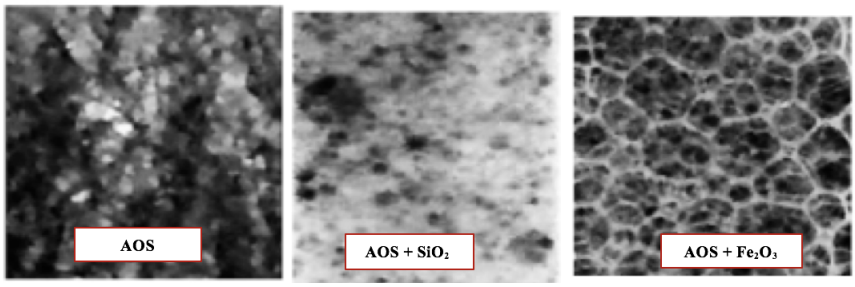

Figure 3.8: Threshold image, of selected section at initial time (0.1 wt% of nanoparticles and 0.5 wt% of AOS).

3.3 Foam Stability

3.3.1 Foam Stability in Absence of Nanoparticles

Surfactants can withstand surface tension changes in the surface area and surface concentration, i.e., explained by the interfacial viscoelasticity, that can stabilize bubble interfaces. Quick adsorption of foam-stabilizer surfactants to the interface along with rapid increase in the gas/liquid interfaces, generate surfactant monolayers that consequently diminish the coarsening process based on the surface mechanical characteristics. In fact, surfactant monolayers capability in forming surface elastic modules that resist against compression, causes a reduction in the coarsening process [74].

It is well-known fact that the foam thickness is strongly correlated with the surfactant concentration. Low surfactant concentrations with no foam-stabilizing agent, such as nanoparticle, led to rapid drainage of solution from lamellae and coalescence of neighboring bubbles, while high concentrations of surfactants, that have been known to stabilize foams, will stabilize lamellae or extend the coalescence. Higher surfactant concentration can generate thicker foam and, consequently, can enhance the foam stability. In other words, the foam half-life increases with increasing the concentration of the surfactant solution.

Figure 3.9 shows the effects of surfactant concentration on the foam stability at 75F and 300 psi. Surfactant concentration was changed from 0.05 to 1 wt%. An interesting result can be observed from the trend of foam stability curves before and after a specific surfactant concentration, referred to as optimal surfactant concentration, which is also associated to the maximum foam stability and foam half-life. The foam stability curve against surfactant concentration had an increasing trend before the optimal surfactant concentration whereas a decreasing behavior is became dominant by further increasing the surfactant concentration after the optimal point. Figure 3.9 also shows that the foam half-life for

concentrations of 0.05 wt%, 0.1 wt%, 0.5 wt%, 0.8 wt% and 1 wt% were 4 minutes, 5 minutes, 55 minutes, around 2 hours and 18 minutes respectively. It has been observed that the optimum surfactant concentration is 0.8 wt% which means that adding more surfactant to the system does not improve the foam stability

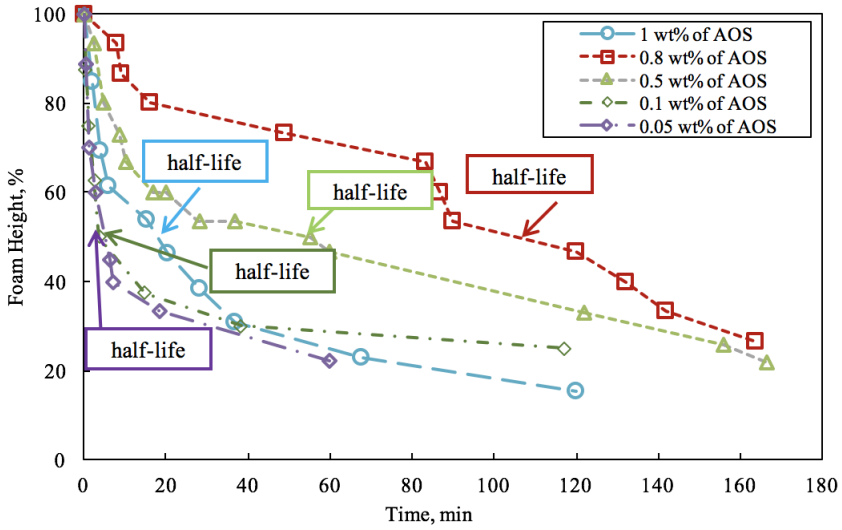

Figure 3.9: Foam height as a function of surfactant concentration at 75°F and 300 psi.

It has also been seen that foam texture is a function of surfactant concentration and thus increases as surfactant concentration increases. Figure 3.10 compares the shape of the foam produced by AOS solution for 0.05 wt% (right), 0.8 wt% (middle), and 1 wt% (right) of AOS solution at the beginning of experiment. It can be seen that denser foam with smaller lamella thickness is formed in higher concentration. Moreover, the bubble sizes at the bottom and top of the HP/HT cell are different due to snap-off mechanism that occurs between foam bubbles. In other words, should small bubbles coalesce at the top of the cell and due to drainage of the film between the bubbles which consequently results in

formation of larger bubbles.

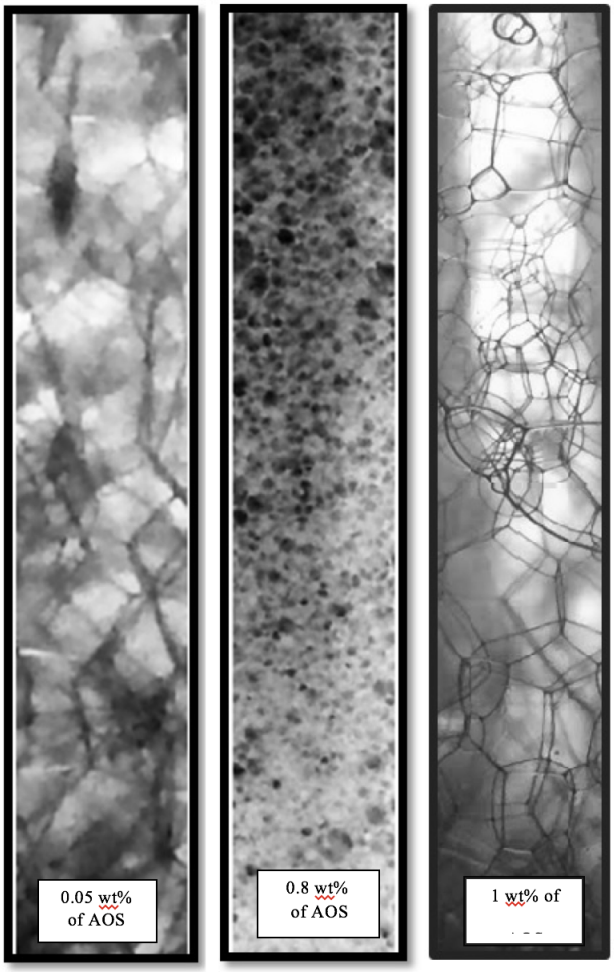

Figure 3.10: Effect of surfactant concentrations on foam texture for 0.05, 0.8, and 1 wt% of AOS solution.

Surfactants may degrade at high temperatures and /or in environments with high-salinity and so adding surfactants to form and stabilize foams in such conditions is not practical. Hence, improving the foam stability and protecting surfactants from being degraded is of great importance and can be achieved by adding nanoparticles, VES, or poly-

mers to the solution. The next section is dedicated to a comprehensive comparison of foam stability between all aforementioned solutions.

3.3.2 Foam Stability in Presence of Nanoparticles

As discussed previously, nanoparticles can be used to improve foam stability. Figure 3.11 shows the results of the foam shake test for 5 ml of the solution in the test glass tube at the ambient conditions, a time interval of 24 hours for the AOS solution (top), two mixtures of the AOS solution and nanoparticles (SiO_2 and Fe_2O_3), the mixed surfactant and guar-gum, and the mixed surfactant and VES solution in the presence of nanoparticles. The basic foam shake test shows that the AOS solution and the mixed AOS and VES solution in the presence of iron oxide can generate stronger foams with fine textures that may remain stable for a longer time (24 hours) at ambient conditions.

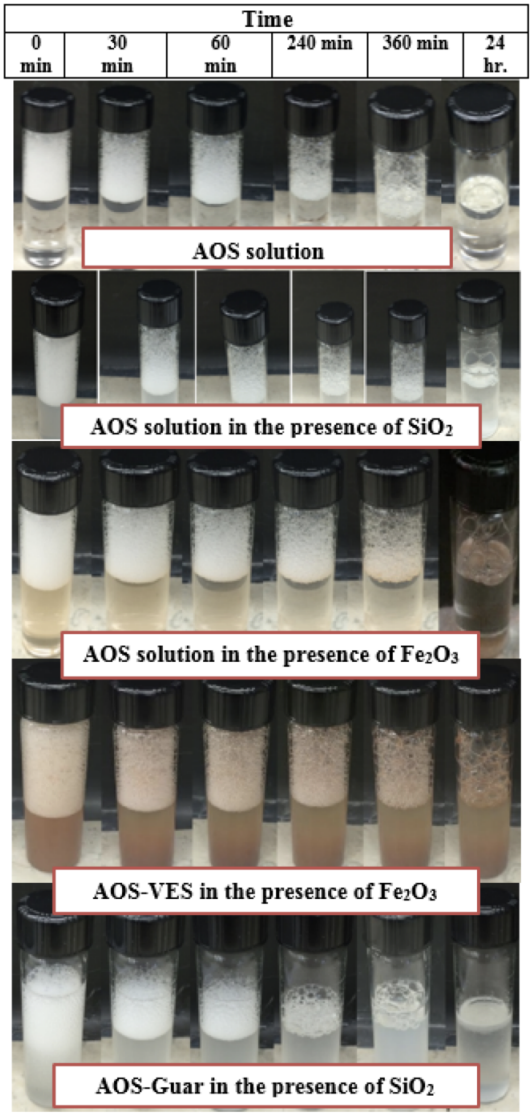

Figure 3.11: Foam shake test for all solutions examined in this study. Concentrations of chemical are 0.5 wt% of AOS, 0.1 wt% of nanoparticles, SiO_2 and Fe_2O_3, 20 ppt guar gum, and 2 vol% of VES.

To evaluate foam stability, the foam height decay against time was measured, and the half-life was determined for the AOS and the AOS solution in the presence of nanopar-

ticles. Figure 3.12 shows that nanoparticles, e.g., SiO_2 and Fe_2O_3, could improve foam stability compared to when an AOS solution was employed alone. The observed foam half-life in the presence of nanoparticles was around 4 hours and 7 hours for SiO_2 and Fe_2O_3, respectively. However, the half-life for the AOS solution was almost 3 hours. Consequently, foam made by AOS solution in the presence of Fe_2O_3 is more stable compared to the two other solutions.

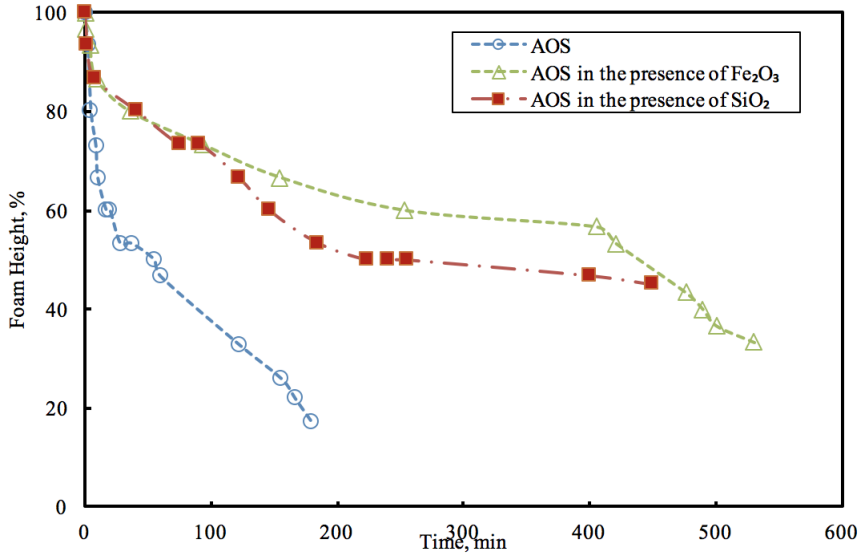

Figure 3.12: A comparison of the foam height in the absence and presence of nanoparticles at 75°F and 300 psi (0.1 wt% of nanoparticles and 0.5 wt% of AOS).

The nanoparticle foam was more stable compared to the surfactant foam. The higher stability is due to the nanoparticle irreversible adsorption onto the interface between the two phases. Surfactants dynamically adsorb to and desorb from two-phase interfaces [13]. Nanoparticles also can minimize contact area between the two phases. Therefore, they

can form a strict barrier that prevents droplet coalescence. The involved adsorption energy to move nanoparticles to the bubble interfaces is noticeably large due to the created strict barrier to coalescence. As a matter of fact, the stronger particle detachment energy, the more force is necessary to interrupt layers between particles and to make coalescence occur [55].

The results also indicated that the electrostatic interaction between Fe_2O_3 and AOS head groups led to a monolayer adsorption of the surfactant at the particle-solution interface and transformed the particles from hydrophilic to hydrophobic. Hence, particles became surface-active and stabilized the bubbles.

Bubbles were circular in shape, and there was almost no interaction between bubbles at initial time. However, the bubbles, as time passes by, will break down to form polyhedral foams. For the basic solution, the initial foam column height was shorter than that of the nanoparticle solutions. This means that the foam column degraded faster for the basic solution in comparison with the nanoparticle solutions. In other words, adding nanoparticles to the solution can form a longer initial foam column, and thus, it takes longer for the initial foam column to reach its half-life. Consequently, nanoparticle solutions may stay stable much longer compared to basic solution. But, silica nanoparticles cannot always improve the foam stability (Figure 3.13).

Therefore, increasing nanoparticle concentrations in the system can only improve foam stability to some extent. There is always an optimum nanoparticle concentration for each solution. In other words, in the absence of nanoparticles, employing surfactant might stabilize foam by reducing the surface tension. However, in the presence of nanoparticles, the concentration of surfactant and also surfactant ability is reduced because of the adsorption on to the particle surfaces. Also, the adsorbed surfactant reduces contact angle of the particles, which is expected to reduce the ability of the particles to stabilize the foam by weakening their steric barrier on the surface of bubbles [56].

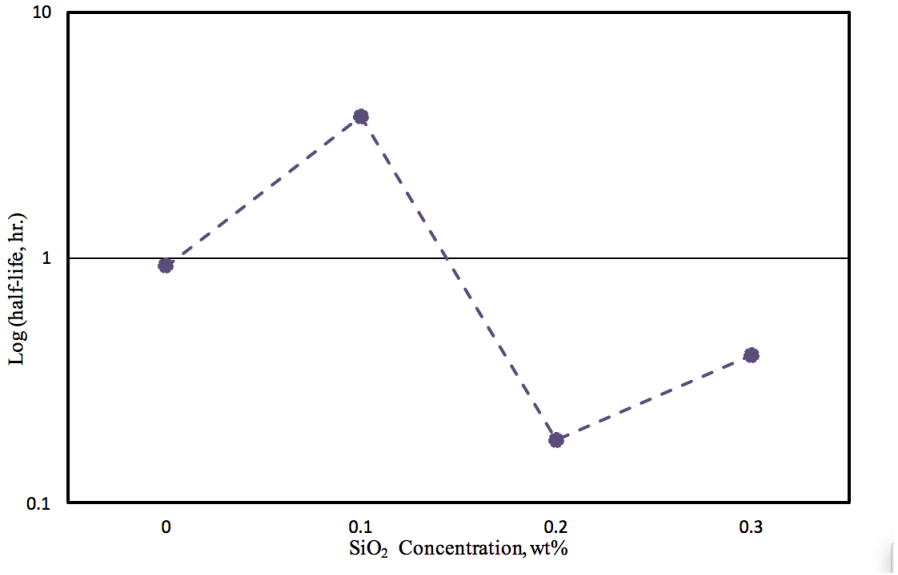

Figure 3.13: Log (half-life time) as a function of nanoparticle concentrations at 75°F and 290 psi.

In the present study, different nanoparticle concentrations (SiO_2 with 100 nm) were used (from 0.1 to 0.3 wt%). The foam half-life for concentrations of 0.1, 0.15, 0.2, 0.25 and 0.3 wt% of SiO_2 at 75°F and 300 psi, were 4 hours, 1 hours, 15 minutes, 18 minutes and 24 minutes, respectively (Figure 3.14-solid line). Therefore, 0.1 wt% of nanoparticles is the optimal concentration that can stabilize foam at 75°F with high surfactant concentration (0.5 wt% of AOS) among all various concentrations of nanoparticles investigated in the present work. In other words, under explained conditions, SiO_2 concentration as low as 0.1 wt% can easily produce foam owing to the fact that the number of particles in the liquid are large enough to attach and absorb at the CO_2 and liquid interface. After 4 hours, the foam height reached to half of its initial height. However, the optimal SiO_2 concentration increased as temperature increased (140°F) or AOS concentration decreased (Figure 3.14-dashed line).

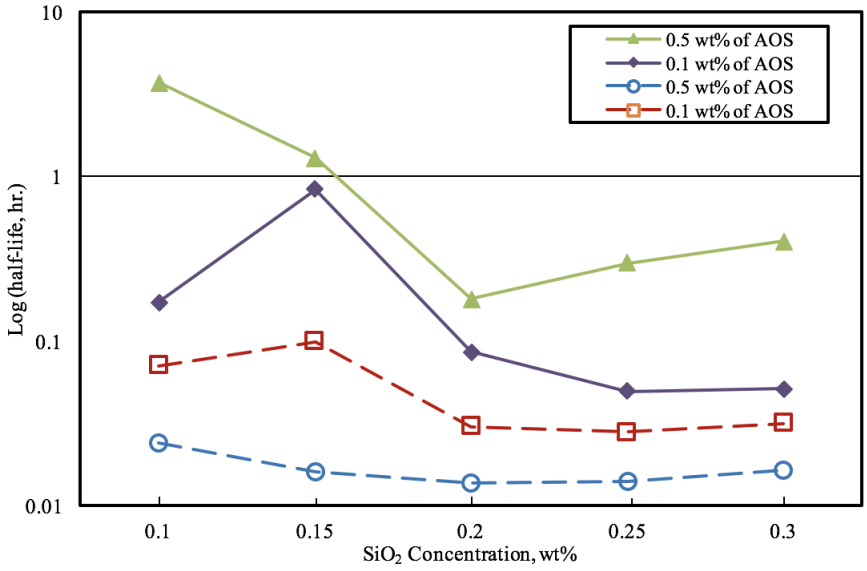

Figure 3.14: The optimal surfactant and nanoparticle concentrations (SiO_2 with 100 nm) for line-bar at 75°F, and dashed-line at 140°F.

Strong hydrophilic SiO_2 is one of the main compounds that can decrease solid particles adsorption energy. As discussed before, the contact angle has a strong effect on the detachment energy and might influence the foam stability. Figure 3.15 shows the contact angle results for 0.5 wt% of AOS in the presence of SiO_2 with 100 nm at 75°F and 300 psi. Nanoparticles could minimize the contact area between the two phases. Furthermore, for a contact angle between 0 and 30° or between 150 to 180°, the detachment energy is pretty small, so the particles cannot stabilize foam anymore. To achieve a larger contact angle with high stability, it is of high importance to generate nanoparticles with smaller bubble sizes [7]. Also, formation of SiOH groups on the silica surface during dispersion of silica particles in solution assists retaining larger contact angles [75]. In fact, further particles aggregation is avoided as a result of the electrostatic repulsion between silica particles. Results show that contact angle in the presence of 0.1 wt% of SiO_2 was 54. It means that

the detachment energy for 0.5 wt% of AOS and 0.1 wt% of SiO_2 at 75°F and 300 psi is higher compared to other concentrations of SiO_2 and at the same conditions. Therefore, foam is more stable at this condition.

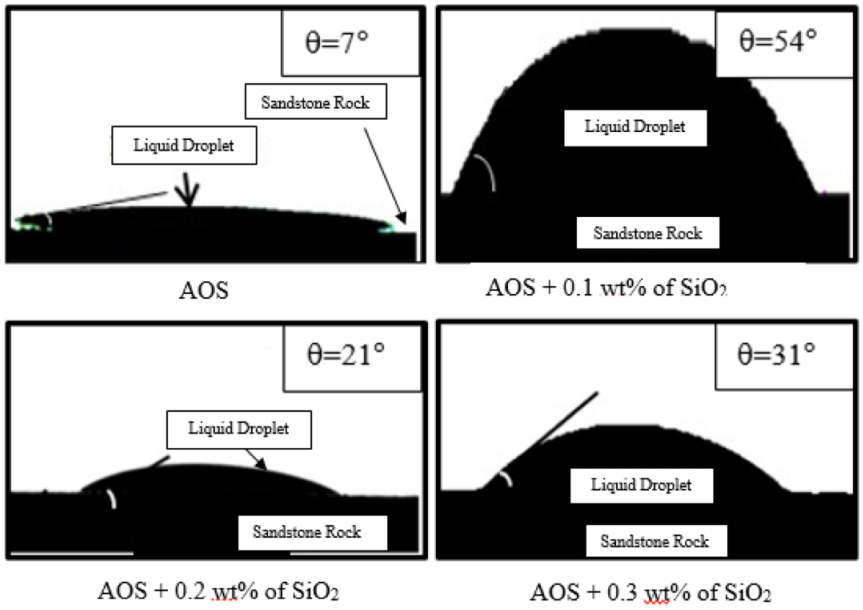

Figure 3.15: Contact angle between solution/sandstone/CO_2 for 0.5 wt% of AOS at 75°F.

Figure 3.16 indicates the bubble texture for 0.5 wt% of AOS at various nanoparticle concentrations as a function of time. The foam bubble size and texture are determined using image processing software known as 'ImageJ' [72]. At the optimal surfactant and nanoparticle concentration, e.g., in the present work 0.5 wt% of AOS and 0.1 wt% of SiO_2 were used, the foam bubble size was smaller and denser at the initial time, which leads to a more stable foam.

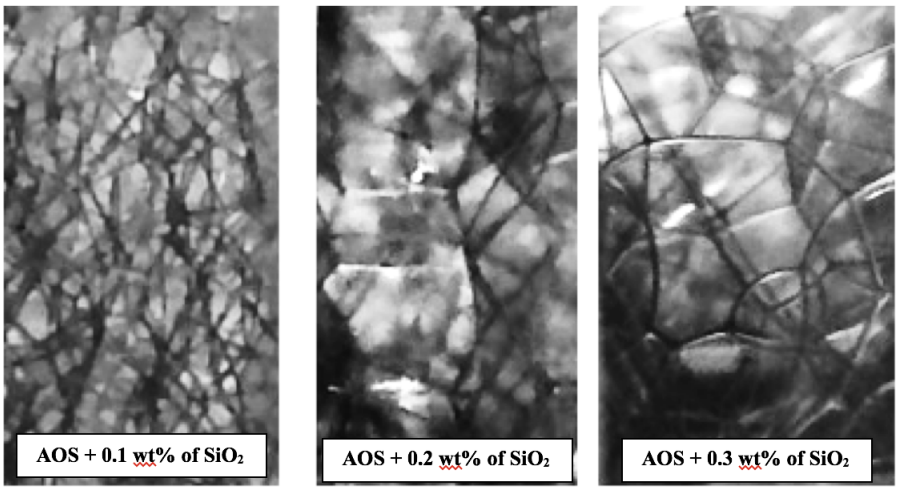

Figure 3.16: The bubble size for 0.5 wt% of AOS at 75°F and initial time.

To study the effect of nanoparticle size on foam stability, two sizes of nanoparticle, e.g., 100 and 140 nm, were used to make the solution. Several different SiO_2 concentrations (from 0.1 to 0.3 wt %) added to the basic solution. All experiment ran at 75°F and 300 psi. Results show the bigger size (140 nm) of particle has better effect on CO_2 foam stability (Figure 3.17). The reason is shown in Figure 3.18 based on contact angle measurement results for these two size of nanoparticles. One may note that high hydrophobicity or hydrophilicity may lead to an unstable foam due to the dispersed distribution of particles either in the aqueous or CO_2 phase. Attar Hamed et al. showed that generating stable foams can be achieved at contact angles above 85 [1]. The θ is 86 for the solution in the presence of SiO_2 with 140 nm, which is more than θ compared to the SiO_2 with 100 nm.

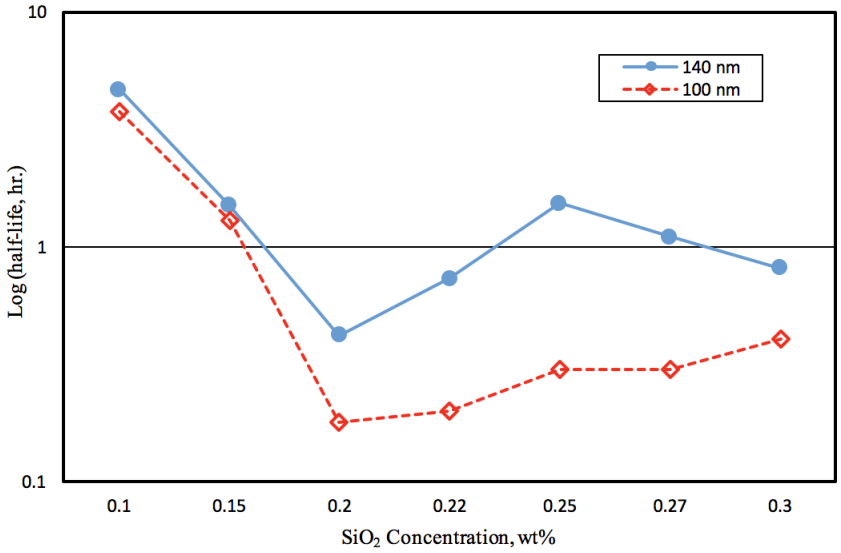

Figure 3.17: A comparison of the foam made by 0.5 wt% of AOS and two different nanoparticle sizes at 75°F.

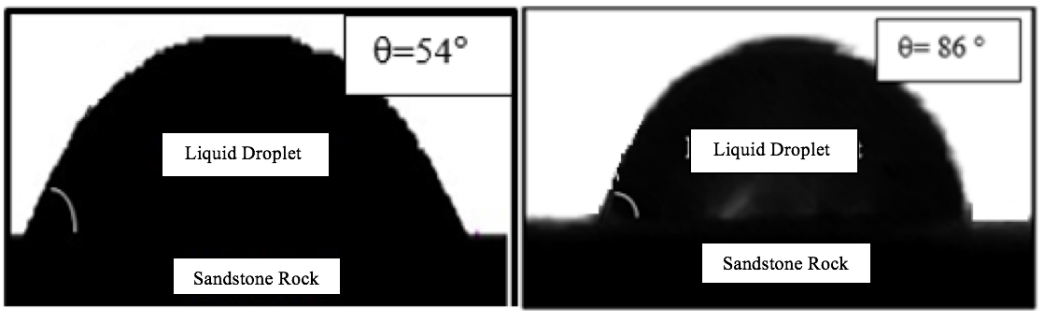

Figure 3.18: Contact angle between solution/sandstone/CO_2 for 0.5 wt% of AOS and SiO_2 with 100 nm (left) and 140 nm (right) at 75°F.

Figure 3.19 shows the pressure effects on the process of generating CO_2 foam at 75°F for 0.1 and 0.5 wt% of AOS solution in the presence of 0.1 wt% of SiO_2. Foam stability decreased as pressure increased. In fact, at high pressures, CO_2 solubility in solution increases, which leads to faster gravity drainage and causes a greater reduction in the foam volume at the same time. In addition, the high surface tension value at low pressure means that the interfacial energy between CO_2 bubbles and the solution is high. Consequently, the CO_2 bubbles collapse, and the foam is not stable. Therefore, based on the current results, i.e., the effects of pressure on the surface tension and the foam stability, a lower surface tension does not always indicate stable foam.

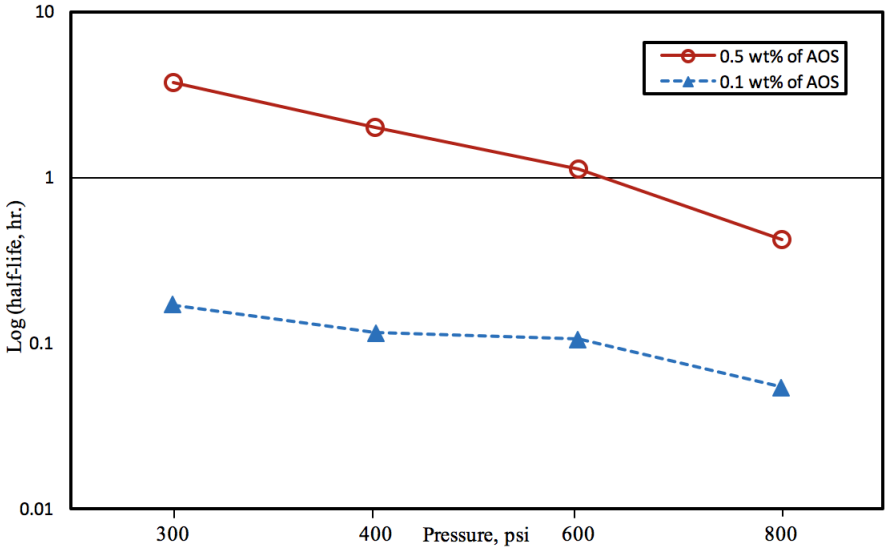

Figure 3.19: Log (half-life) as a function of pressure at 75°F in the presence of 0.1 wt% of SiO_2 with 100 nm for 0.1 and 0.5 wt% of AOS.

Temperature plays a pivotal role in foam applications in hydraulic fracturing and EOR.

To probe the effects of the temperature on the CO_2 foam stability in all experiments, pressure was fixed at 300 psi, while temperature varied in the range of 75 to 176°F. Results show that the bubble size increased as temperature increased (Figure 3.20). Results also indicate that at higher temperatures, bubbles collapsed faster compared to 75°F (Figure 3.21).

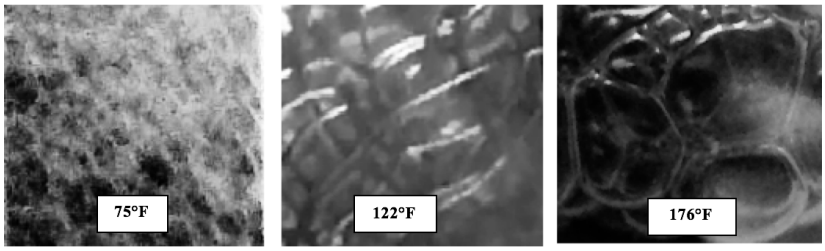

Figure 3.20: The bubble size increases as temperature increases.

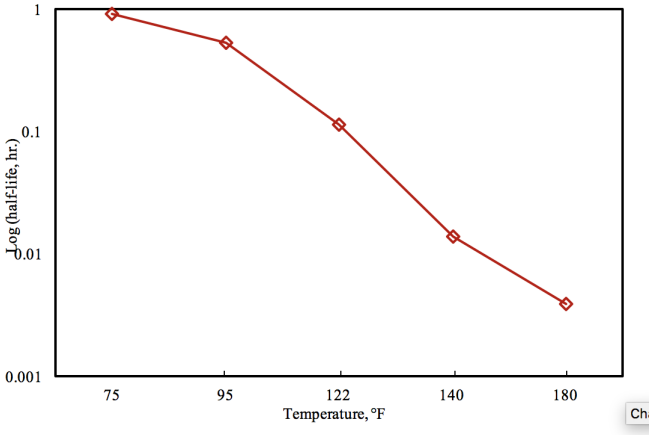

Figure 3.21: Log (half-life time) as a function of temperature at 300 psi and 0.5 wt% of AOS.

Moreover, the height of the foam decreased as temperature increased. As the temperature went beyond 140°F, no foam was observed in the cell. Furthermore, the drainage half-life decreased as temperature increased. Two reasons might cause this phenomenon. First, it might occur due to the decrease in liquid viscosity as temperature increases. In fact, viscosity slows down the drainage of liquid at initial time and keeps the liquid film thicker, which causes the foam to stay at a stable state for a longer time [74]. Second, increasing temperature can reduce the density of the CO_2 phase.

Using nanoparticles in the solution is one way to increase foam stability. Figure 3.22 shows that foam stability could be improved when nanoparticles were added to the solution at high temperatures. However, the optimal nanoparticle concentration at 140°F was 0.1 wt%, as no foam can be generated at temperatures higher than 140°F.

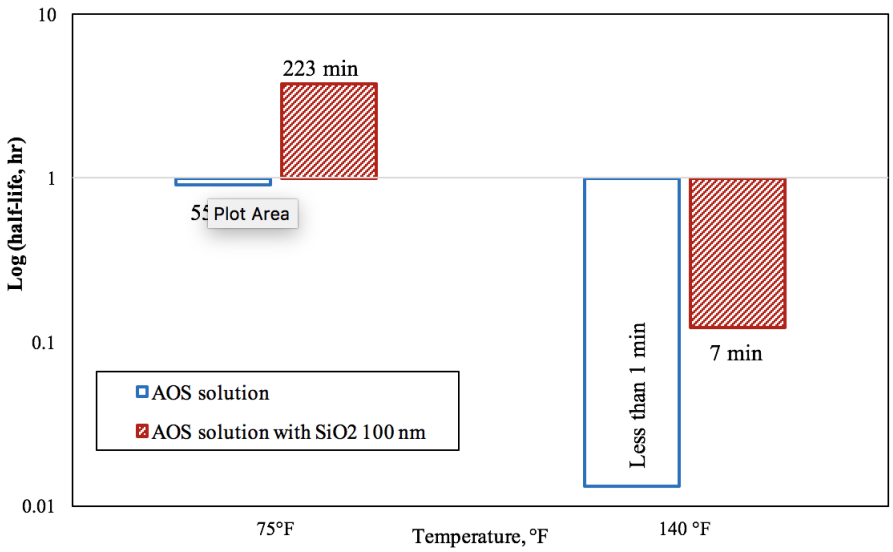

Figure 3.22: Log (half-life time) as a function of a nanoparticle concentration for 75°F and 140°F at 300 psi for 0.5 wt% of AOS.

Based on the obtained results in the current and previous section, using a high nanoparticle concentration with lower surfactant concentration at high temperatures provides the optimum composition and concentration for obtaining stable foam. In fact, surfactant degrades at high temperatures. This explains the low concentration of surfactant at high temperatures. On the other hand, at ambient conditions, surfactant can increase liquid viscosity, and thus, using a higher surfactant concentration leads to more stable foam.

To investigate the effects of salt concentration on the CO_2 foam stability, various concentrations of NaCl (1, 3, and 5 wt%) were used to prepare the solution in the presence of different SiO_2 concentrations. Results show that the foam stability decreased as salt concentration increased in the solution (Figure 3.23). In other words, foam was no longer stable if the salinity was too high. The reason is that once salt was added to the solution, the particle electrostatic repulsions were reduced, which resulted in aggregation of the particles [5].

The foam stability 0.5 wt% of AOS solution in the presence of 0.1 wt% of SiO_2 is plotted as a function of salt concentration for 1, 3, and 5 wt% of NaCl. The results show that the foam stability can be improved in the presence of nanoparticles. For example, the foam stability changed from 3 hours to 8 hours for 0.1 wt% of SiO_2 in the present experiment.

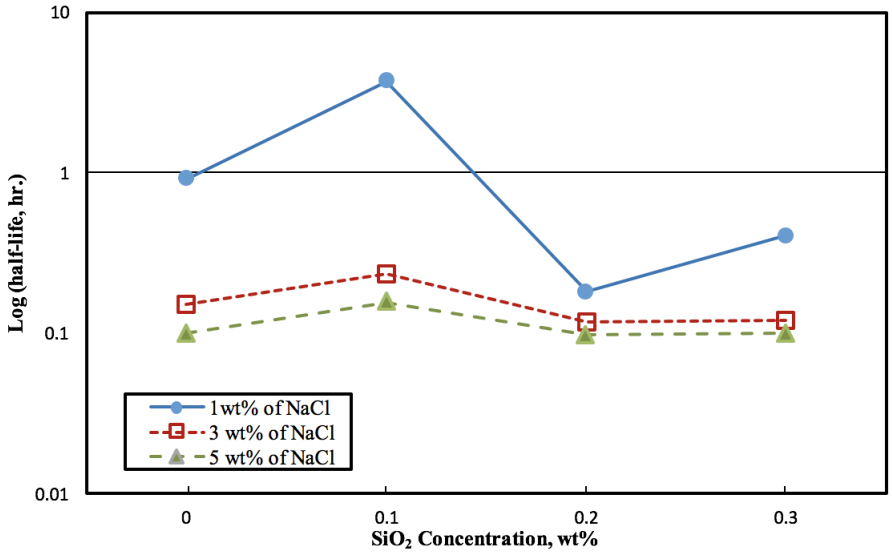

Figure 3.23: A comparison of the log (half-life) of CO_2 foam at 75°F temperature and 300 psi for 0.5 wt% of AOS in the presence of SiO_2 with 100 nm for different salt concentrations.

3.3.3 Foam Stability in Presence of Polymer

Foamability of the dispersion was studied by performing a shake test. To generate foam, 200 cm^3 of solutions including nanoparticles, with and without guar-gum, were shaken for 20 minutes at ambient conditions (Figure 3.24).

The foamability test shows that the guar-gum solution without surfactant and in the presence of 0.1 wt% of SiO_2 cannot generate foam (Figure 3.24(a)). Surfactant type and system dynamics govern foam formation. In other words, the presence of surfactants is essential to form foam in all solutions because they facilitate nanoparticle adsorption. In contrast to guar-gum solutions, the AOS-guar solution, in the presence of either nanoparticles, SiO_2 or Fe_2O_3, can generate foam (Figure 3.24(b, c)). The AOS solution with SiO_2

nanoparticles generates the most stable foam compared to other solutions (Figure 3.24(d)).

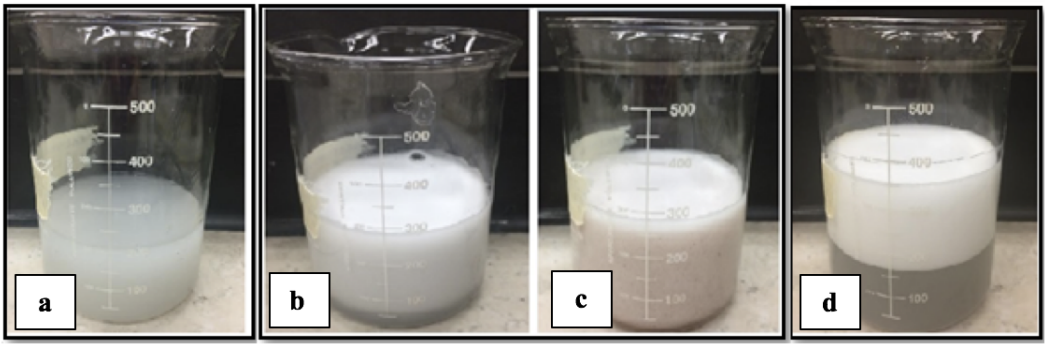

Figure 3.24: A comparison of the foamability at ambient conditions for: (a) 20 ppt guar + 0.1 wt% SiO_2, (b) 0.5 wt% AOS + 20 ppt guar + 0.1 wt% SiO_2, (c) 0.5 wt% AOS + 20 ppt guar + 0.1 wt% Fe_2O_3, and (d) 0.5 wt% AOS + 0.1 wt% SiO_2. Experiments showed that all dispe dispersions ((b), (c), and (d)) could generate foam except for the dispersion (a) which contains no surfactant.

High foamability may lead to lower foam stability, and Figure 3.25 illustrates this point. Even though the AOS-guar solution with Fe_2O_3 has higher foamability at ambient conditions compared to the AOS solution with SiO_2, results show that the foam stability of the AOS-guar solution with Fe_2O_3 is less than that of AOS solution with SiO_2. Foamability depends on the initial foam volume given a specified amount of system energy. However, the foam stability is obtained with respect to foam decay through determining the variation in the percentage of foam or coalescence of the bubbles over time. Therefore, high foam stability may imply relatively less foamability.

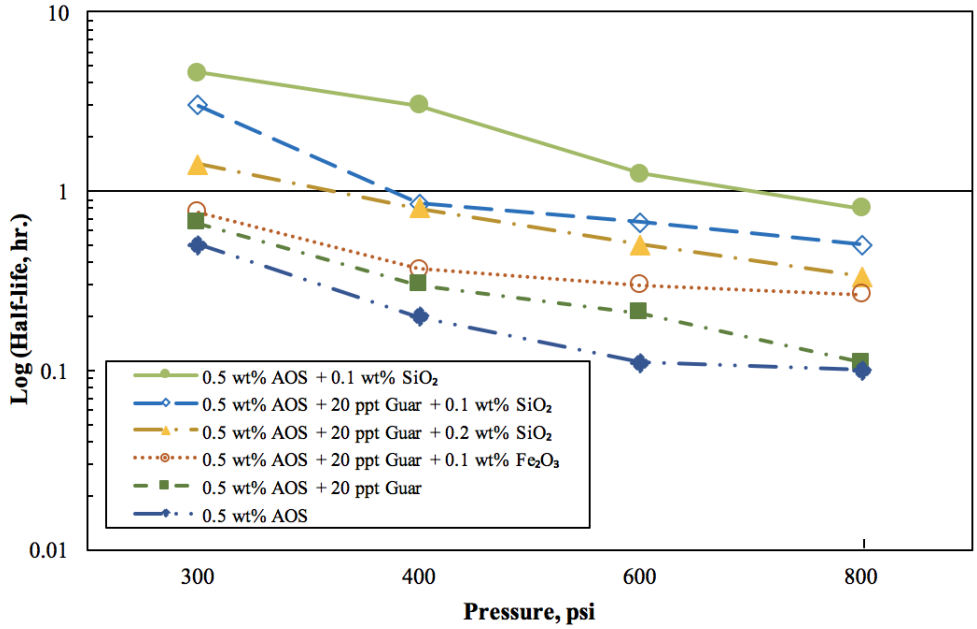

Figure 3.25: Effect of pressure on log (half-life) for the AOS-guar and AOS solutions in the presence of nanoparticles at 77°F.

Polymer-based solutions (AOS + Guar-Gum) generate foams with low stability owing either to the size of the polymer molecules or their adsorption rate. During the foam generation, large polymer molecules fail to adsorb onto the bubble surfaces due to insufficient interaction time [35]. Figure 3.25 also shows that AOS-guar foams collapsed within 30 minutes at 300 psi (less than one hour). Foam stability increased as nanoparticles were added to the solution. For instance, the half-life increased from 30 minutes to 3 hours for AOS-guar solution in the presence of 0.1 wt% SiO_2 at 300 psi. Figure 3.26 shows an optical micrograph of the foam film. Image J, an image processing software, was used to measure lamella layer thickness in this work. Mixed solutions containing nanoparticles stabilize foam films by creating thicker lamella layer, of size 5.96 μm, in the middle of lamella layer, compared to that of AOS solution with a thickness of 2.93 μm.

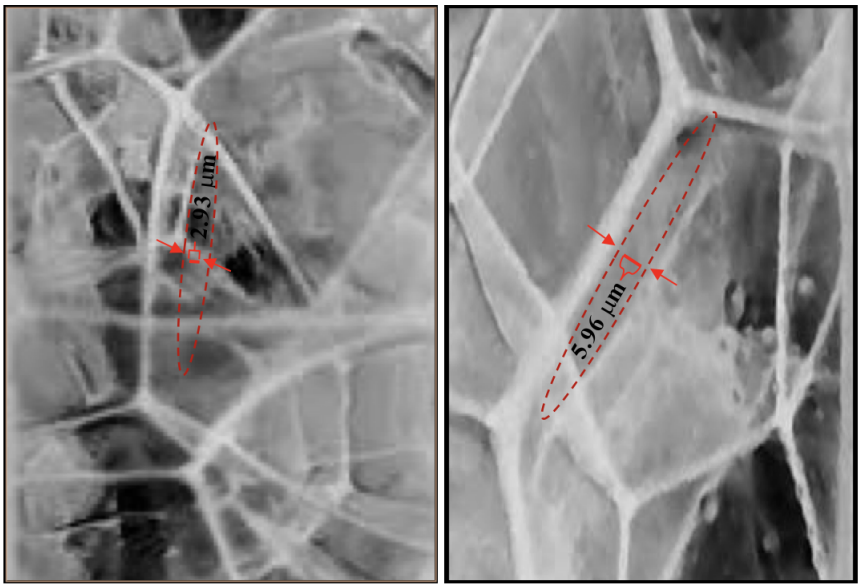

Figure 3.26: Compression of the thickness for (a) 0.5 wt% AOS + 20 ppt guar, and (b) 0.5 wt% AOS + 20 ppt guar + 0.1 wt% SiO_2. Nanoparticles create lamella layer two times thicker than that of the solution without nanoparticles.

The thermal properties and surface energy for nanoparticles are normally very high, compared to polymer, because of their nanoscale dimensions that allow them to mix well with the polymer chain [48]. Optical micrographs of foams stabilized by 0.5 wt% AOS solutions with 20 ppt guar-gum in the presence of 0.1 wt% nanoparticles at initial time (Figure 3.27((a), (b), and (c)) and after two days (Figure 3.27((d), (e), and (f)). The nanoparticles can attach at the lamella layer between gas-liquid interface, which can improve foam stability by reducing liquid-liquid interfacial area (Figure 3.27 ((a), (b), and (c)). The most common destabilizing mechanism is known to be coalescence which encompasses the process of collapsing smaller nanoparticles into each other to generate larger nanoparticles (Figure 3.27((d) and (e)). Nanoparticles (Fe_2O_3) in guar-based solutions had a tendency

to agglomerate because of the high surface energy of these nanoparticles (Figure 3.27 (f)). Therefore, it is hard to disperse foam flooding solutions containing nanoparticles and guar-gum, which might be a disadvantage of such solutions.

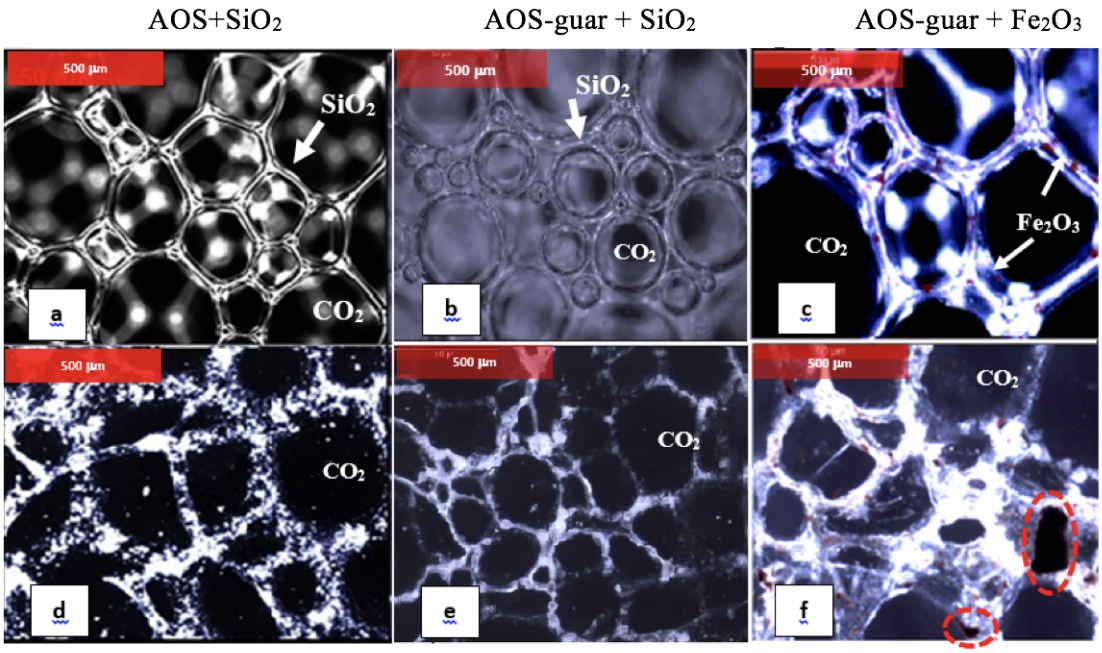

Figure 3.27: Optical micrographs of foams stabilized by 0.5 wt% AOS solutions with 20 ppt guar gum in the presence of 0.1 wt% nanoparticles at initial time (a, b, and c) and after two days (d, e, and f). (a, b, and c) show that the nanoparticles attach to the lamella between bubbles that help to stabilize foam. (d) and (e) show that the bubble size and shape changes with time. (f) shows clearly that there is agglomeration for Fe_2O_3 into the AOS + guar-gum solutions.

The micrograph images of the foam show the Fe_2O_3 agglomeration (Figure 3.28). The classical Derjaguin-Landau-Verwey-Overbeek (DLVO) theory describes the particle-

particle agglomeration. According to the DLVO theory, the attractive and repulsive forces among particles are pivotal factors in agglomeration and stability of the particles [76]. Attractive forces between particles occur because of the van der Waals force, which is defined by zeta potential and will be discussed later. The electrostatic repulsion is the electrical double-layer interaction surrounding each particle. Therefore, particle agglomeration into a large cluster of particles can decrease in the presence of suitably high repulsion force, which helps to enhance system stability. In other words, if a system does not have a repulsion mechanism, particle agglomeration will occur.

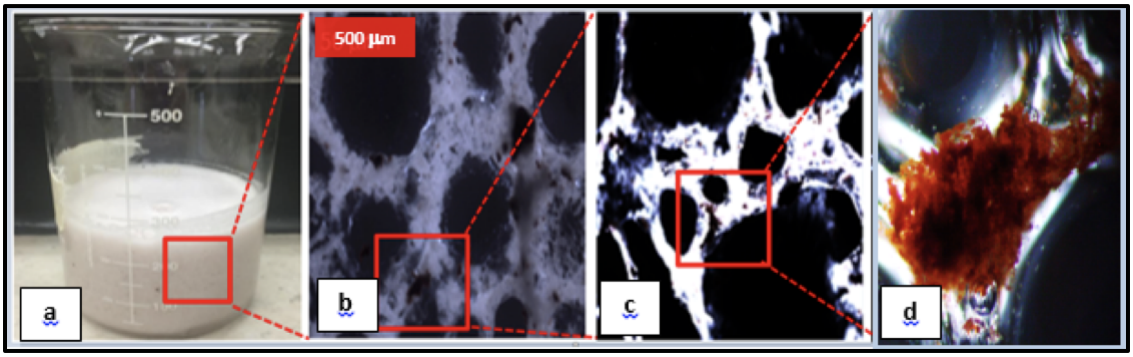

Figure 3.28: Agglomeration of nanoparticles for the AOS-guar solution in the presence of Fe_2O_3 at ambient conditions. (a) foam at ambient conditions, (b)-(d) magnified images of the squared areas in (a)-(c) using electron microscope to show Fe_2O_3 agglomeration.

Figure 3.29 shows the size of the agglomeration of Fe_2O_3 nanoparticles in the AOS-guar solution calculated by employing ImageJ software and the input image to the ImageJ system is captured by TEM (Transmission Electron Microscopy). An increase in the size of nanoparticle diameter from 50 nm to 162 nm is observed.

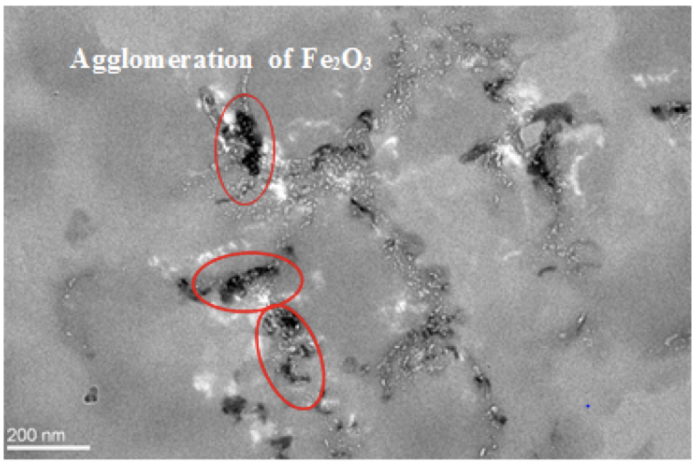

Figure 3.29: TEM image of Fe_2O_3 nanoparticle agglomeration in the AOS-guar solution.

Temperature is another important parameter that affects foam stability. Figure 3.30 shows a comparison of the half-life for the AOS with SiO_2, the polymer-based solutions including two types of nanoparticles, SiO_2 and Fe_2O_3, and polymer-based solutions at different temperatures. As mentioned before, nanoparticles can enhance the foam stability for both the AOS and the polymer-based solutions. Results also demonstrate that there is an optimum nanoparticle concentration at which foam half-life reaches its highest value and thus at concentrations higher than the optimum, half-life time decreases. Such improvement occurs due to detachment energy (Eq. 2.1) and attractive force between nanoparticles, which are determined by contact angle and zeta potential, respectively.

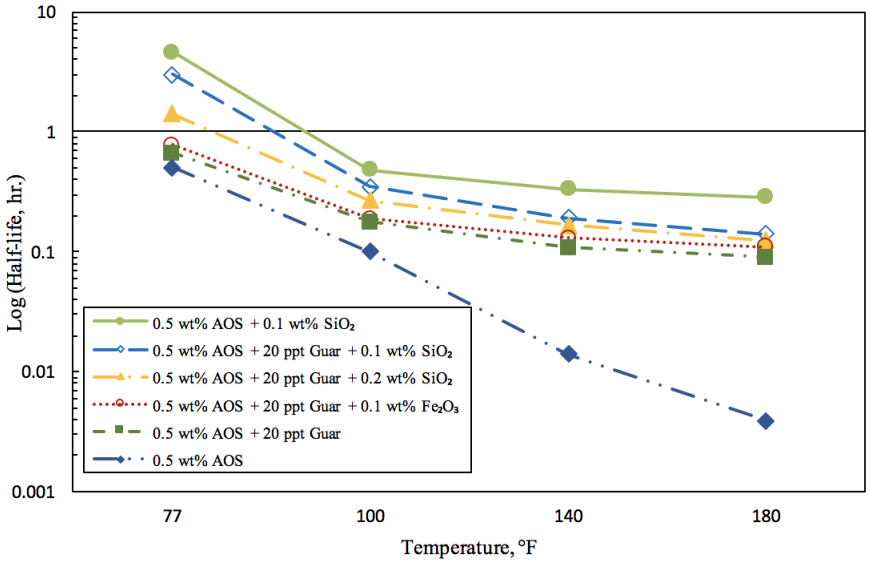

Figure 3.30: Log (Half-life) for the AOS-guar and AOS solutions in the presence of nanoparticles at various temperatures and 300 psi.

The AOS solution with SiO_2 can remain stable for a longer time compared to polymer-based solutions. The half-life for the AOS solution with SiO_2 was almost five hours, while the half-life for the AOS-guar with SiO_2 and AOS-guar solutions were three hours and less than one hour, respectively. Bubbles were spherical in shape at initial time (Figure 3.31 (a and b)). However, small bubbles merge to form larger bubbles and expand as time passes, and they also break down to form polyhedral- shaped bubbles. The smaller the bubble size is, the higher the pressure inside the bubble would be. Once bubbles of different sizes interact, the higher pressure within the smaller ones disperses to the liquid phase between the bubble walls. This process continues until the bubbles coalesce and form a larger bubble. Nanoparticles dispersion into the solution can thus form foam with more uniform structure compared to the AOS solution (Figure 3.31(c and d)). Nanoparticles can form a viscoelastic layer around the bubble surface, which can make the foam film thicker and

protect bubbles against shrinkage [77]. Consequently, nanoparticle dispersions enhance the foam stability.

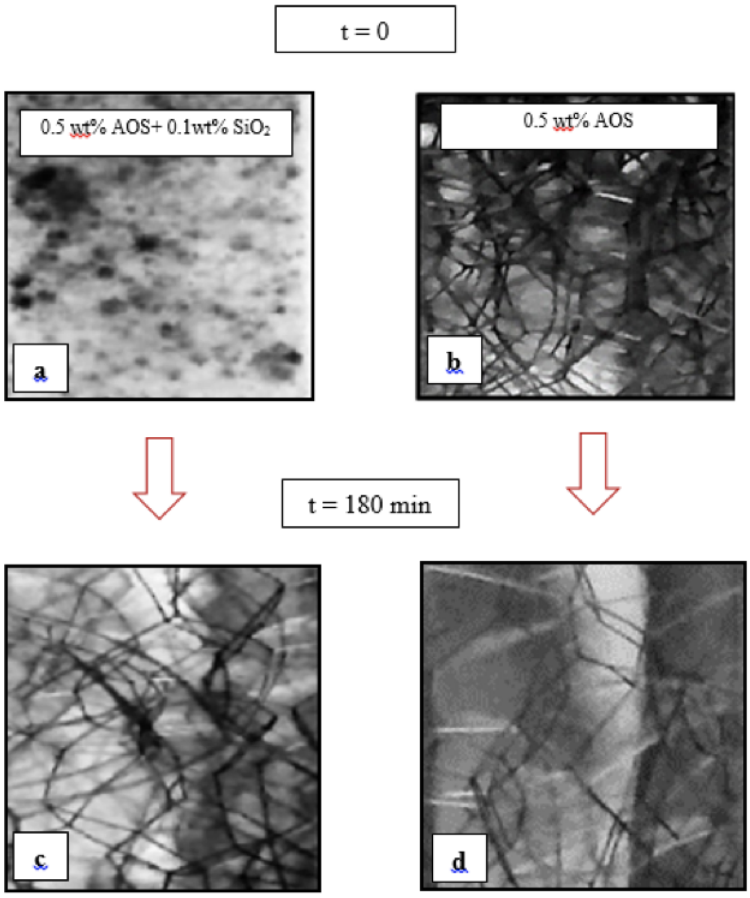

Figure 3.31: The behavior of the foam over time for AOS solution: (a) and (c) in the presence of SiO_2, and (b) and (d) in the absence of SiO_2. Small bubbles merge to form and expand larger bubbles as time passes (c) and (d).

Figure 3.32 (a) shows the foam generated by AOS. In absence of nanoparticles, the probability of bubbles coalescence is higher compared to that of the foam in presence

of nanoparticles. An interesting observation was that using nanoparticles as a stabilizer generates foam with smaller bubble size (16 μm) compared to the case that solution contains no nanoparticles (bubble size is 58 μm). The primary bubble shape stays unchanged, spherical or ellipsoidal, while the volume of each bubble grows larger with time. The coalescence of smaller bubbles due to adsorption of nanoparticles on the gas/solution interface creates stronger foam [78, 79]. The surface area available for inter-bubble gas diffusion decreases due to the attached nanoparticles on the bubble surfaces. The nanoparticles attach to the lamella between bubbles, which can enhance foam stability in contrast to Ostwald ripening and bubble thermal stability by making a 3D network structure in the liquid phase (Figure 3.32 (b)).

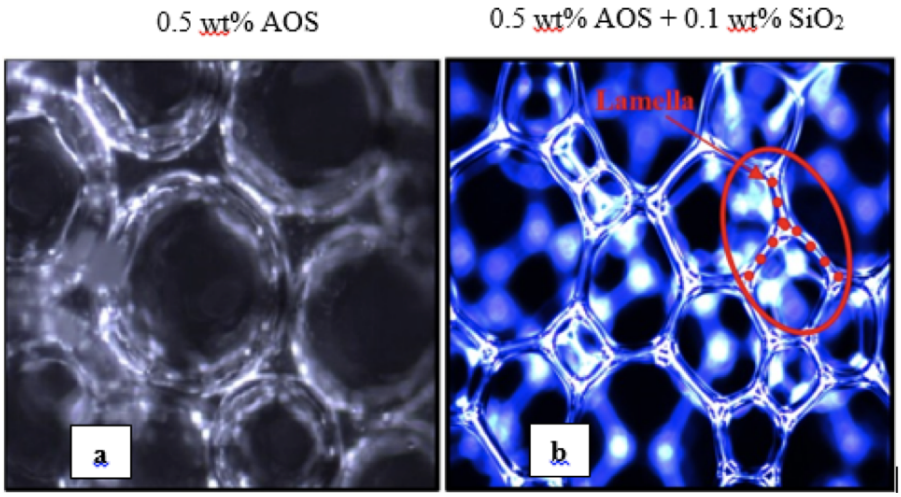

Figure 3.32: Optical micrographs showing a 3D network structure in the lamella layer for: (a) 0.5 wt% AOS and (b) 0.5 wt% AOS + 0.1 wt% SiO_2.

3.4 Contact Angle

The hydrophilicity or hydrophobicity of the nanoparticles helps researchers to understand and accurately predict the interactions between the nanoparticles and the bubbles. For contact angles between 0 and 30° or between 150 to 180°, detachment energy will be rather low and according to the Eq. 2.1, the nanoparticles cannot stabilize the foam. However, the closer the angle is to 90, the higher the energy is. Stronger particle detachment energy requires larger forces to break layers between particles and make coalescence process occurs. Unlike surfactants, nanoparticles will be irreversibly adsorbed at the gas-liquid interfaces, which improve foam stability [55]. For the present study, contact angles were measured for the AOS solutions, and the AOS-guar solution both in the presence of SiO_2 and Fe_2O_3. Figure 3.33 shows that no foam was generated for θ between 0 and 30°. A stable foam was generated for θ between 50 and 85 as well as for θ greater than 85. However, for the latter case, foam stays stable longer compared to the former case.

Nanoparticle size is another important factor that affects foam stability. With smaller sizes, agglomeration should occur more readily [78]. Nanoparticle agglomeration as a physical response occurs in systems with high surface energy that leads to a decrease in this energy. It is observed, in the current experiment, that the agglomeration trend for guar solutions, including Fe_2O_3 nanoparticles with 50 nm diameter, tends to happen faster compared to that of the other solutions owing to the low detachment energy.

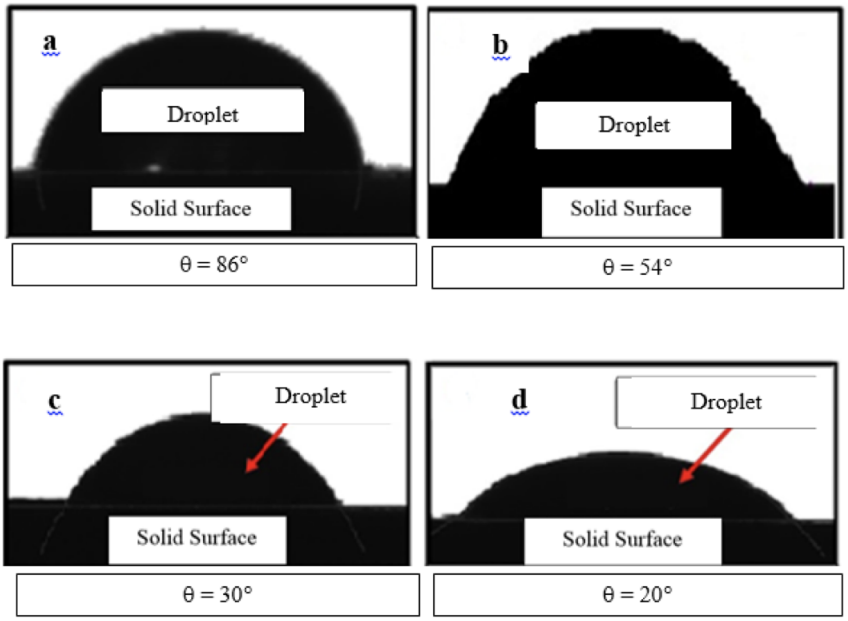

Figure 3.33: Contact angle for 0.5 wt% of AOS and (a) 0.1 wt% of SiO_2 (b) 20 ppt guar + 0.1 wt% of SiO_2, (c) 20 ppt guar + 0.2 wt% SiO_2, and (d) 20 ppt guar + 0.1 wt% Fe_2O_3 at 77°F.

Acquiring foam stability requires the nanoparticles remain attached to the interface, which in turn avoids bubbles coalescence. Owing to the colloidal nanoparticles high attachment energy at the interfaces, such nanoparticles tend to irreversibly adsorb at the interface while surfactants adsorption at the interface is reversible. Obtaining detachment energy requires measuring surface tension and contact angle accordingly. Several experiments were conducted, and (Table 3.1) summarizes the results associated with surface tension for AOS and guar-gum solutions in the present of SiO_2. Note that in the absence of nanoparticles, surface tension of a surfactant solution tends to decrease as temperature increases (from 33 to 30 mN/m) similar to the case that the surfactant solution contains

nanoparticles. Surface tension of AOS in presence of SiO_2 nanoparticles is less than that of the plain AOS solution due to the repulsive interaction between negatively charged silica nanoparticles and negatively charged AOS molecules. Consequently, more AOS molecules can move from the bulk phase to the interface [80]. The guar-based foam with θ less than 30° was not stable compared to the AOS solutions. The energy decreases as contact angle decreases (Figure 3.34). The AOS solution with SiO_2 is more stable compared to the guar-based solution.

Aqueous Dispersion	Temperature, °F	Surface Tension, mN/m
0.5 wt% AOS + 0.1 wt% SiO_2	77	30.80
0.5 wt% AOS + 0.1 wt% SiO_2	100	30.56
0.5 wt% AOS + 0.1 wt% SiO_2	140	30.02
0.5 wt% AOS + 0.1 wt% SiO_2	180	29.12
0.5 wt% AOS + 20 ppt guar-gum + 0.1 wt% SiO_2	77	32.08
0.5 wt% AOS + 20 ppt guar-gum + 0.2 wt% SiO_2	77	29.20
0.5 wt% AOS + 20 ppt guar-gum + 0.1 wt% Fe_2O_3	77	32.51

Table 3.1: The surface tension between CO_2 and different aqueous dispersions at 300 psi.

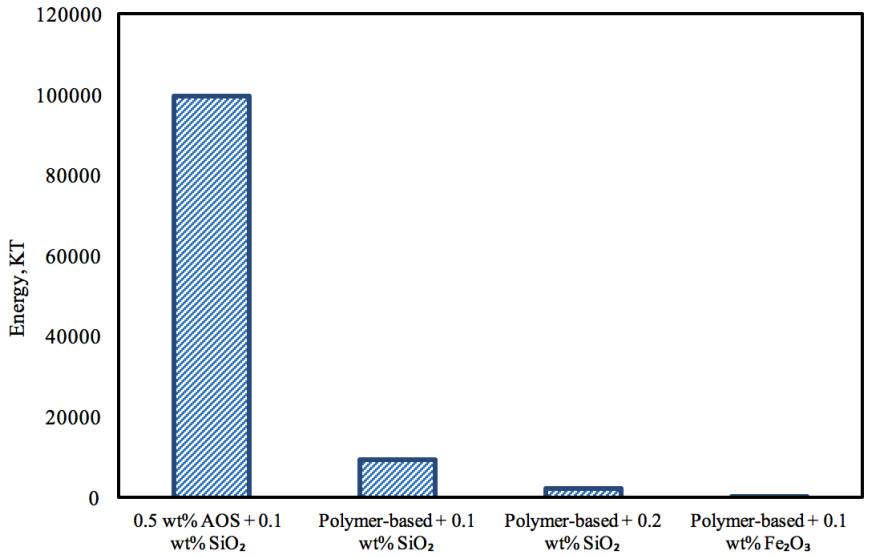

Figure 3.34: Comparison of the detachment energy for different dispersions at 77°F. KT represents an energy unit which is called Boltzmann constant (KT = 4.11 $\times 10^{-21}$ Joule).

Figure 3.35 shows the contact angle for the optimum solution, 0.5 wt% of AOS solution in the presence of 0.1 wt% of SiO_2, at different temperatures. The contact angle (θ) decreased as temperature increased. SiO_2 with contact angles less than 40° failed to stabilize foam, whereas nanoparticles with θ = 86° successfully stabilized foam.

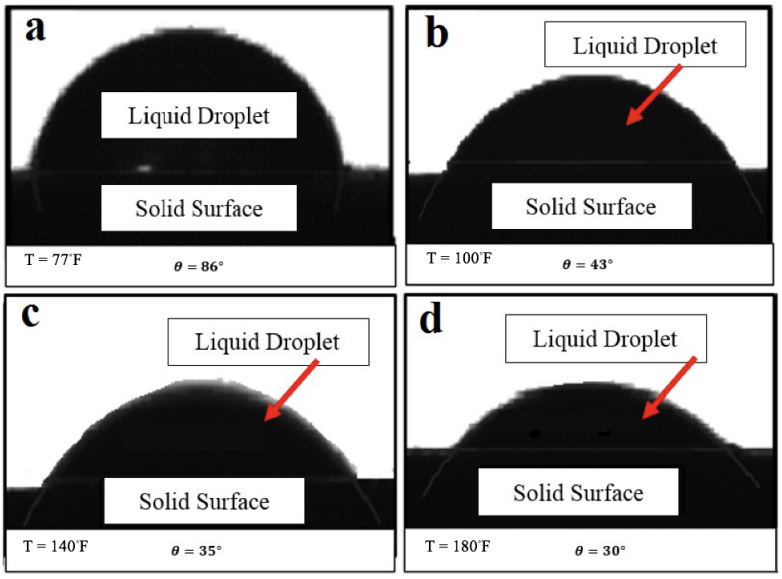

Figure 3.35: Contact angle for 0.5 wt% AOS + 0.1 wt% SiO_2 at (a) 77°F, (b) 100°F, (c) 140°F, and (d) 180°F.

Figure 3.36 shows the detachment energy (E) for AOS solution including SiO_2 from 77 to 180°F. It is proposed that the extreme variation of the detachment energy with wettability and temperature has a major influence on the ability of nanoparticles of different wettability and temperature to stabilize foam.

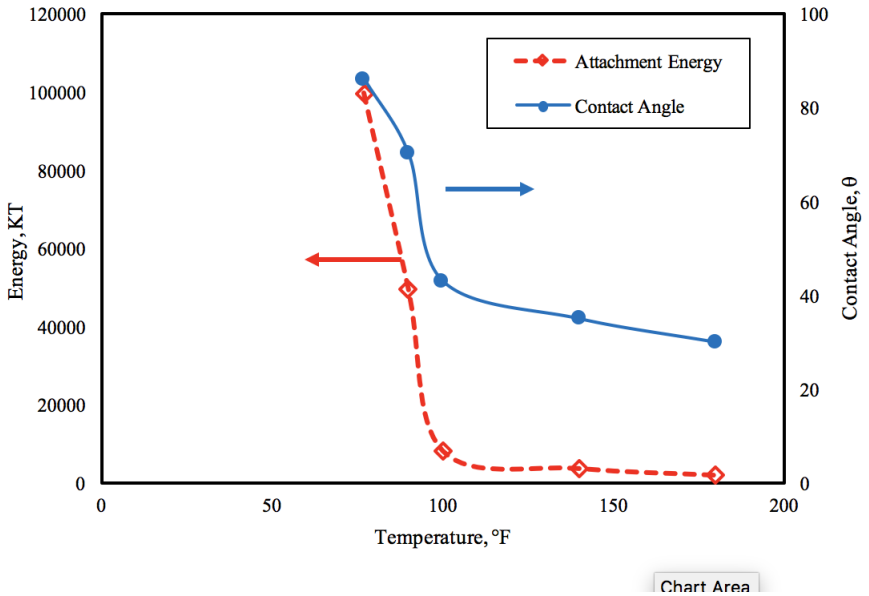

Figure 3.36: Detachment energy for the AOS solutions in the presence of 0.1 wt% of SiO_2 nanoparticles as a function of temperature.

3.5 Zeta Potential

Zeta potential is another parameter that can determine stability of colloidal dispersions. High gas-liquid interfacial areas of colloidal dispersions result in the foam instability since system's free energy increased. Accordingly, minimizing the free energy of the system is of great importance in acquiring stable foam. The electrokinetic properties of a colloidal system can be described using zeta potential. With a low zeta potential value, agglomeration might happen because of attraction between nanoparticles as a result of the van der Waals force as mentioned previously [81].

Zeta potential can also indicate the repulsion degree between adjacent nanoparticles in a dispersion. The surface potential value is related to the electrical double-layer thickness and the surface charge. Figure 3.37 shows that zeta potential values for four different dis-

persions, AOS, and AOS-guar solution in the presence of two different nanoparticles, SiO_2 and Fe_2O_3. The most negative values were observed for the AOS solution in the presence of nanoparticles. A high absolute value of the zeta potential will show stability for small nanoparticles that survive nanoparticle aggregation to enter the solution. In contrast to the high value, a low zeta potential value means that the attraction force is greater than the repulsion force between nanoparticles.

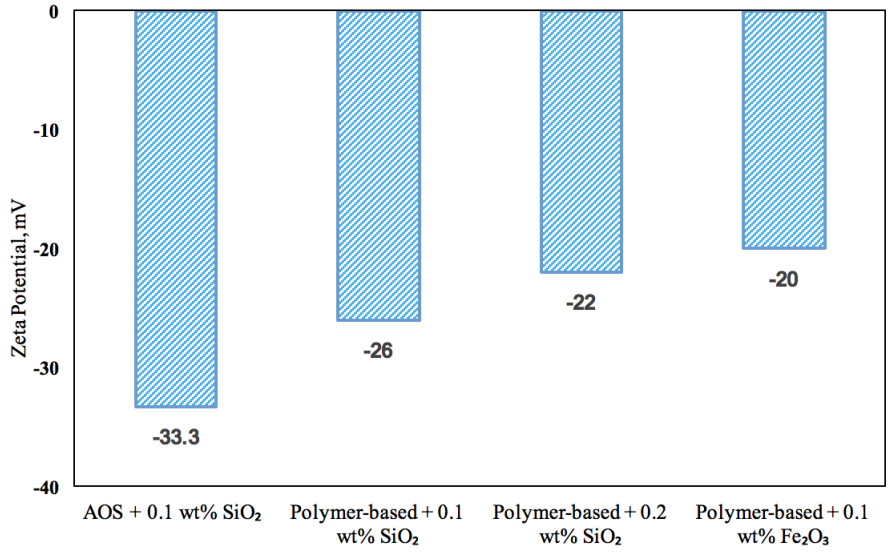

Figure 3.37: Zeta potential of nanoparticles for the AOS solution and the AOS-guar solution in the presence of nanoparticles at 77°F.

Higher stability is observed for nanoparticle suspensions with the 0.5 wt% AOS and 0.1 wt% SiO_2. Adding polymers to the solution that contains surfactant and nanoparticles results in nanoparticle agglomeration. This is due to the low zeta potential of such suspension wherein the repulsion force is less than attraction force and thus Fe_2O_3 nanoparticles

start to agglomerate.

3.6 Coreflood

CO_2-foam, consisting of low amounts of water and high amounts of compressed gas, minimize formation damage to unconventional reservoirs through fast cleanup and recovered permeability, as most of the gas flows back after depressurization [82]. However, CO_2-foams have some potential weaknesses. Foams are thermodynamically and kinetically unstable because the surface energy of gas/liquid interfaces tends to decrease as they degenerate into separate gas and liquid phases. At high-temperature reservoir conditions, surfactants generally tend to degrade. In addition, surfactant loss in a reservoir due to adsorption in the porous medium leads to a large chemical consumption especially in CO_2-foam flooding. Thus, high reservoir temperature can be a major feature governing the economic viability of CO_2-foam flooding, and can also be another factor of foam instability.

Foam stability improvement, especially in severe reservoir conditions, is a pivotal parameter to increase sweep efficiency. The addition of thickeners such as polymers for the CO_2-foam has been addressed to improve the foam stability [83]. Mixing surfactant and polymer may reduce fluid viscosity at high temperatures. However, adding nanoparticles to the mixture may enhance the liquid phase viscosity and stabilize CO_2-foam at high pressures and high temperatures (HP/HT). It is known that nanoparticles can adsorb at the gas/liquid interfaces to stabilize bubbles in foams by creating a rigid protective barrier around dispersed bubbles, which can reduce liquid film drainage.

Nanoparticles have been researched extensively as a means to stabilize foams used in oil production operations [67, 13]. Various other aspects of the nanoparticle-stabilized foams, such as the effect of salinity on the nanoparticle concentrations, have been established by [4]. They showed foam stability was improved as nanoparticle concentration

increased under high salinity conditions. Although longer-lasting foams have been generated by various systems, the stability of these foams in the presence of crude oil and corefloods at high temperature has not been explored extensively.

Foam was introduced by [84] more than 35 years ago to be a candidate for improving sweep efficiency and mobility control of oil-recovery drive fluids. Foams improve the oil recovery by decreasing the interfacial tension between the crude oil and the drive fluid. Moreover, foam has a greater percentage of gas (70-90%), which decreases the amount of water. Therefore, less water can be used to decrease CO_2 mobility. [5] showed that the equilibrium adsorption of nanoparticles in different porous media is very low. Also, nanoparticles cannot change the core permeability based on their coreflood tests.

The purpose of this part is to investigate ways to improve foam properties and increase MRF in nanoparticle-based foams when used as hydraulic fracturing fluids. The experimental studies included: (1) foam stability and foamability study for different solutions, and (2) coreflooding tests to understand the effect of nanoparticles and polymers on MRF at high salinity and high temperature. To achieve this objective, coreflood tests were conducted on Buff Berea sandstone cores at temperatures from 77 up to 250°F. CO_2 was injected with the prepared solutions simultaneously to generate foam with 80% quality. The breakthrough time was monitored for each solution compared to 5 wt% NaCl brine.

3.6.1 Foamability

Foamability of the solutions was studied by performing a shake test. To generate foam, 5 cm3 of solutions, with and without SiO_2, were shaken at ambient conditions for one minute. Figure 3.38 shows the results of the foam shake test at the 77°F and subsequent foam degradation over a time interval of 24 hours for the AOS solution (a), a mixture of the AOS solution and SiO_2 nanoparticles (b), and a mixture of the AOS solution, guar, and SiO_2 nanoparticles (c). Larger bubbles continuously coalesced with smaller ones which

mean bubble size rapidly expands over time owing to the pressure differences produced by the Young-Laplace effect [85].

The basic foam test also shows that the mixture of the AOS solution and nanoparticles can generate stronger foams with fine textures that may remain stable longer (24 hours). This behavior is due to the nanoparticle's adsorption to the interface between the two phases and minimizes the contact area between them; as a result, it can build a strict barrier that prevents droplets coalescence. Note that SiO_2 nanoparticle with size of 140 nm rader than Fe_2O_3 is selected and employed in all coreflood experiments as it is observed to significantly outperform Fe_2O_3 in stabilizing foam.

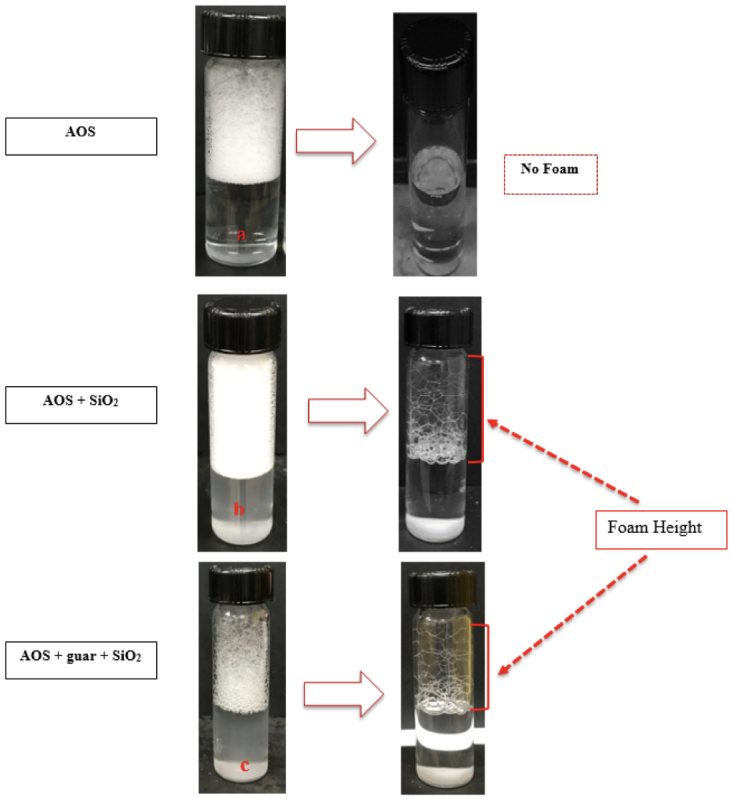

Figure 3.38: Foam shake test for 0.5 wt% of AOS in the absence (a), presence of 0.1 wt% of SiO_2 (b), and presence of 4 ppt guar-gum and SiO_2 (c) at ambient conditions for 5 wt% of NaCl.

3.6.2 Foam Stability

Foam as a hydraulic fracturing fluid is generated on the surface and then injected into the well and passed into the formation. The temperature of the foam is a function of well's depth that means its temperature is increased as it penetrates deeper in the formation. Foam stability decays at high temperatures which can negatively affect the fluid fracturing performance. Adding nanoparticles and polymer to the surfactant solution improves foam stability at high temperatures. Thus, the half-life of nanoparticle and polymer-based solu-

tions has been studied at different temperatures in this work to illustrate their influence on the foam stability.

Figure 3.39 indicates half-life four solutions, the AOS solution, the AOS + SiO_2 solution, the polymer-based solution, and the polymer-based + SiO_2 solution. As mentioned previously, the nanoparticle-based solution was made by stabilizing basic solution with SiO_2 with diameters of 140 nm. To generate other solutions, the basic solution was stabilized using 20 ppt guar-gum. All experiments were run at 300 psi, while temperature increased from 77 to 180°F. Foam half-life decreases as the temperature increases. Furthermore, results show that nanoparticle foams were more stable over time compared to those stabilized by guar-gum at both temperature examined. Results also show that the bubble size for polymer-based solution increased as temperature increased (Figure 3.40). In addition, bubbles collapsed faster at 140°F compared to 77°F. As the temperature went beyond 140°F, the foam disappeared very quickly and was not observed in the cell. Using nanoparticles in the solution is one way to increase foam stability. Consequently, foam stability improved when nanoparticles were added to both the AOS and the polymer-based solutions at high temperatures.

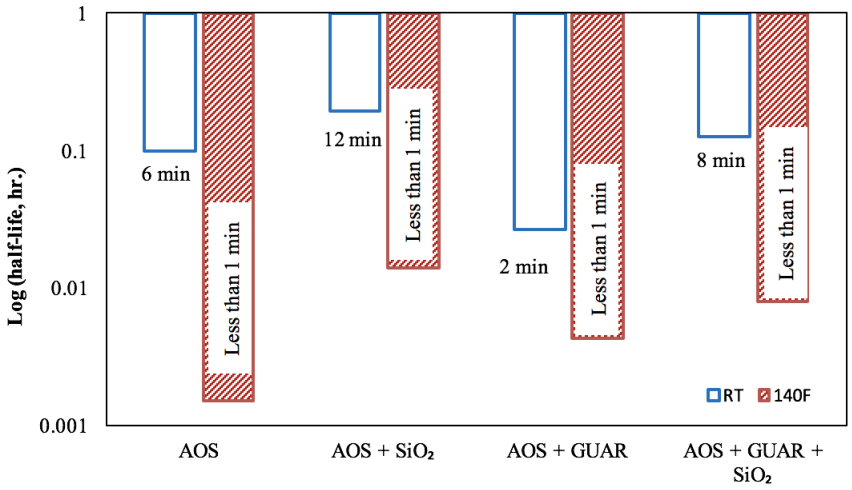

Figure 3.39: Log (half-life) for room temperature (77°F) and 140°F at 300 psi for 0.5 wt% of AOS.

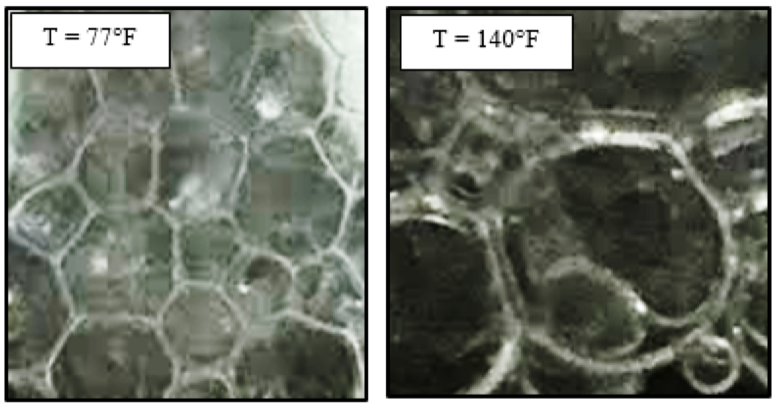

Figure 3.40: Threshold image, of selected section at initial time (polymer-based). The bubble size increases as temperature increases.

To measure pressure drop across the core, the core was flooded with brine (5 wt% of NaCl) of 2 PV. Then AOS solution (0.5 wt% of AOS) was injected at a flow rate of 120 ml/hr. Figure 3.41 presents the pressure drop across the core in the case of foam (CO_2 + AOS) in comparison to the baseline pressure drop for brine-CO_2 coinjection at 77°F. The pressure drop for the brine-CO_2 coinjection stabilized around 7 psi, where no changes occurred in the fluid saturations and the relative permeability inside the core. In the case of foam, the pressure drop across the core continuously increased as a result of replacing the low viscosity fluids (CO_2 gas or water) with high apparent viscosity for the foam [43]. As the two cases having the same flow rate (total flowrate = 10 cm^3/min) and percentage of gas (80%), Eq. 2.3 was used to calculate the MRF. The MRF for the foam (CO_2 + AOS solution) increased with time to three after injection of six pore volumes. The presence of AOS in the foam solution as an anionic surfactant improved the MRF by 300%. In other words, the apparent foam viscosity is three times that of the brine/CO_2 viscosity.

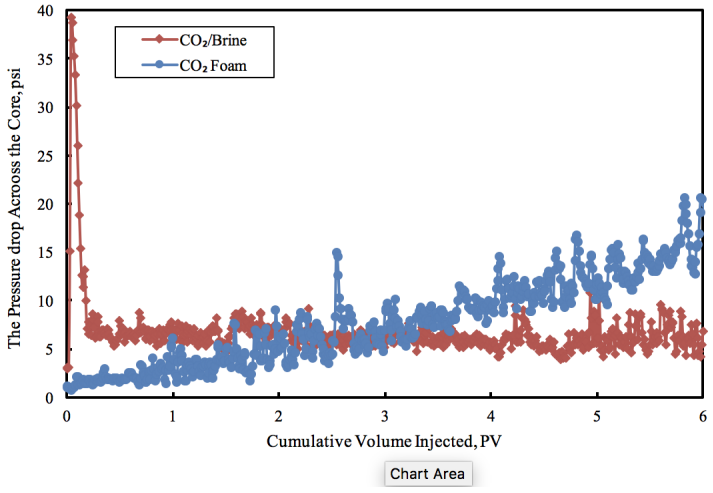

Figure 3.41: A comparison of the drop pressure across the core between CO_2-Foam injection and brine-CO_2 Coinjection at 77°F.

3.6.3 Nanoparticles Effect

Figure 3.42 shows the effect of nanoparticles on pressure drop for foam solutions. The addition of SiO_2 with 140 nm to the AOS solution improved foam stability and increased the pressure drop at ambient conditions. The presence of nanoparticles in foam solution increases the foam stability and form fine texture foam.

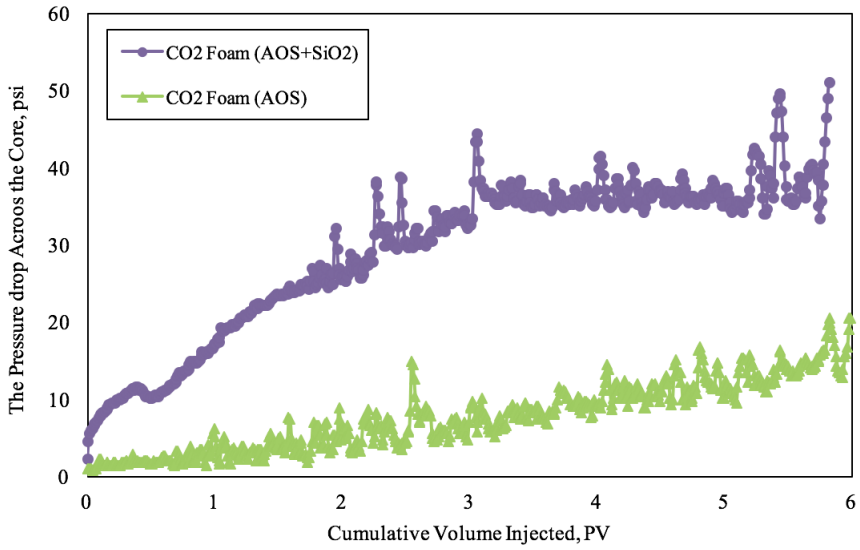

Figure 3.42: A comparison of the pressure drop between AOS solution in the absence and presence of nanoparticles and 77°F.

Figure 3.43 show the foam height at the core outlet in the presence and in the absence of nanoparticles of the AOS solution before and after breakthrough. These results confirm the increases in the MRF in case of the presence of nanoparticles. This comparison gives qualitatively an indicator for foam stability in both cases, where the foam was more stable in the case AOS solution in the presence of nanoparticles. The foam in the pres-

ence nanoparticles (Figure 3.43 (a)) is more stable, longer life time, and with fine texture compared to the foam with the absence of nanoparticles (Figure 3.43 (b)).

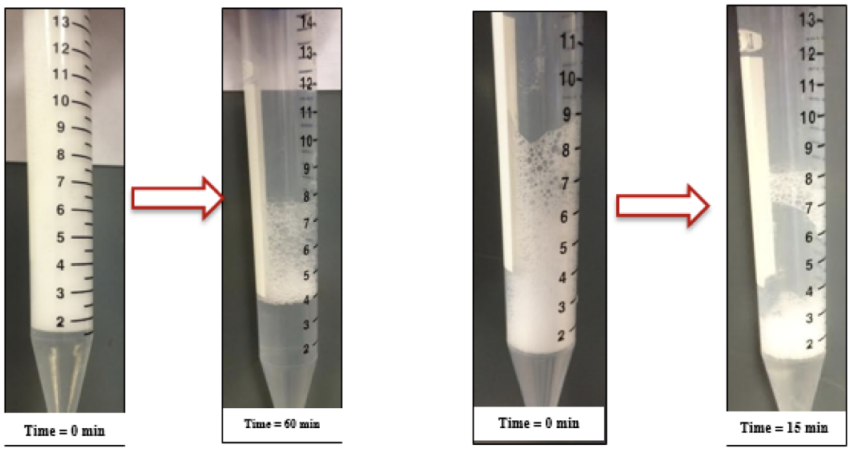

Figure 3.43: A comparison of the foam height for AOS solution in the (a) presence and (b) absence of SiO_2 nanoparticles at 77°F.

Foam breakthrough tends to have the maximum pressure drop at the outlet (Figure 3.44). Due to coalescence of the bubbles caused by diffusion and breaking of the foam films pressure drops after breakthrough. However, the behavior of the pressure drop after the foam breakthrough for nanoparticle-based foam was observed to be very small compared to that of the solution without nanoparticle which implies that foam coalescence barely happened and is an indicator of very stable foam.

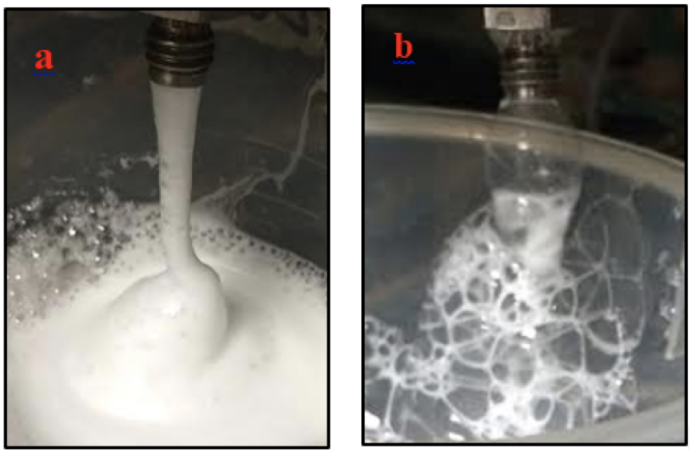

Figure 3.44: A comparison of the outlet production (a) before breakthrough and (b) after breakthrough for AOS + SiO_2 solution.

Figure 3.45 shows the effect of nanoparticles on MRF for foam solutions. The addition of SiO_2 with 140 nm to the AOS solution improved foam stability and increased the MRF to eight after injection of six pore volumes at ambient conditions (which is double the MRF for in the absence of nanoparticles). Addition of nanoparticles leads to formation of fine texture foam which increases foam apparent viscosity and thus can improve foam stability and the mobility control factor. Since, the number of foam lamellae films within a given volume of the porous rock has increased. Furthermore, foams with higher gas fraction, i.e., a high quality and very stable foam, necessitate more deformation to happen and flow has lower mobility. On the other hand, when the foam quality is low, wet foams are produced. Wet foams are more mobile than dry foams because the bubbles in wet foams are more spherical and uniform; hence, there is very small interference between bubbles, thus resisting flow [70].

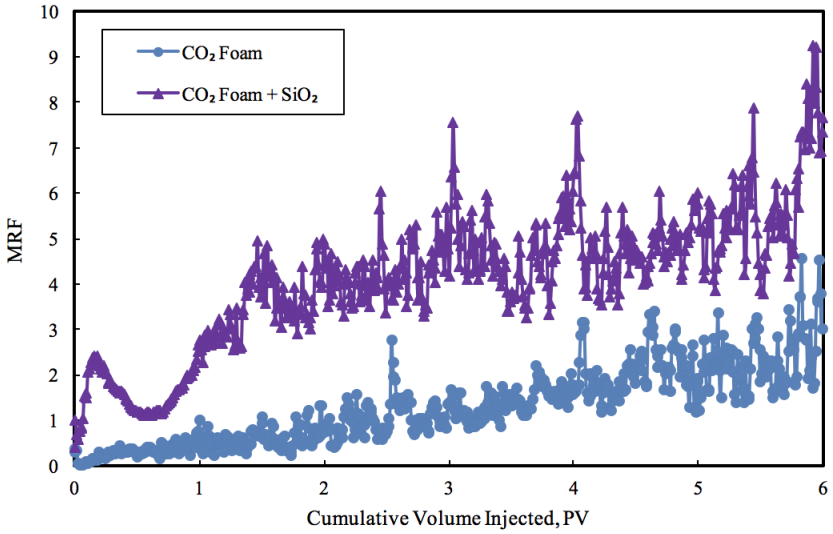

Figure 3.45: A comparison of the MRF between AOS solution in the absence and presence of nanoparticles and 77°F.

3.6.4 Temperature Effects

As mentioned previously, temperature plays a critical role to control foam stability by influencing the diffusion rate and surfactant adsorption at the gas/water interface and rock surface [29]. To examine the performance of nanoparticles at high-temperature, the previous two experiments were repeated at 250°F.

Figure 3.46 plots the pressure drop across the core in the case of foam injection, both AOS and polymer-based solutions, and brine-CO_2 coinjection. At high-temperature the gap between the pressure drops across the core significantly increased. This is a result of viscosity reduction for the brine from 0.9 to 0.106 cp at 77 and 250°F, respectively [86].

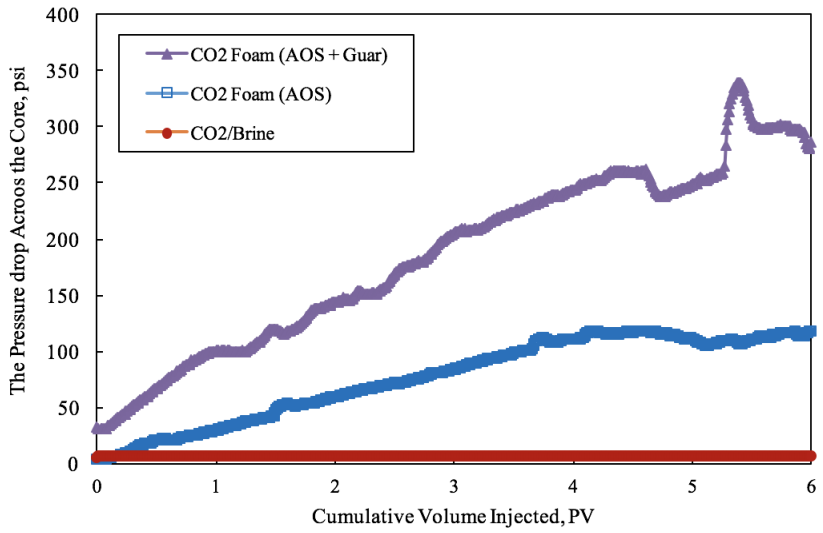

Figure 3.46: A comparison of the pressure drop between CO_2-Foam (AOS and AOS + Guar) and CO_2 Gas at 250°F.

Figure 3.47 shows the same MRF value for both solutions, AOS alone and AOS with SiO_2 nanoparticles at 250°F. No change was observed, which was anticipated from the foam stability measurements at this temperature. The drainage half-life decreased as temperature increased. Two reasons might cause this phenomenon. First, the density of the CO_2 gas was reduced by increasing temperature. Second, it might occur due to the decrease in liquid viscosity as temperature increases.

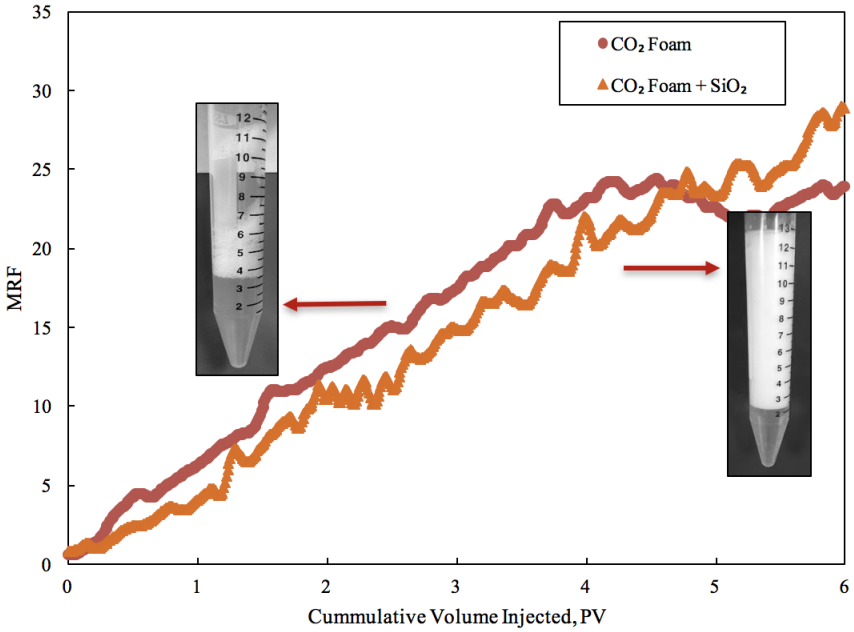

Figure 3.47: A comparison of the MRF between AOS in the presence and absence of SiO_2 at 250°F

3.6.5 Polymer Effect

It has been observed that polymer based solutions generate foams that tend to show a very unstable behavior. Owing to weak attachment of polymer molecules to the bubbles' surface and low adsorption at the interface, polymer based foams rapidly decay at less than 10-20 second. A mixture of polymer and surfactant (polymer-based solution) might considerably enhance foam stability. In fact, thanks to instant adsorption of surfactant molecules and as a result of the Marangoni effect, the process of foam film thinning is decelerated which leads to a longer adsorption time and consequently longer film stabilization time (Figure 3.25 and Figure 3.30).

Figure 3.48 compares pressure drop across the core between the polymer-based and

baseline solutions at 77°F. As one can see, pressure drop increases for polymer-based solution.

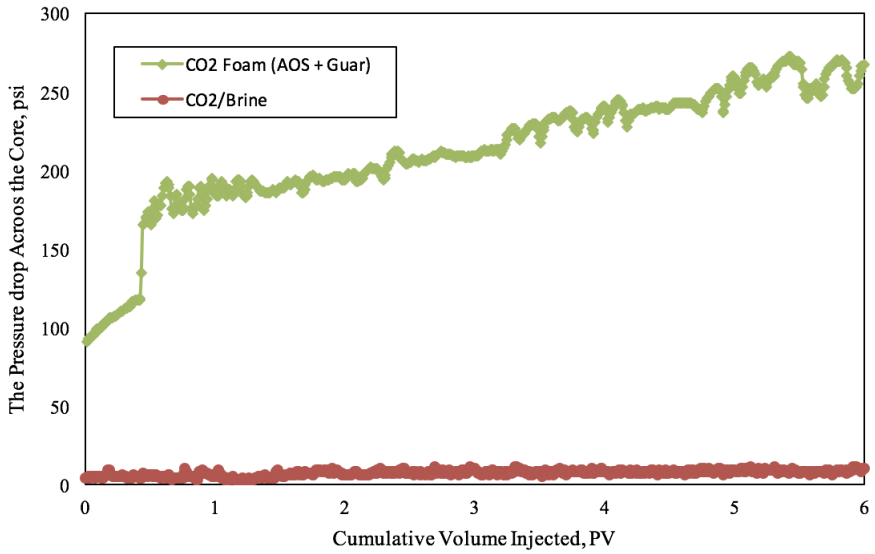

Figure 3.48: A comparison of the drop pressure between CO_2-Foam injection (AOS + Guar) and brine-CO_2 Coinjection at 77°F.

Figure 3.49, Figure 3.50, and Figure 3.51 indicate that the MRF value for guar-gum solution, polymer-based solution in the presences of SiO_2 nanoparticles at 77, 140 and 250°F respectively. Results show that MRF for the polymer-based solution with SiO_2 nanoparticles is higher compared to the solution without nanoparticles. The polymer-based solution in the presence of nanoparticle (SiO_2) shows a higher MRF comparing to the other two solutions. In a regular waterflood practice, a polymer with high-molecular-weight and viscosity-enhancing property is entered into the water which remarkably reduces the flood water mobility and subsequently increase sweep efficiency characteristic of the waterflood.

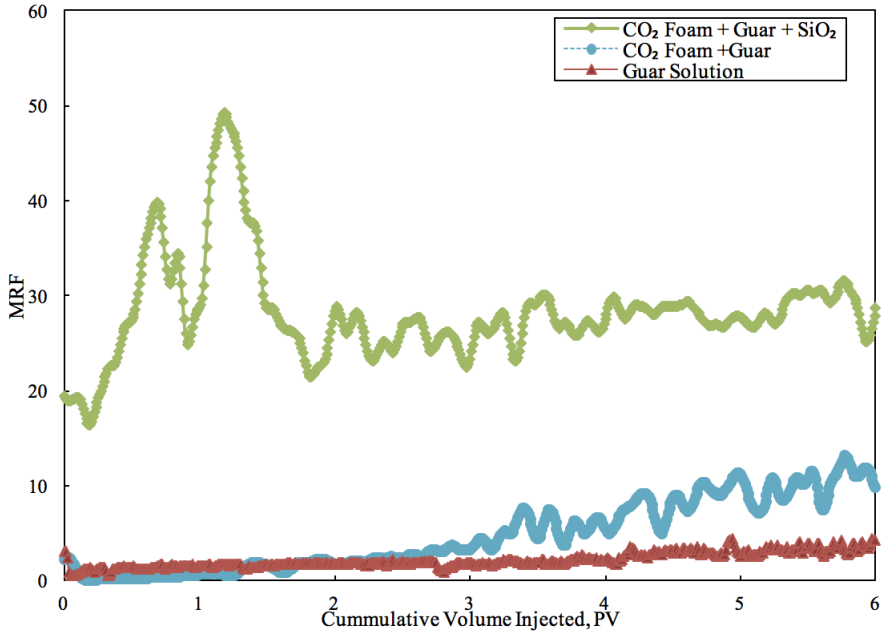

Figure 3.49: A comparison of the MRF between guar solution, CO_2-Foam (AOS+ guar) in the presence, and absence of SiO_2 at 77°F.

As discussed in the previous section, the high temperature decreases the liquid viscosity and foam stability. By adding guar-gum to the solution, the liquid viscosity increases, and the viscosity slows down the drainage of liquid at initial time and keeps the liquid film thicker that causes the foam to stay at a stable state for a longer time. Thus, adding polymer and nanoparticles to the base solution can improve foam stability under harsh reservoir conditions (high-temperature and high salinity). Note that, 40% damage on Berea sandstone was observed while injecting polymer-based solution at 140°F.

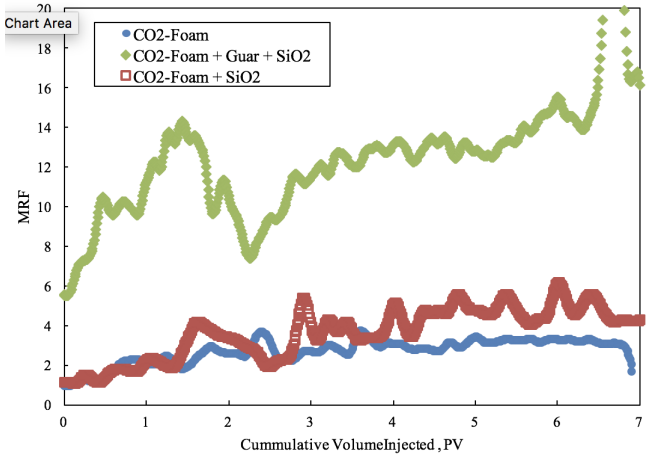

Figure 3.50: A comparison of the MRF between CO_2-Foam and CO_2-Foam + guar in the presence and absence of SiO_2 at 140°F.

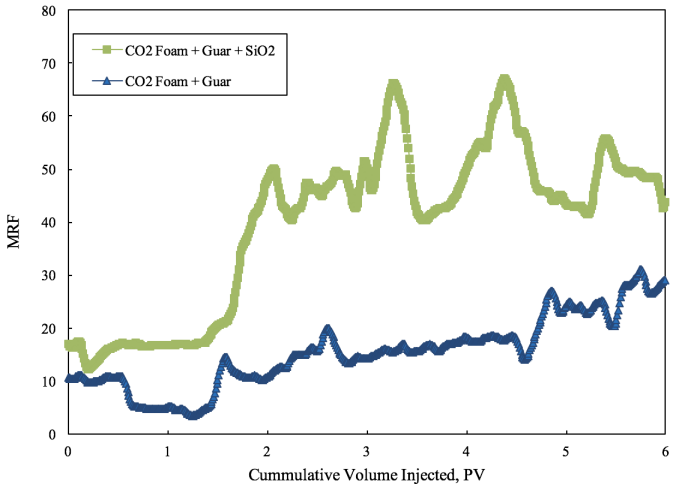

Figure 3.51: A comparison of the MRF between CO_2-Foam + guar in the presence and absence of SiO_2 at 250°F.

The addition of SiO_2 nanoparticles to the AOS solution generates more stable foam with a fine texture that increases the mobility control factor. As a result, the performance of foam as an EOR fluid improved by increasing the sweep efficiency. No improvement on the MRF was found by adding the nanoparticles, but adding a viscosifier to the AOS solution allows the nanoparticles to increase the MRF at high temperature. Designing field development plans for EOR practices requires considering quite a few essential parameters like high risk of unfavorable instances and capital sensitivity to name a few. Hence, it is of paramount importance to select the best recovery method for underlying reservoirs. Moreover, acquiring an efficient enhanced oil recovery method necessitates expertise along with many other assumptions on properties of reservoir and fluid flow within the porous medium [87].

4. CONCLUSIONS AND RECOMMENDATIONS

4.1 Surface Tension Measurement to Find the CMC Value

The choice of the surfactant concentration is a critical step in preparing a more stable foam. However, surface adsorption, cost, surfactant loss or degradation under a high temperature reservoir limits the economic viability of the surfactants usage. Using nanoparticles as a stabilizer to form foam can be another substitute for harsh reservoir conditions. In the present study, a new foaming solution was introduced in order to evaluate and optimize the surfactant concentration in formations of stable CO_2-foams in unconventional reservoirs. Based on the experiments conducted and results obtained for the experiments, the following conclusions are summarized:

1. The dynamic surface tension continuously decreased until reaching a constant value after 2 hours at ambient temperature. The dynamic surface tension reduction may be explained by the adsorption of CO_2 into the AOS solution.

2. The equilibrium surface tension decreased as the pressure, temperature, and salt concentration increased.

3. Based on the experiments conducted and the results obtained for the experiments, the surface tension decreased with increasing surfactant concentrations and pressures for all electrolyte concentrations until it reached a minimum. The surface tension values changed slightly after this minimum and remained constant afterward. The minimum point is known as a CMC value. The CMC value for the CO_2/AOS solution was 0.025 wt% at ambient conditions in the presence of 1 wt% NaCl.

4. Surface tension decreased when salt concentrations increased since in the presence of salt, ionic repulsions between the head-groups decreased so, the double-layer thickness decreased. However, the dependence of surface tension on temperature was more complex

than that on either pressure or salinity.

5. In the presence of nanoparticles, the equilibrium time for saturation of the solution decreased.

6. The CMC value decreased as salt concentration increased or temperature decreased. Also, the CMC value decreased while nanoparticles were added to the solution. As a result, surfactant concentrations must be above the CMC value to obtain proper properties for foaming foams.

7. Nanoparticles were observed to promote CO_2-foam formation in AOS solutions. Adding a small amount of nanoparticles (0.1 wt%) to AOS solutions could improve the CO2-foam stability.

4.2 Foam Stability

8. Nanoparticles can promote CO_2-foam formation in AOS solutions at HP/HT and high salinity.

9. The contact angle has a strong effect on the detachment energy. It also influences the foam stability in the presence of nanoparticles. An optimal value for contact angle has been calculated to increase foam stability.

10. At high temperatures, the optimum composition and concentration to stabilize foam is obtained by a high nanoparticle concentration with a lower surfactant concentration.

11. By adding guar-gum to the solution, the liquid viscosity increases, and the viscosity slows down the drainage of liquid and keeps the liquid film thicker, thus causing the foam to stay at a stable state for a longer time.

12. In contrast to the guar-based solutions, a mixture of SiO_2 nanoparticles and guar, can improve foam stability because the interfacially active nanoparticles can adsorb at the gas-liquid interface and stabilize foams.

13. Foam stability of polymer-based solutions was strongly reduced as compared to that of the AOS solution in the presence of nanoparticles. Stabilizing foams using nanoparticles results in more stable foams in contrast to when polymer-based is utilized to do so. This is mainly because of high adsorption energy of the nanoparticles at interfaces comparing to low adsorption energies of polymer-based.

14. Polymer-based solutions with Fe_2O_3 had a tendency to agglomerate in the solution because of the high surface energy of these nanoparticles.

15. With a high zeta potential value, the 0.5 wt% AOS + 0.1 wt% SiO_2 showed high stability for nanoparticle suspensions. However, when the zeta potential of a suspension was low (-20.5 mV), as in polymer-based solution with Fe_2O_3, it means the attraction force is more than repulsion force; therefore, nanoparticles start to agglomerate.

4.3 Core Flood

Utilizing CO_2-foam improves CO_2 effective viscosity that introduces a better sweep efficiency and provides mobility control. CO_2-foams can be stabilized by increasing the viscosity of the liquid phase through employing polymers along with surfactants. The interfacial tension and the amount of water used in the system can also be minimized using polymer-based foams. Therefore, they are a suitable choice of interest for ultra-tight gas reservoirs and coalbed methane wells that contain water. The problem with using the mixture of surfactant and polymer is that it may reduce fluid viscosity at high temperatures. Adding nanoparticles to the mixture may enhance the liquid phase viscosity and stabilize CO_2-foam at HP/HT. This study investigates the effect of polymer and nanoparticles in addition to surfactant on foam stability and MRF calculation in porous media. The main conclusions are summarized as follow:

16. Results show that, in the absence of nanoparticles, the pressure drop across the core is lower than in all cases where nanoparticles are present.

17. The CO_2-foam can provide enough viscosity so that it can be used as a hydraulic fracturing fluid.

18. Addition of nanoparticles increases the foam stability, which greatly increases the MRF of the injected gas compared to surfactant.

19. At 250°F, CO_2-foam has a higher pressure drop compared the gas/brine solution.

20. No change was found for MRF value by adding nanoparticles to the foam solution at 250°F. Foam stability and MRF value increased when guar-gum is added to the AOS solution.

4.4 Recommendation

Oil production using enhanced oil recovery techniques and especially through performing hydraulic fracturing has been increased in recent years. This in turn significantly escalates the demand for high performance fracturing fluids which cause low formation damage in porous medium. Traditional fracturing fluids use water viscosifying agents such as guar-gum and its derivatives to support and carry the proppant. However, guar gum forms an insoluble residue in the formation, and these insoluble materials plug pore throats, causing formation damage that could be fatal to the reservoirs. Recent advances in foam fracturing techniques has attracted many researchers and engineers to focus on the foaming fluids particularly due to the small liquid volume of such fracturing fluids which drastically decreases the formation damage in sensitive reservoirs.

Based on the obtained results, adding polymer and nanoparticles to the base solution can improve foam stability under harsh reservoir conditions. Note that, 40% damage on Berea sandstone was observed while injecting polymer-based solution. Formation damage can be decreased or completely avoided either by adding polymer breaker to polymer-based solution or though adding nanoparticle to surfactant-based solution.

REFERENCES

[1] F. AttarHamed, M. Zoveidavianpoor, and M. Jalilavi, "The incorporation of silica nanoparticle and alpha olefin sulphonate in aqueous CO_2 foam: Investigation of foaming behavior and synergistic effect" in Journal of Petroleum Science and Technology, vol. 32, no. 21, pp. 2549–2558, 2014.

[2] Y. Chen, A. S. Elhag, B. M. Poon, et al., "Ethoxylated cationic surfactants for CO_2 EOR in high temperature, high salinity reservoirs" in SPE Improved Oil Recovery Symposium, Society of Petroleum Engineers, SPE-154222-MS, 2012.

[3] L. Ribeiro, and M. Sharma, "Fluid selection for energized fracture treatments" in SPE Hydraulic Fracturing Technology Conference, Society of Petroleum Engineers, SPE-163867-MS, 2013.

[4] D. A. Espinoza, F. M. Caldelas, K. P. Johnston, et al., "Nanoparticle-stabilized supercritical CO_2 foams for potential mobility control applications" in SPE Improved Oil Recovery Symposium, Society of Petroleum Engineers, SPE-129925-MS, 2010.

[5] J. Yu, N. Liu, L. Li, et al., "Generation of nanoparticle-stabilized supercritical CO_2 foams" in Carbon Management Technology Conference, Carbon Management Technology Conference, CMTC-150849-MS, 2012.

[6] D. Mo, J. Yu, N. Liu, et al., "The application of nanoparticle-stabilized CO_2 foam for oil recovery" in SPE International Symposium on Oilfield Chemistry, Society of Petroleum Engineers, SPE-164074-MS, 2013.

[7] A. Worthen, H. Bagaria, Y. Chen, et al., "Nanoparticle stabilized carbon dioxide in water foams for enhanced oil recovery" in SPE Improved Oil Recovery Symposium, Society of Petroleum Engineers, SPE-154285-MS, 2012.

[8] A. Habibi, M. Ahmadi, P. Pourafshary, et al., "Reduction of fines migration by nanofluids injection: an experimental study" SPE Journal, vol. 18, no. 02, pp. 309–318, SPE-144196-MS, 2012.

[9] M. G. Aarra, P. A. Ormehaug, A. Skauge, et al., "Experimental study of CO_2-and methane-foam using carbonate core material at reservoir conditions" in SPE Middle East Oil and Gas Show and Conference, Society of Petroleum Engineers, SPE-141614-MS, 2011.

[10] J. Solbakken, A. Skauge, and M. Aarra, "Supercritical CO_2 foam-the importance of CO_2 density on foams performance"in SPE Enhanced Oil Recovery Conference, Society of Petroleum Engineers, SPE 165296-MS, 2013.

[11] L. L. Schramm, Surfactants: fundamentals and applications in the petroleum industry. Cambridge University Press, 2000.

[12] J. Sheng, Enhanced oil recovery field case studies. Gulf Professional Publishing, 2013.

[13] D. Mo, J. Yu, N. Liu, et al., "Study of the effect of different factors on nanoparticle-stablized CO_2 foam for mobility control" in SPE Annual Technical Conference and Exhibition, Society of Petroleum Engineers, SPE-159282-MS, 2012.

[14] R. Farajzadeh, A. Andrianov, R. Krastev, et al., "Foam–oil interaction in porous media: Implications for foam assisted enhanced oil recovery" Advances in Colloid and Interface Science, vol. 183, pp. 1–13, 2012.

[15] J. A. Rushing, K. E. Newsham, K. C. Van Fraassen, et al., "Laboratory measurements of gas-water interfacial tension at hp/ht reservoir conditions" in CIPC/SPE Gas Technology Symposium 2008 Joint Conference, Society of Petroleum Engineers, SPE-114516-MS, 2008.

[16] M. A. Malik, M. A. Hashim, F. Nabi, et al., "Anti-corrosion ability of surfactants: a review" Int. J. Electrochem. Sci, vol. 6, no. 6, pp. 1927–1948, 2011.

[17] M. J. Rosen, and J. T. Kunjappu, "Surfactants and interfacial phenomena" John Wiley & Sons, 2012.

[18] J. Salager, J. Morgan, R. Schechter, et al., "Optimum formulation of surfactant/water/oil systems for minimum interfacial tension or phase behavior" Society of Petroleum Engineers Journal, vol. 19, no. 02, pp. 107–115, SPE-7054-PA, 1979.

[19] J. Sheng, Modern chemical enhanced oil recovery: theory and practice. Gulf Professional Publishing, 2010.

[20] D. Oussoltsev, I. Fomin, K. Butula, et al., "Foam fracturing: New stimulation edge in western siberia (russian)" in SPE Russian Oil and Gas Technical Conference and Exhibition, Society of Petroleum Engineers, SPE-115558-RU, 2008.

[21] D. Gupta "Unconventional fracturing fluids for tight gas reservoirs" in SPE Hydraulic Fracturing Technology Conference, Society of Petroleum Engineers, SPE-119424-MS, 2009.

[22] H. Nasr-El-Din, and A. Al-Ghamdi, "Effect of acids and stimulation additives on the cloud point of nonionic surfactants" in SPE Formation Damage Control Symposium, Society of Petroleum Engineers, SPE-31106-MS, 1996.

[23] L. B. Romero-Zeron, and A. Kantzas, "The effect of wettability and pore geometry on foamed-gel-blockage performance" SPE Reservoir Evaluation & Engineering, vol. 10, no. 02, pp. 150–163, SPE-89388-PA, 2007.

[24] J.-S. Tsau, A. E. Syahputra, H. Yaghoobi, et al., "Use of sacrificial agents in CO_2 foam flooding application" in SPE annual technical conference, SPE 56609-MS, 1999.

[25] L. P. Singh, S. K. Bhattacharyya, R. Kumar, et al., "Sol-gel processing of silica nanoparticles and their applications" Advances in Colloid and Interface Science, vol. 214, pp. 17–37, 2014.

[26] C. Vashisth, C. P. Whitby, D. Fornasiero, et al., "Interfacial displacement of nanoparticles by surfactant molecules in emulsions" Journal of Colloid and Interface Science, vol. 349, no. 2, pp. 537–543, 2010.

[27] A. Andrianov, R. Farajzadeh, M. Mahmoodi Nick, et al., "Immiscible foam for enhancing oil recovery: bulk and porous media experiments" Industrial & Engineering Chemistry Research, vol. 51, no. 5, pp. 2214–2226, 2012.

[28] R. Farajzadeh, R. Krastev, and P. Zitha, "Foam films stabilized with alpha olefin sulfonate (aos)" Colloids and Surfaces A: Physicochemical and Engineering Aspects, vol. 324, no. 1, pp. 35–40, 2008.

[29] R. Farajzadeh, A. Andrianov, H. Bruining, et al., "Comparative study of CO_2 and N_2 foams in porous media at low and high pressure- temperatures" Industrial & Engineering Chemistry Research, vol. 48, no. 9, pp. 4542–4552, 2009.

[30] G. Kubala, "Aqueous gelling and/or foaming agents for aqueous acids and methods of using the same" Sept. 22 1987. US Patent 4,695,389.

[31] K. E. Cawiezel, and D. Gupta, "Successful optimization of viscoelastic foamed fracturing fluids with ultralightweight proppants for ultralow-permeability reservoirs" SPE Production & Operations, vol. 25, no. 01, pp. 80–88, SPE-119626-PA, 2010.

[32] A. Belhaij, A. AlQuraishi, O. Al-Mahdy, et al., "Foamability and foam stability of several surfactants solutions: The role of screening and flooding" in SPE Saudi Arabia Section Technical Symposium and Exhibition, Society of Petroleum Engineers, SPE-172185-MS, 2014.

[33] K. Malysa and K. Lunkenheimer, "Foams under dynamic conditions" Current Opinion in Colloid & Interface Science, vol. 13, no. 3, pp. 150–162, 2008.

[34] S. S. Adkins, X. Chen, I. Chan, et al., "Morphology and stability of CO_2-in-water foams with nonionic hydrocarbon surfactants" Langmuir, vol. 26, no. 8, pp. 5335–5348, 2010.

[35] R. Petkova, S. Tcholakova, and N. Denkov, "Foaming and foam stability for mixed polymer–surfactant solutions: effects of surfactant type and polymer charge" Langmuir, vol. 28, no. 11, pp. 4996–5009, 2012.

[36] D. Langevin, "Complexation of oppositely charged polyelectrolytes and surfactants in aqueous solutions. a review" Advances in Colloid and Interface Science, vol. 147, pp. 170–177, 2009.

[37] G. A. Pope, K. Tsaur, R. S. Schechter, et al., "The effect of several polymers on the phase behavior of micellar fluids" Society of Petroleum Engineers Journal, vol. 22, no. 06, pp. 816–830, SPE-8826-PA, 1982.

[38] J. E. Tackett Jr, "Process for enhanced delayed in situ gelation of chromium polyacrylamide gels" Dec. 3 1991. US Patent 5,069,281.

[39] R. Sydansk, "Polymer-enhanced foams part 1: laboratory development and evaluation" SPE Advanced Technology Series, vol. 2, no. 02, pp. 150–159, SPE-25168-PA, 1994.

[40] C. Romero, J. Alvarez, A. Müller, et al., "Micromodel studies of polymer-enhanced foam flow through porous media" in SPE/DOE Improved Oil Recovery Symposium, Society of Petroleum Engineers, SPE-75179-MS, 2002.

[41] S. Kutay, L. Schramm, "Structure/performance relationships for surfactant and polymer stabilized foams in porous media" Journal of Canadian Petroleum Technology,

vol. 43, no. 02, PETSOC-04-02-01, 2004.

[42] N. Kristen-Hochrein, A. Laschewsky, R. Miller,et al., "Stability of foam films of oppositely charged polyelectrolyte/surfactant mixtures: effect of isoelectric point" The Journal of Physical Chemistry B, vol. 115, no. 49, pp. 14475–14483, 2011.

[43] C. Shen, Q. P. Nguyen, C. Huh, et al., "Does polymer stabilize foam in porous media?" in SPE/DOE Symposium on Improved Oil Recovery, Society of Petroleum Engineers, SPE-99796-MS, 2006.

[44] W. R. Rossen, "Mechanistic studies of improved foam EOR processes" 2003.

[45] R. Petkova, S. Tcholakova, and N. Denkov, "Role of polymer–surfactant interactions in foams: effects of ph and surfactant head group for cationic polyvinylamine and anionic surfactants" Colloids and Surfaces A: Physicochemical and Engineering Aspects, vol. 438, pp. 174–185, 2013.

[46] A. Stocco, W. Drenckhan, E. Rio, et al., "Particle-stabilised foams: an interfacial study" Soft Matter, vol. 5, no. 11, pp. 2215–2222, 2009.

[47] M. Safwat, H. A. Nasr-El-Din, K. Dossary, et al., "Enhancement of stimulation treatment of water injection wells using a new polymer-free diversion system" in Abu Dhabi International Petroleum Exhibition and Conference, Society of Petroleum Engineers, SPE-78588-MS, 2002.

[48] M. Saha, M. E. Kabir, and S. Jeelani, "Enhancement in thermal and mechanical properties of polyurethane foam infused with nanoparticles" Materials Science and Engineering: A, vol. 479, no. 1, pp. 213–222, 2008.

[49] B. P. Binks, M. Kirkland, and J. A. Rodrigues, "Origin of stabilisation of aqueous foams in nanoparticle–surfactant mixtures" Soft Matter, vol. 4, no. 12, pp. 2373–2382, 2008.

[50] S. I. Karakashev, O. Ozdemir, M. A. Hampton, et al., "Formation and stability of foams stabilized by fine particles with similar size, contact angle and different shapes" Colloids and Surfaces A: Physicochemical and Engineering Aspects, vol. 382, no. 1, pp. 132–138, 2011.

[51] Q. Lv, Z. Li, B. Li, et al., "Study of nanoparticle–surfactant-stabilized foam as a fracturing fluid" Industrial & Engineering Chemistry Research, vol. 54, no. 38, pp. 9468–9477, 2015.

[52] F. Ravera, M. Ferrari, L. Liggieri,et al., "Liquid–liquid interfacial properties of mixed nanoparticle–surfactant systems" Colloids and Surfaces A: Physicochemical and Engineering Aspects, vol. 323, no. 1, pp. 99–108, 2008.

[53] E. Santini, J. Krägel, F. Ravera, et al., "Study of the monolayer structure and wettability properties of silica nanoparticles and ctab using the langmuir trough technique" Colloids and Surfaces A: Physicochemical and Engineering Aspects, vol. 382, no. 1, pp. 186–191, 2011.

[54] B. Bai, M. Elgmati, H. Zhang, et al., "Rock characterization of fayetteville shale gas plays" Fuel, vol. 105, pp. 645–652, 2013.

[55] B. P. Binks, "Particles as surfactantsâĂŤsimilarities and differences" Current Opinion in Colloid & Interface Science, vol. 7, no. 1, pp. 21–41, 2002.

[56] T. N. Hunter, E. J. Wanless, G. J. Jameson, et al., "Non-ionic surfactant interactions with hydrophobic nanoparticles: Impact on foam stability" Colloids and Surfaces A: Physicochemical and Engineering Aspects, vol. 347, no. 1, pp. 81–89, 2009.

[57] A. Maestro, E. Guzmán, F. Ortega, et al., "Contact angle of micro-and nanoparticles at fluid interfaces" Current Opinion in Colloid & Interface Science, vol. 19, no. 4, pp. 355–367, 2014.

[58] T. Mohd, M. Shukor, N. A. Ghazali, et al., "Relationship between foamability and nanoparticle concentration of carbon dioxide (CO_2) foam for enhanced oil recovery (EOR)" in Applied Mechanics and Materials, vol. 548, pp. 67–71, Trans Tech Publ, 2014.

[59] Å. Haugen, M. A. Fernø, A. Graue, et al., "Experimental study of foam flow in fractured oil-wet limestone for enhanced oil recovery" SPE Reservoir Evaluation & Engineering, vol. 15, no. 02, pp. 218–228, SPE-129763-PA, 2012.

[60] J. F. Gadberry, M. J. Engel, J. D. Nowak, et al., "Thickened viscoelastic fluids and uses thereof" May 17 2016. US Patent 9,341,052.

[61] J. Gauthier, "Rheology and Settling Dynamics of a Particle Filled Aqueous Polymer Gel for Hydraulic Fracturing Fluid Systems" The Ohio State University, 2015.

[62] J. Andreas, E. Hauser, and W. Tucker, "Boundary tension by pendant drops1" The Journal of Physical Chemistry, vol. 42, no. 8, pp. 1001–1019, 1938.

[63] W. Xu, S. C. Ayirala, D. N. Rao, et al., "Measurement of surfactant-induced interfacial interactions at reservoir conditions" SPE Reservoir Evaluation & Engineering, vol. 11, no. 01, pp. 83–94, SPE-96021-PA, 2008.

[64] S. Bachu, "Screening and ranking of sedimentary basins for sequestration of CO_2 in geological media in response to climate change" Environmental Geology, vol. 44, no. 3, pp. 277–289, 2003.

[65] C. Aggelopoulos, M. Robin, E. Perfetti, et al., " CO_2/$CaCl_2$ solution interfacial tensions under CO_2 geological storage conditions: influence of cation valence on interfacial tension" Advances in Water Resources, vol. 33, no. 6, pp. 691–697, 2010.

[66] A. Maestro, E. Rio, W. Drenckhan, et al., "Foams stabilised by mixtures of nanoparticles and oppositely charged surfactants: relationship between bubble shrinkage and

foam coarsening" Soft matter, vol. 10, no. 36, pp. 6975–6983, 2014.

[67] R. Singh, and K. K. Mohanty "Synergistic stabilization of foams by a mixture of nanoparticles and surfactants" in SPE Improved Oil Recovery Symposium, Society of Petroleum Engineers, SPE-169126-MS, 2014.

[68] M. B. Alotaibi, R. A. Nasralla, H. A. Nasr-El-Din, et al., "Wettability studies using low-salinity water in sandstone reservoirs" SPE Reservoir Evaluation & Engineering, vol. 14, no. 06, pp. 713–725, SPE-149942-PA, 2011.

[69] Y. Liu, R. B. Grigg, B. Bai, et al., "Salinity, ph, and surfactant concentration effects on CO_2-foam" in SPE International Symposium on Oilfield Chemistry, Society of Petroleum Engineers, SPE-93095-MS, 2005.

[70] K. Osei-Bonsu, N. Shokri, and P. Grassia, "Fundamental investigation of foam flow in a liquid-filled hele-shaw cell" Journal of Colloid and Interface Science, vol. 462, pp. 288–296, 2016.

[71] G. Yin, R. B. Grigg, Y. Svec, et al., "Oil recovery and surfactant adsorption during CO_2-foam flooding" in Offshore Technology Conference, Offshore Technology Conference, OTC-19787-MS, 2009.

[72] C. A. Schneider, W. S. Rasband, and K. W. Eliceiri, "NIH Image to ImageJ: 25 years of image analysis," Nature Methods, vol. 9, no. 7, pp. 671, 2012.

[73] T. EREN, "Foam characterization: Bubble size and texture effects". PhD Dissertation, Middle East Technical University, 2004.

[74] A.-L. Fameau and A. Salonen, "Effect of particles and aggregated structures on the foam stability and aging" Comptes Rendus Physique, vol. 15, no. 8, pp. 748–760, 2014.

[75] B. P. Binks and T. S. Horozov, "Aqueous foams stabilized solely by silica nanoparticles" Angewandte Chemie, vol. 117, no. 24, pp. 3788–3791, 2005.

[76] H. H. Liu, S. Surawanvijit, R. Rallo, et al., "Analysis of nanoparticle agglomeration in aqueous suspensions via constant-number monte carlo simulation" Environmental Science & Technology, vol. 45, no. 21, pp. 9284–9292, 2011.

[77] C. Zhang, Z. Li, Q. Sun, et al., " CO_2 foam properties and the stabilizing mechanism of sodium bis (2-ethylhexyl) sulfosuccinate and hydrophobic nanoparticle mixtures" Soft Matter, vol. 12, no. 3, pp. 946–956, 2016.

[78] Q. Sun, Z. Li, S. Li, et al., "Utilization of surfactant-stabilized foam for enhanced oil recovery by adding nanoparticles" Energy & Fuels, vol. 28, no. 4, pp. 2384–2394, 2014.

[79] Q. Sun, Z. Li, J. Wang, et al., "Aqueous foam stabilized by partially hydrophobic nanoparticles in the presence of surfactant" Colloids and Surfaces A: Physicochemical and Engineering Aspects, vol. 471, pp. 54–64, 2015.

[80] N. R. Biswal, N. Rangera, and J. K. Singh, "Effect of different surfactants on the interfacial behavior of the n-hexane–water system in the presence of silica nanoparticles" The Journal of Physical Chemistry B, vol. 120, no. 29, pp. 7265–7274, 2016.

[81] R. J. Hunter, Zeta potential in colloid science: principles and applications, vol. 2. Academic press, 2013.

[82] C. Xiao, S. N. Balasubramanian, L. W. Clapp, et al., "Rheology of supercritical CO_2 foam stabilized by nanoparticles" in SPE Improved Oil Recovery Conference, Society of Petroleum Engineers, SPE-179621-MS, 2016.

[83] J. Fang, C. Dai, Y. Yan, et al., "Enhanced foam stability by adding dispersed particle gel: A new 3-phase foam study" in SPE Asia Pacific Enhanced Oil Recovery

Conference, Society of Petroleum Engineers, SPE-174597-MS, 2015.

[84] J. B. Lawson, J. Reisberg, "Alternate slugs of gas and dilute surfactant for mobility control during chemical flooding" in SPE/DOE Enhanced Oil Recovery Symposium, Society of Petroleum Engineers, SPE-8839-MS, 1980.

[85] P. Stevenson, "Inter-bubble gas diffusion in liquid foam" Current Opinion in Colloid & Interface Science, vol. 15, no. 5, pp. 374–381, 2010.

[86] D. Meehan, "Estimating water viscosity at reservoir conditions" Petrol. Eng, vol. 52, no. 8, pp. 117–118, 1980.

[87] S. Afra and E. Gildin, "Tensor based geology preserving reservoir parameterization with higher order singular value decomposition (HOSVD)" Computers & Geosciences, vol. 94, pp. 110–120, 2016.

APPENDIX A

The foam texture, lamella thickness, and bubble size are obtained by using an image processing tool known as ImageJ. A visual HP/HT cell is employed to acquire two dimensional images. A microscope with a strong magnifier that can easily enlarge initial images is utilized to capture foam images. Images are then captured by placing the lens of a digital camera to the lid of the microscope at size of 2400x1800 pixels. The software can calculate area and pixel value statistics of user-defined selections. Image J software also can measure distances and angles. It also can create density histograms and line profile plots for particle or bubble distribution.

PROCEDURE:

1) Open the ImageJ software.

2) In ImageJ employ the file menu to open an image.

3) On the toolbar of ImageJ, select the line tool. Hold down the shift key and draw a straight line along the length of the scale bar of the image being as precise as possible.

4) Select analyze, then set scale. For the known distance type in the distance of your scale bar, and then enter the units (microns or nm). Check global so that this measurement is applied to all of the images taken with the same magnification.

5) Select a region of interest by choosing the box tool, to the far left of the line drawing tool, and draw a box around the area of interest. Only include in the box the particles you want to analyze.

6) Under the Image tab select crop.

7) Under the Image tab select adjust then threshold.

8) Adjust the threshold by sliding the bars so that only the bubbles or particles you

wish to analyze are selected.

9) Under the analyze tab select set measurements and check the measurements to take.

10) On the ImageJ toolbar, select the red arrows that indicate that there are more tools, and select drawing tools. Use the eraser tool to erase any particles do not to measure.

11) Under analyze select analyze particles. Check display results and other settings to use.

12) The measurements will show up in a chart. Then cut and paste these measurements into excel in order to analyze the data and create graphs.